**Molecular Photovoltaic Systems Based on Solid-Supported Phospholipids/Alkanethiol Hybrid Bilayer Matrices: Photocurrent Generation and Modulation**

by

Lixia Liu

A dissertation submitted to the Graduate Faculty of
Auburn University
in partial fulfillment of the
requirements for the Degree of
Doctor of Philosophy

Auburn, Alabama
August 3, 2013

Keywords: Molecular Photovoltaics, Phospholipids,
Hybrid bilayer matrix, Photoelectric Chemistry



Approved by

Wei Zhan, Chair, Associate Professor of Chemistry and Biochemistry
Rik Blumenthal, Associate Professor of Chemistry and Biochemistry
Curtis Shannon, Professor of Chemistry and Biochemistry
Xinyu Zhang, Associate Professor of Polymer and Fiber Engineering

## Abstract

Stimulated by the energy crisis and inspired by natural photosynthesis, several molecular photovoltaic (artificial photosynthetic) systems were developed and investigated within the current research. These molecular photovoltaic cells are based on solid-supported hybrid bilayer matrices which are composed of a self-assembled monolayer (SAM) of alkanethiols/octadecyltrichlorosilane and a phospholipid monolayer on gold or ITO substrate. Various chromophores including fullerenes $C_{63}$, ruthenium tris(bipyridyl) complexes ($Ru(bpy)_3^{2+}$) and zinc porphyrin (ZnP) were incorporated in the lipid layer to enable photo-excitation, charge separation and thus photocurrent generation. To further develop and improve these photovoltaics, some natural compounds, such as lutein and cholesterol, were co-assembled in the lipid layer to modulate the photocurrent and photovoltage generation by the photoactive agents. The modulation effect was also successfully applied by altering the underlying SAM layer. A combination of UV-Vis, fluorescence and impedance spectroscopy, cyclic voltammetry (CV), atomic force microscopy (AFM) as well as photoelectrochemical techniques were used to characterize and investigate these systems.

This dissertation begins with an introduction to the concept of photovoltaic system and its development, the formation of solid-supported hybrid bilayer as well as the photo-sensitizers commonly used for molecular photovoltaics. Four research projects are then discussed separately, which include the investigation on the photocurrent modulation

generated by fullerene $C_{63}$ through co-incorporating a natural compound lutein in an alkanethiol/lipid hybrid bilayer matrix; the studies with the modulation of porphyrin and fullerene's photocurrent and photovoltage generation by using polar alkanethiol to form the underlying SAM layer as well as the involved mechanisms form several perspectives; the discussion on the dual impacts of cholesterol on lipid membranes and thus induced different effects on the photovoltaic responses of fullerene co-assembled in hybrid bilayer matrices; as well as photovoltaic systems built on modified Indium Tin Oxide (ITO) and the difficulties of forming well-packed SAM layers on ITO surface. Which is followed by a conclusion and a brief future outlook.

Acknowledgments

I would like to graciously thank Dr. Wei Zhan for his continuous guidance and support throughout the entire Ph.D. program. I would like to thank my committee, which consists of Dr. Rik Blumenthal, Dr. Curtis Shannon, Dr. Xinyu Zhang and the outside reader Dr. Minseo Park, for their help and advices in completing this program and finishing this dissertation. Additional appreciation goes to Dr. Anne Gorden for providing the UV-Vis spectrophotometer, Dr. Christopher Easley for the Gamry electrochemical impedance analyzer system, and Dr. Aleksandr Simonian from the Materials Engineering department for providing the electrochemical impedance instrument. I am also very grateful to my previous and current lab mates: Dr. Kai Jiang, Dr. Chenguo Hu, Dr. Hong Xie, Ms. Ana Dmytrejchuk and Mr. Mingming Wang.

My greatest thanks goes to my parents, my husband Dr. Dan Clary and all my other family members for their support and encouragement throughout the graduate school.

Table of Contents

List of Tables

List of Figures

List of Abbreviations

| | |
|---|---|
| HBM | Hybrid Bilayer Membrane |
| SAM | Self-Assembled Monolayer |
| POPC | 1-palmitoyl-2-oleoyl-sn-glycero-3-phophocholine |
| DOPE | 1,2-dioleoyl-*sn*-glycero-3-phosphoethanolamine |
| DPPC | 1,2-dipalmitoyl-*sn*-glycero-3-phosphocholine |
| BT | Benzothiadiazole |
| ITO | Indium Tin Oxide |
| LHC | Light-Harvesting Complexes |
| $C_{12}SH$ | 1-dodecanethiol |
| $C_{63}$ | Monomalonic fullerenes |
| ZnP | Zinc Porphyrin |
| HEPES | 4-(2-hydroxyethyl)piperazine-1-ethanesulfonic acid |
| $Bu_4NBF_4$ | Tetrabutylammonium Tetrafluoroborate |
| MV | Methyl Viologen |
| CV | Cyclic Voltammetry |
| OTS | n-Octadecyltrichlorosilane |
| OPV | Organic Photovoltaics |
| HIB | Hole-Injection Barrier |
| $Ru(bpy)_3^{2+}$ | Ruthenium tris(bipyridyl) complexes |
| ET | Electron Transfer |
| $C_{10}F_{17}SH$ | Heptadecafluoro-1-decanethiol |

| | |
|---|---|
| OLED | Organic Light Emitting Diode |
| DSSC | Dye Sensitized Solar Cell |

# Chapter One

# Introduction

## 1.1 Introduction

Today fossil fuels still make up the predominant share of the global energy supply, which not only are unsustainable but also can potentially cause detrimental climate fluctuations. The alternative energy sources, such as nuclear energy, unfortunately, are not problem free, such as their waste generation, vulnerability to accidents and the undesirable spread of nuclear technology and materials.[1] Another potentially renewable energy source is solar based, which is abundant but currently contributes to less than half a percent in the total energy consumption. Several factors, such as the diffusiveness of sunlight and its seasonal and diurnal fluctuations, will have to be addressed before this inexhaustible energy source can become a major contender to replace of fossil fuels. To achieve such goals, therefore, continuous research and development in the harvesting, conversion and storage of solar energy are clearly needed.

Mimicking various aspects of natural photosynthesis using semiconducting and biological materials, i.e., artificial photosynthesis, represents a powerful approach to efficient solar energy utilization. Natural photosynthesis converts sunlight, water and carbon dioxide into carbohydrates and oxygen which is illustrated in a simplified manner in Figure 1.1.[2] The light reactions of photosynthesis include light absorption, charge

separation, water splitting and electron/proton transfer .[2] The light-harvesting complexes in photosynthesis have two functions which include increasing the solar spectrum range that can be captured and shortening the time of passing excitation energy to reaction center.[3] Artificial photosynthesis refers to a system that involves a chemical process that mimics the natural photosynthesis process occurring in plants: this term is commonly used to illustrate any setup for capturing and storing the energy from sunlight. A lot of researchers around the world have been trying to build efficient artificial photosynthetic systems to generate electricity. But unfortunately, so far, no components have been built which are efficient and strong enough to be incorporated into a system for solar fuel production. Most of the research has been done to design new molecular photovoltaic systems or to improve the efficiency of existed ones.

The current investigation focuses on the development of a series of new artificial photosynthetic systems that are assembled in several solid-supported lipid bilayers. Mimicking the phospholipid lipid bilayer which comprises most cell membranes in nature, a lipid layer will be constructed on top of a base layer which is assembled onto either a gold or indium tin oxide (ITO) electrode. The objective will be to incorporate and investigate various chromophores within the outer lipid layer which enable photoexcitation and charge separation. Some natural compounds will be embedded into the lipid layer with chromophores to modify the photocurrent generation by either altering the electron transfer pathway or changing the properties of the lipid layer. The effect of different base layer on the performance of photovoltaic system will also be studied and the electrode material to which a base layer is fixed will serve as the terminal electron donor/acceptor. Specifically, I describe in this dissertation:

1) The modulation of fullerene's photocurrent generation by the co-assembled lutein (a natural carotenoid species) via electron transfer mechanism in an alkanethiol/lipid based bilayer photovoltaic system.
2) The modulation of Porphyrin and fullerene's photovoltaic responses by polar alkanethiols SAMs through dipole-induced modification of work function of the metal substrates.
3) The different effects of cholesterol on fullerene's photocurrent output in different lipid matrices by regulating the properties of the lipid membrane, such as, ordering, rigidity, and passive permeability.
4) The study of photovoltaic cells based on modified Indium Tin Oxide (ITO) substrates and the formation of SAMs on ITO surface.

This approach is unique because it has the potential to provide an avenue to supply much needed, usable energy by harnessing the energy of sunlight through an environmentally "green" approach which mimics nature.

The main process involved in molecular photovoltaic systems is to mimic the light driven charge separation and electron transfer which occurs in the light reaction centers of natural photosynthesis.[2] So a successful molecular photovoltaic system must at least consists of an electron donor, a photo sensitizer which can absorb visible light, an electron acceptor, and an organized orientation which favors electron transfer from donor to acceptor .[4]

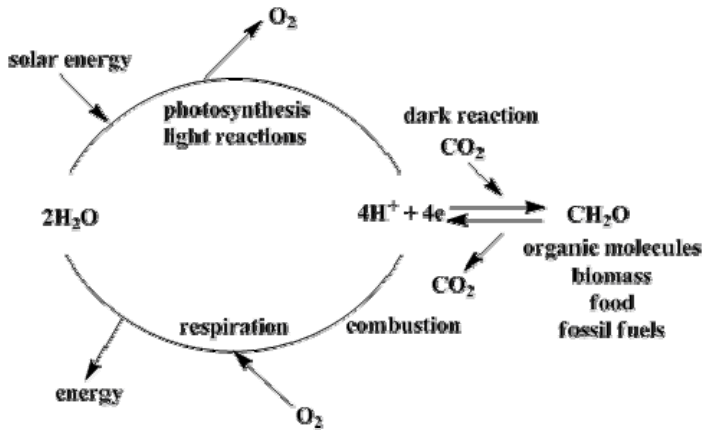


**Figure 1.1.** Diagrammatic representation of natural photosynthesis.

### 1.1.1 The development and different types of photovoltaics

The photovoltaic effect refers to the conversion of sunlight into electrical power and was first discovered by Alexandre-Edmond Becquerel in 1839.[5,6] Photovoltaics, which have been practically utilized in different ways, are setups that convert solar radiation into direct current electricity or chemical fuels such as hydrogen as illustrated in Figure 1.2.[7] The term photovoltaics originally represented the unbiased operating mode of a photodiode in which the current flow through is entirely generated by sunlight energy.[5] In early developments of photovoltaics, all the materials utilized by photovoltaic devices were semiconductor and the most common type was crystalline silicon. The basic structure of a semiconductor-based solid state photovoltaic cell composes a p-type semiconductor wafer on top of a back metal plate, which is followed by a n-type semiconductor wafer, on tope of which is a antireflective coating and then a front metal/transparent conductor plate.[8] The general concept of semiconductor-based photovoltaics involves the generation of electron-hole pairs upon irradiation of the semiconductor with visible light and the subsequent creation of an electrical potential

difference across the interface between two different semiconductor materials.[7] The benefits of this type of photovoltaics are high efficiency and reliability. For example, the efficiency of crystalline silicon photovoltaic cells can reach as high as 25%. [9] The disadvantages include band gap limitation and expensive production. Because of these disadvantages, traditional semiconductor materials were challenged by nanocrystalline semiconductor and conducting polymers, which are relatively cheaper and more flexible.[7,9]

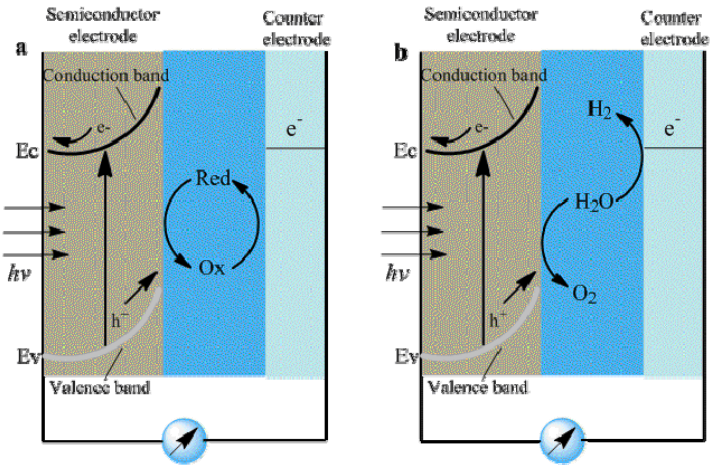


**Figure 1.2.** Photovoltaic system that generates electrical current (a) and hydrogen (b) through water splitting.

Later on, the solid phase in contact with the semiconductor was replaced by electrolyte containing proper redox couples. Since semiconductor has a typical band gap from 2.7 to 3.2 electron volts (eV), so it cannot efficiently adsorb the light with a longer wavelength than 460 nm. Inspired by this fact, the dye sensitized electrochemical photovoltaics came along (Figure 1.3).[7] For the first time, dye sensitized photovoltaics separates light absorption and charge carrier transport processes, which opens up wide options for molecular absorber material. The dye sensitizer first absorbs light producing an electronically excited state, the excited electron is then injected into the conduction

band of the adjacent semiconductor which enables current flow from the semiconductor to the electrode and then to the external circuit. The neutral dye sensitizer can be regenerated by the oxidation reaction of redox couples in the electrolyte and the mediator can then be reduced to its original state at the cathode by the electrons flowing through the external circuit, which is followed by a new cycle.[10] The maximum voltage generated by the cell upon radiation depends on the energy separation between the redox potential of the electrolyte and the Fermi level of electron in the modified solid electrode.[11]

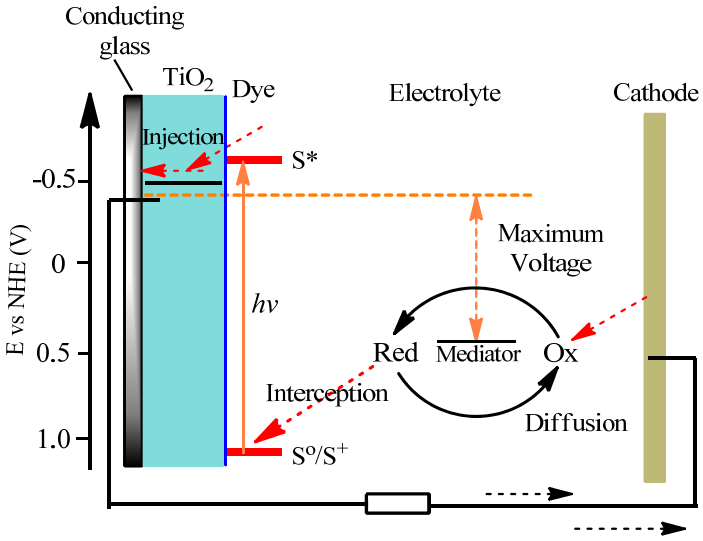


**Figure 1.3.** Representation of dye sensitized electrochemical photovoltaics.

The dye sensitized photovoltaics possess several advantages compared to the earlier silicon based photovoltaics, such as higher photosensitivity, lower cost and more flexibility. But it also bears some faults which include instability due to the temperature sensitivity of the liquid electrolyte and relatively low efficiency (typically between 5% to 13%) compared to crystalline silicon photovoltaic cell. Early studies with dye sensitized photovoltaics focused on depositing dye on flat electrodes which means that only the first layer of the adsorbed dye can efficiently capture light and inject electrons into the semiconductor. But one single sensitizer layer can only adsorb less than 1% of the

incident light because of the area occupied by one dye molecule is much larger than the optical pass way for light capture. [12,13] By applying nanoporous semiconductor materials on the flat electrodes, the surface area for dye molecules to be adsorbed on can be enhanced by 100 to 1000 fold which will accordingly increase the efficiency of light harvesting and electron transfer significantly.[14] The first nanoporous $TiO_2$ based dye sensitized photovoltaics was reported by Grätzel group.[11]

With the development of different photovoltaic systems, molecular photovoltaics based on solid supported lipid bilayer, which mimics the structure and mechanism of natural photosynthesis, has emerged and been growing in recent years. The most common lipid used for building up this bilayer structure is phospholipid which is the major component of all cell membranes. The solid substrate offers a robust and stable structure, and the lipid bilayer can act as a barrier to suppress the charge recombination.[15] The photoactive agent can be placed either on the substrate surface or incorporated in the lipid bilayer. One type of system is illustrated in Figure 1.4 which utilizes fullerene $C_{63}$ as the chromophore in the phospholipid bilayer on an indium tin oxide (ITO) electrode.[16] There are several reasons for the emergence and development of this type of molecular photovoltaic. First, it mimics the natural photosynthetic process. Second, different, or different combinations of, photo sensitizers can be inserted into the lipid bilayer to modify the molecular photovoltaic system. Third, the lipid bilayer can enable biofunctionalization of some inorganic solid surface, such as ITO, gold-coated surface and semiconductors. Forth, the lipid bilayer structure can provide a well-defined orientation.[15] On top of these advantages, both anodic and cathodic photocurrent can be generated with this molecular photovoltaic based on the electron donor or acceptor agent

added in the solution. When electron donor is added in the solution, the photo-excited chromophore is first reduced by the donor, which then injects an electron into the electrode and generates anodic current. The cathodic current generation can be realized with the excited chromophore reducing the electron acceptor in the solution and then being reduced back to its original state by the electrode.[15]

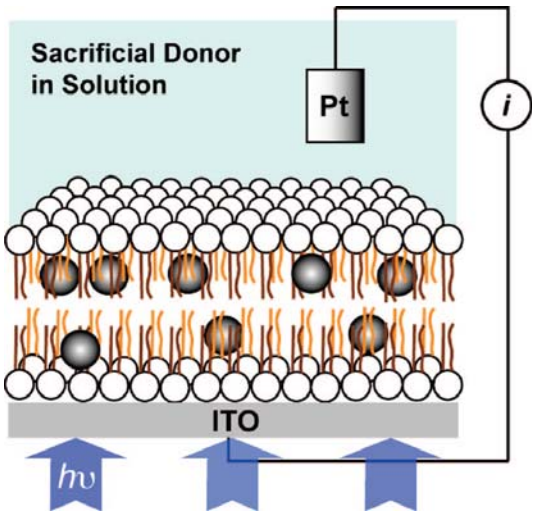


**Figure 1.4.** Molecular photovoltaics based on solid supported lipid bilayer. Taken with permission from Ref.7 [16].

One advancement in this category of photovoltaics involves the self-assembling of an alkanethiol monolayer on a gold substrate and a subsequently phospholipid layer with embedded $Ru(bpy)_3^{2+}$ as a photosensitizer as illustrated in Figure 1.5.[15] This form of hybrid bilayer based photovoltaics offers advantages over the lipid bilayer-based version, such as greater stability because of the strong bond between the bottom monolayer and substrate, more variety of combinations and increased opportunity for systemic modification. Both the bottom alkanethiol layer and top lipid layer can be separately modified to improve the photocurrent generation efficiency of this system. Similarly,

both anodic and cathodic photocurrent generation can be obtained with this hybrid bilayer system.

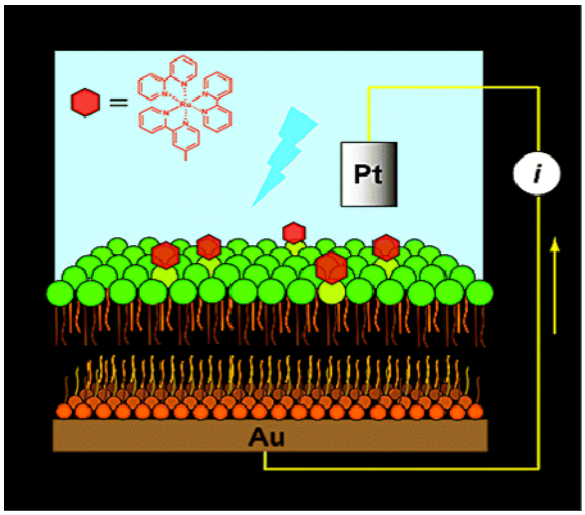


**Figure 1.5.** Molecular photovoltaics based on solid supported lipid bilayer. Taken with permission from Ref .8.[15]

### 1.2 The formation of solid supported hybrid bilayer

There are two methods to form the bottom layer on the solid surface, one of which is self-assembly which will be discussed here. Another method involves Langmuir–Blodgett transfer. Self-assembly provides a simple process to organize organic molecular on solid surface. Highly ordered self assembled monolayers (SAMs) can be formed spontaneously through chemisorptions and self organization of long chain organic molecules on suitable substrates.[17,18] Molecules that can be used to form SAMs typically have three parts: the headgroup, which provides chemisorption to the substrate: the tail group (-$CH_3$) that provides a surface for the modified substrate: and the alkyl chain (-$(CH_2)_n$-) that links the head and tail group. The formation of SAMs can be simply carried out by placing the substrate in a dilute solution containing the molecule of interest

(Figure 1.6).[17] Two different classes of SAMs will be introduced in this chapter. One class is alkanethiol SAMs whereas the other is alkylsilane SAMs.

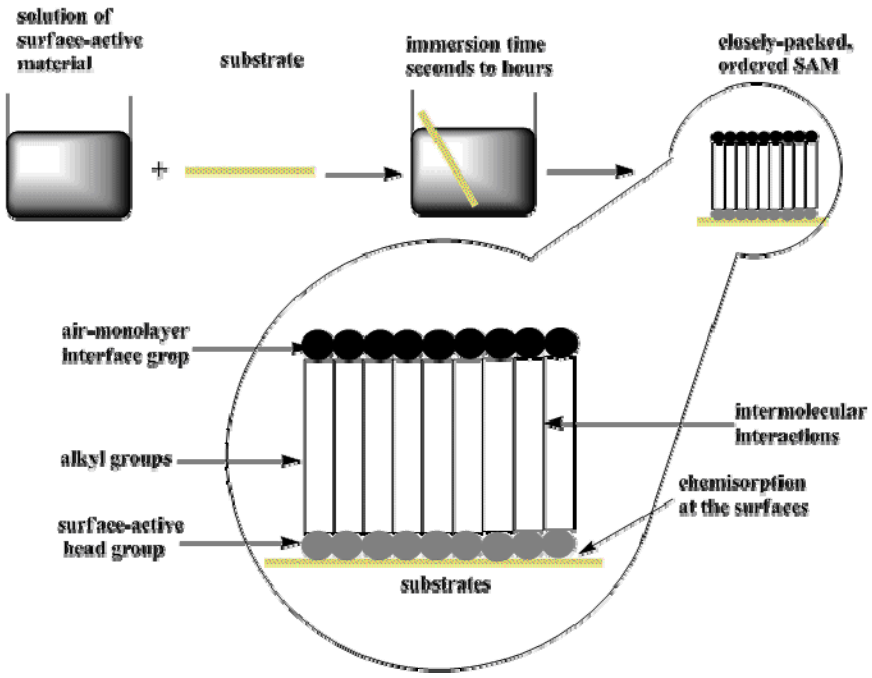


**Figure 1.6.** The formation of SAMs on solid substrates.

The most studied and well known example of alkanethiol SAMs is based on the strong metal-sulfur interaction on the gold substrate. The formation of alkanethiol SAMs on gold can provide a well defined hydrophobic surface for the following layer. Because octadecanethiol offers the ability to form a well ordered and tightly packed monolayer, it is a very common choice for hybrid bilayer formation on gold substrate.[19] Another popular and well-studied class of SAMs are alkylsilanes on silicon, which will induce the formation of a three-dimensional, cross-linked (silane to silicon and silane to silane) network of Si-O-Si bonds to the surface of the substrates. Compared to the alkanethiol SAMs on gold, the silane terminated monolayers offer a higher physical and chemical stability. But on another hand, the alkylsilane molecules show a lower reactivity than

alkanethiol, which makes the formation process of silane SAMs a little bit more difficult than the assembly of alkanethiol monolayers onto gold substrates.[20] Other than the silane SAMs on silicon, the assembly of silane monolayers through Si-O bonds on glass, ITO and some other semiconductors have also been widely studied. Among the wide variety of alkylsilane compounds, trichlorosilanes, such as n-octadecyltrichlorosilane (OTS), are the most popular class of SAM formation.

The formation of well-packed SAMs is very crucial for the formation of the following layer. There are several parameters that can affect the quality of SAMs, such as the selected solvent, the concentration of the immersing solution, the immersing time, the solution temperature, and the water concentration which is especially important for the formation of silane monolayers. There are also two methods for applying the top lipid layer onto the SAMs-modified surface: vesicle fusion and lipid transfer from an air-water interface.[19] Several studies have shown that vesicles in aqueous buffer solutions can fuse onto SAM-modified hydrophobic surface spontaneously to form a hybrid bilayer (Figure 1.7).[19]

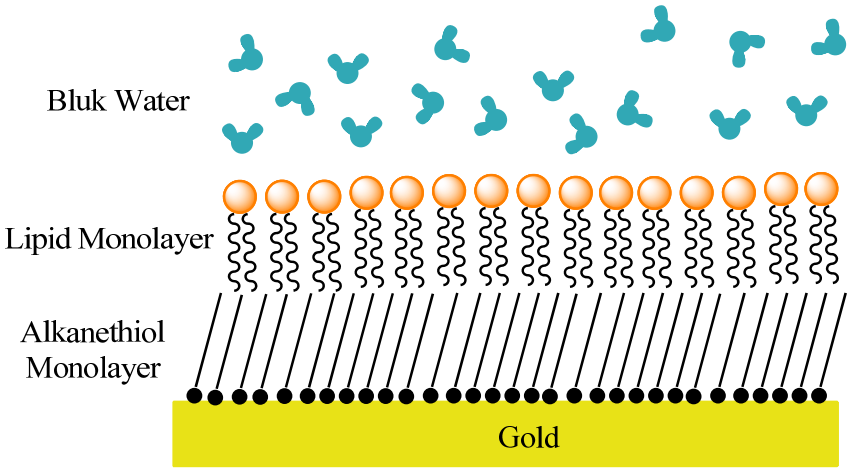


**Figure 1.7.** Schematic illustration of a lipid/ alkanethiol hybrid bilayer

There are several advantages of utilizing hybrid bilayer membranes for molecular photovoltaics as compared to using lipid bilayer structures, such as more stability due to the strong interactions between SAMs and substrate, and greater freedom of variation since the chemical and physical properties of a hybrid bilayer can be altered through the use of different SAM precursors, lipids and membrane additives.

### 1.3 Common photosensitizers for molecular photovoltaics

The efficiencies of silicon based inorganic solar cells have reached 10-25%, but the high cost has limited its application and development. The efficiencies of earlier solid organic solar cells were very low due to the slow electron/hole dissociation and small exciton diffusion range.[21] Then the dye-sensitized molecular photovoltaics came along which offer fast photoinduced charge separation and slow charge recombination. A lot of chromophores have been incorporated into different molecular photovoltaic cells, such as porphyrin, fullerene and its derivatives, polythiophene derivatives, benzothiadiazole (BT), $[Ru(bpy)_3]^{2+}$ etc.[22-25] A favorable orientation of the chromophores can increase the efficiency of photovoltaics by at most a factor of 2 through enhancing vertical electron transfer. Among all the potential chromophores, the fullerenes and porphyrin have obtained most of the attention because of their unique electrical and photochemical properties. Fullerenes possess unique properties which include narrow HOMO-LUMO gap (~1.8 eV), long-lived photoinduced charge separation and low reorganization energy. With a capacity of up to six electrons, fullerenes can serve as excellent electron acceptors.[16,26,27] On another hand, porphyrin molecules can be great electron donors and

moreover, they typically possess several strong visible light absorption bands because of the π – π * electron transitions and have long-lived excited state counterparts.[28,29] Because the redox potential of excited-state porphyrins and that of fullerenes match well in addition to their unique properties, they have been frequently incorporated together into photovoltaic cells either as covalently linked porphyrin-fullerene arrays or as two individuals.[22,30,31] This combination of both chromophores offers efficient light absorption, prolonged charge separation and fast photoinduced electron transfer.[32] Other than these synthesized chromophores, some natural compounds can also be utilized in molecular photovoltaics to enhance the efficiency, such as chlorophylls, carotenoids, cholesterol.[33-36]

**References:**


1. Nash Kenneth, L.; Lumetta Gregg, J.; Clark Sue, B.; Friese, J. In *Separations for the Nuclear Fuel Cycle in the 21<sup>st</sup> Century*; American Chemical Society: 2006; Vol. 933, p 3-20.

2. Barber, J. Photosynthetic energy conversion: natural and artificial. *Chemical Society Reviews*. **2009**, *38*, 185-196.

3. Woller, J. G.; Hannestad, J. K.; Albinsson, B. Self-Assembled Nanoscale DNA–Porphyrin Complex for Artificial Light Harvesting. *Journal of the American Chemical Society*. **2013**, *135*, 2759-2768.

4. Gust, D.; Moore, T. A.; Moore, A. L. Mimicking Photosynthetic Solar Energy Transduction. *Accounts of Chemical Research*. **2000**, *34*, 40-48.

5. Kippelen, B.; Bredas, J.-L. Organic photovoltaics. *Energy & Environmental Science*. **2009**, *2*, 251-261.

6. Bredas, J.-L.; Durrant, J. R. Organic Photovoltaics. *Accounts of Chemical Research*. **2009**, *42*, 1689-1690.

7. Gratzel, M. Photoelectrochemical cells. *Nature*. **2001**, *414*, 338-344.

8. Green, M. A.; Basore, P. A.; Chang, N.; Clugston, D.; Egan, R.; Evans, R.; Hogg, D.; Jarnason, S.; Keevers, M.; Lasswell, P.; O'Sullivan, J.; Schubert, U.; Turner, A.; Wenham, S. R.; Young, T. Crystalline silicon on glass (CSG) thin-film solar cell modules. *Solar Energy*. **2004**, *77*, 857-863.

9. Sun, B.; Findikoglu, A. T.; Sykora, M.; Werder, D. J.; Klimov, V. I. Hybrid Photovoltaics Based on Semiconductor Nanocrystals and Amorphous Silicon. *Nano Letters*. **2009**, *9*, 1235-1241.

10. Wei, D. Dye Sensitized Solar Cells. *International Journal of Molecular Sciences.* **2010**, *11*, 1103-1113.

11. Hagfeldt, A.; Grätzel, M. Molecular Photovoltaics. *Accounts of Chemical Research*. **2000**, *33*, 269-277.

12. O'Regan, B.; Gratzel, M. A low-cost, high-efficiency solar cell based on dye-sensitized colloidal TiO2 films. *Nature*. **1991**, *353*, 737-740.

13. Grätzel, M. Solar Energy Conversion by Dye-Sensitized Photovoltaic Cells. *Inorganic Chemistry*. **2005**, *44*, 6841-6851.

14. O'Regan, B.; Schwartz, D. T.; Zakeeruddin, S. M.; Grätzel, M. Electrodeposited Nanocomposite n–p Heterojunctions for Solid-State Dye-Sensitized Photovoltaics. *Advanced Materials*. **2000**, *12*, 1263-1267.

15. Jiang, K.; Xie, H.; Zhan, W. Photocurrent Generation from Ru(bpy)32+ Immobilized on Phospholipid/Alkanethiol Hybrid Bilayers. *Langmuir*. **2009**, *25*, 11129-11136.

16. Zhan, W.; Jiang, K. A Modular Photocurrent Generation System Based on Phospholipid-Assembled Fullerenes. *Langmuir*. **2008**, *24*, 13258-13261.

17. Prashar, D. Self Assembled Monolayers-A Review. *Self*. **2012**, *4*, 258-265.

18. Fihr, I. A. Supported membranes: scientific and practical applications. *Science*. **1996**, *271*, 43.

19. Castellana, E. T.; Cremer, P. S. Solid supported lipid bilayers: From biophysical studies to sensor design. *Surface Science Reports*. **2006**, *61*, 429-444.

20. Haensch, C.; Hoeppener, S.; Schubert, U. S. Chemical modification of self-assembled silane based monolayers by surface reactions. *Chemical Society Reviews*. **2010**, *39*, 2323-2334.

21. Tributsch, H. Dye sensitization solar cells: a critical assessment of the learning curve. *Coordination Chemistry Reviews*. **2004**, *248*, 1511-1530.

22. Imahori, H.; Fukuzumi, S. Porphyrin - and Fullerene - Based Molecular Photovoltaic Devices. *Advanced Functional Materials*. **2004**, *14*, 525-536.

23. Chen, J.; Cao, Y. Development of novel conjugated donor polymers for high-efficiency bulk-heterojunction photovoltaic devices. *Accounts of Chemical Research*. **2009**, *42*, 1709-1718.

24. Yanagida, S.; Yu, Y.; Manseki, K. Iodine/iodide-free dye-sensitized solar cells. *Accounts of Chemical Research*. **2009**, *42*, 1827-1838.

25. Roncali, J. Molecular bulk heterojunctions: an emerging approach to organic solar cells. *Accounts of Chemical Research*. **2009**, *42*, 1719-1730.

26. Li, L.; Davande, H.; Bedrov, D.; Smith, G. D. A molecular dynamics simulation study of C60 fullerenes inside a dimyristoylphosphatidylcholine lipid bilayer. *The Journal of Physical Chemistry B*. **2007**, *111*, 4067-4072.

27. Guldi, D. M.; Prato, M. Excited-state properties of C60 fullerene derivatives. *Accounts of Chemical Research*. **2000**, *33*, 695-703.

28. Griffith, M. J.; Mozer, A. J. Porphyrin Based Dye Sensitized Solar Cells.

29. Griffith, M. J.; Sunahara, K.; Wagner, P.; Wagner, K.; Wallace, G. G.; Officer, D. L.; Furube, A.; Katoh, R.; Mori, S.; Mozer, A. J. Porphyrins for dye-sensitised solar cells: new insights into efficiency-determining electron transfer steps. *Chemical Communications*. **2012**, *48*, 4145-4162.

30. Zhan, W.; Jiang, K.; Smith, M. D.; Bostic, H. E.; Best, M. D.; Auad, M. L.; Ruppel, J. V.; Kim, C.; Zhang, X. P. Photocurrent generation from porphyrin/fullerene complexes assembled in a tethered lipid bilayer. *Langmuir*. **2010**, *26*, 15671.

31. Luo, C.; Guldi, D.; Imahori, H.; Tamaki, K.; Sakata, Y. Sequential energy and electron transfer in an artificial reaction center: formation of a long-lived charge-separated state. *Journal of the American Chemical Society*. **2000**, *122*, 6535-6551.

32. Liddell, P. A.; Sumida, J. P.; Macpherson, A. N.; Noss, L.; Seely, G. R.; Clark, K. N.; Moore, A. L.; Moore, T. A.; Gust, D. Preparation and Photophysical Studies of Porphyrin-$C_{60}$ Dyads. *Photochemistry and Photobiology*. **1994**, *60*, 537-541.

33. Brown, J. S. Functional Organization of Chlorophyll a and Carotenoids in the Alga, Nannochloropsis salina. *Plant Physiology*. **1987**, *83*, 434-437.

34. Baruah, T.; Pederson, M. R. DFT Calculations on Charge-Transfer States of a Carotenoid-Porphyrin-C60 Molecular Triad. *Journal of Chemical Theory and Computation*. **2009**, *5*, 834-843.

35. Osuka, A.; Yamada, H.; Maruyama, K.; Mataga, N.; Asahi, T.; Yamazaki, I.; Nishimura, Y. Picosecond dynamics of intramolecular singlet excitation energy transfer and photoinduced electron transfer in covalently-linked carotenoid—porphyrin and carotenoid—porphyrin—pyromellitimide molecules. *Chemical Physics Letters*. **1991**, *181*, 419-426.

36. Han, Y.-Y.; Zhou, R.-L.; Yang, Y.-G.; Zhou, W.; Ruan, X.-L. Effects of liquid crystal states on photovoltaic effects of chlorophyll-a. *Chinese Journal of Chemistry*. **1995**, *13*, 118-123.

## Chapter Two

# Molecular Photovoltaic System Based on Fullerenes and Carotenoids Co-Assembled in Lipid/Alkanethiol Hybrid Bilayers

## 2.1 Introduction

Interest in studying photocurrent/photovoltage generation from small number of layers of photoactive electron donors/acceptors, i.e., molecular photovoltaics, have grown significantly in recent years.[1-3] Through precise control of energetics and organization of involved species, these systems offer well-defined models for systematic probing of various physiochemical parameters critical in a photoconversion process, which may be convoluted or inaccessible in conventional organic photovoltaic systems. Using several solid-supported lipid bilayers as general structural scaffolds, we have developed a series of modular molecular photovoltaic systems.[4-6] In the new two-component system described here, we show that the addition of lutein (a natural carotenoid species) in the lipid matrix can significantly modulate fullerene's photocurrent output, whereas the system containing lutein alone is found to be inefficient in generating photocurrent.

Carotenoids present a unique set of light-harvesting pigments that is being employed by Nature in photosynthesis alongside chlorophylls and bilins.[7] In green plants and photosynthetic algae, carotenoids generally fulfill three major biological functions.[7-10] First, in terms of light harvesting, they can absorb light efficiently in the spectral region

where chlorophylls lack significant absorption (i.e., blue-green region); and thus absorbed solar energy can be further directed into the photosynthetic process via energy transfer from carotenoids to neighboring chlorophylls. In addition, carotenoids can photochemically protect the photosynthetic apparatus by quenching excited triplet chlorophylls and singlet oxygen. Finally, carotenoids also serve as building blocks to stabilize the structure of photosynthetic protein complexes. In particular the carotenoid studied here, lutein is the most abundant carotenoid in the higher photosynthetic apparatus and can be found in essentially all light-harvesting complexes (LHCs).[11,12]

Unlike chlorophylls and their synthetic analog porphyrins, which have received extended investigations over the years, efforts of adopting carotenoids as a light-absorbing pigment in organic photovoltaic systems are relatively scarce. This disparity might be due to several reasons. Structurally, many of the linear, heavily conjugated carotenoids lack convenient sites for functionalization, whereas others can only be modified at the distal end(s). Spectroscopically, the very short-lived excited states of carotenoids,[13,14] e.g., <50 ps for first singlet state ($S_1$) and <200 fs for second singlet state ($S_2$) of β-carotene, often make it difficult to capture the absorbed light as electrochemical energy in artificial systems. Among the few reported attempts,[15-17] Moore, Sereno and coworkers[16,17] studied photocurrent generation from two carotene derivatives Langmuir-Blodgett deposited on indium tin oxide electrodes. Interestingly, although the two carotenoids differ only by one functional group, i.e., from a carboxylic to an amino group at one end of the structure, significant differences in their electrochemical and photochemical behaviors were observed. These results demonstrate the dependence of the photoconversion efficiency on structural symmetry and electronic coupling strength of

the participating carotenoids, and also imply the possibility of modifying such factors in photovoltaics using carotene-based materials. Although we are not aware of any previous work that employs carotenoids together with fullerenes for direct photocurrent generation, it has previously been shown that the inclusion of carotenoids in photoactive electron donor/acceptor complexes[18,19] can significantly prolong the charge separation by suppressing the charge recombination processes.

Here, we describe a new molecular photovoltaic system based on fullerene and lutein co-assembled in self-assembled hybrid bilayers of alkanethiols and phospholipids on gold electrodes. At modest loadings of 1-3 mol%, the photoinduced electron transfer between lutein and fullerene can effectively compete with the fast relaxation of excited lutein, resulting in a significant modulation of the photocurrents generated by the co-assembled fullerenes. These results can be understood by evaluating the orientation of lutein in lipid membranes, the energetics and relative position of these photoactive species in the hybrid bilayer matrix.

## 2.2 Experimental Section

### 2.2.1 Reagents

Phospholipid 1-palmitoyl-2-oleoyl-*sn*-glycero-3-phosphocholine (POPC) was obtained from Avanti Polar Lipids. Synthesis of monomalonic fullerene ($C_{63}$) was reported previously.[4] Lutein was obtained from Indofine Chemical Company, Inc. Sodium sulfate and sodium chloride were obtained from Fisher Scientific. Other reagents, including dodecanethiol ($C_{12}SH$), 4-(2-hydroxyethyl)piperazine-1-ethanesulfonic acid (HEPES), methyl viologen dichloride hydrate ($MV^{2+}$), tetrabutylammonium

tetrafluoroborate ($Bu_4NBF_4$, 99%), L(+)-ascorbic acid sodium salt (sodium ascorbate), D-(+)-glucose, glucose oxidase (type X-S, *from Aspergillus niger*), and catalase from bovine liver were purchased from Sigma-Aldrich. All solutions employed in these experiments were prepared using 18.2 MΩ·cm deionized water (Millipore).

### 2.2.2 Assembly of Hybrid Bilayers

Gold-coated substrates were fabricated by sputtering gold onto chromium-coated silicon wafers. The thickness of the gold layer was about 200 nm. Prior to the self-assembly of alkanethiol monolayers, the gold-coated substrates were cleaned in piranha solution (3:1 v/v concentrated $H_2SO_4$/30% $H_2O_2$ solution) for 15 min and thoroughly rinsed with water and ethanol and dried in an argon stream. Thus cleaned gold electrodes were incubated in 1 mM alkanethiol in ethanol solution at room temperature for at least 12 h. After that, the SAM-modified gold substrates were rinsed with copious amount of ethanol and DI water, dried in argon, and then assembled in a home-made Teflon photoelectrochemical cell for further use.

Liposomes of various compositions are prepared by an extrusion-based method which is illustrated in Figure 4.1. Briefly, appropriate quantities of POPC/lutein/$C_{63}$ in chloroform were thoroughly mixed in a flask and then dried to a film by rotary evaporation. This mixture was then sonicated (Bransonic, model: 3510-DTH) in HEPES buffer solution (10 mM HEPES, 100 mM NaCl, pH 7.7) at room temperature for 2h. The resulting solution was then extruded consecutively through polycarbonate membranes (Nuclepore, Whatman) of 400 and 80 nm-diameter pore at room temperature. The total

lipids concentration of the final product was approximately 1.25 mM. The exact concentration of the compositions used in the preparation will be specified later.

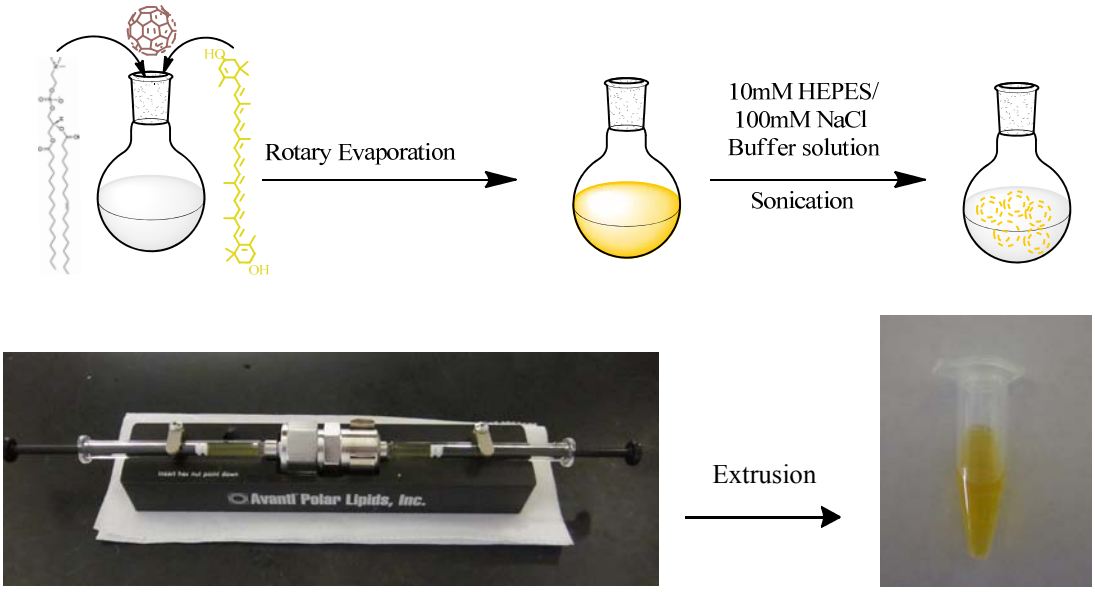


**Figure 2.1.** The preparation of liposome with extrusion-based method

The formation of phospholipid/alkanethiol hybrid bilayers was done by adding a 300-μL liposome solution (total lipid concentration: 1.25 mM) onto an SAM above prepared and incubated for 2 h. Afterwards, the unbound liposome solution was completely removed from the cell by thorough solution exchange with the buffer solution for about 30 times (10 mM HEPES, 100 mM NaCl, pH 7.7).

### 2.2.3 Impedance Spectroscopy

The impedance measurements of the alkanethiol/lipid hybrid bilayers were carried out with a μAutolab Type III/FRA2 electrochemical impedance analyzer system (Metrohm Autolab B.V., Netherlands). Impedance measurements were analyzed by FRA

4.8 software. A conventional three-electrode setup was employed, which contains bilayer-modified gold electrodes as the working electrodes, a Ag/AgCl (KCl saturated) reference electrode and a Pt wire as the counter electrode. The electrochemical cells were biased with a 5 mV a.c. voltage operated in the frequency range from 10 to 10 kHz. The obtained impedance data were fitted to a series-*RC* circuit model using a modeling package included in FRA 4.8. The typical fitting errors were less than ±5%.

### 2.2.4 Electrochemical Measurements

The cyclic voltammetry of lutein was run by a computer-operated potentiostat (CHI 910B, CH Instruments) in dichloromethane with 0.1 M tetrabutylammonium hexfluorophosphate ($Bu_4NBF_4$) as the supporting electrolyte. The three-electrode setup contains a 1-mm gold disk electrode as the working electrode, a Pt wire counter electrode, and a Ag wire as the reference electrode. The voltammetric scan rate was 100 mV/s. Unless otherwise mentioned, all potentials are reported versus a standard Ag/AgCl reference electrode.

### 2.2.5 UV-vis Absorption Spectroscopy

UV-vis spectroscopy was carried out using a UV-visible spectrophotometer (Cary 50 Bio, Varian). To obtain absorption spectra of lutein in hybrid bilayers, a home-machined Teflon cell was fitted to the sample holder of the same spectrometer and so optically aligned. The cell is designed to have an all-through liquid reservoir that can be sandwiched between two planar substrates. One of the substrates is semi-transparent gold

substrates (10 nm Au coated on glass slides, Sigma-Aldrich), on which the hybrid bilayers are formed; while the other is microscope cover slides (VWR).

### 2.2.6 Photoelectrochemical Measurements

The photoelectrochemical measurements were carried out in a three-electrode Teflon photoelectrochemical cell. The three-electrode setup contains the gold substrate with a lipid/SAM bilayer as the working electrode, a Pt counter electrode and an Ag/AgCl (KCl-saturated) reference electrode. The effective area of the gold electrode is ~1.13 $cm^2$. For the photocurrent generation and potential bias measurements, the electrolytes contain either 50 mM ascorbate (anodic) in HEPES buffer or methyl viologen (cathodic) in 0.1 M $Na_2SO_4$. The cell was irradiated with light from a Hg lamp (X-Cite, series 120 PC, EXFO) filtered at 417±30 nm (average intensity: ~40 $mW/cm^2$). In the case of anodic current generation, oxygen in the cell was removed by adding 50 mM glucose, 50 units/mL glucose oxidase, and 200 units/mL catalase in the solution. To obtain the photocurrent action spectra, the bilayer samples were irradiated with monochromated light from a Xe lamp (100 W), and the resulting photocurrents were recorded by a potentiostat (CHI 910B, CH Instruments). The spectral variation of excitation light intensity was corrected with a photometer (Thorlabs).

## 2.3 Results and Discussion

The hybrid-bilayer based photoelectrochemical system was prepared in two steps similar to previous reports.[5,20] As detailed in the Experimental Section, an alkanethiol monolayer is first formed on gold via self assembly, on which a lipid monolayer is then

deposited through lipid fusion by incubating the SAM in a liposome solution. Since the lipid fusion process is primarily driven by hydrophobic/hydrophobic interaction between hydrocarbon chains of alkanethiols and phospholipids, and the dose of fullerene and lutein in the liposome is relatively low (i.e., 1-3 mol % vs. the amount of POPC), a proportional incorporation of these photoactive agents, according to their concentration in liposomes, in the final bilayer structure can be expected.

The capacitance of the hybrid bilayer was measured to be 0.93 μF/cm$^2$ for both C12SH/POPC/2% $C_{63}$ and C12SH/POPC/2% $C_{63}$ + 2% Lutein, and the value of 1.51 μF/cm$^2$ was used for the capacitance of C12SH SAM. [20] So the capacitance of the lipid layer can be calculated by following the equation: $C_{\text{lipid}}^{-1} = C_{\text{BL}}^{-1} - C_{\text{SAM}}^{-1}$. Then the dielectric thickness $d$ of the lipid layer can be calculated with the relation $1/C = d/\varepsilon\varepsilon_0$, where $\varepsilon$ is the dielectric constant of the separating medium which is 2.7 for POPC, and $\varepsilon_0$ is the permittivity of free space ($\varepsilon_0 \approx 8.854\times10^{-12}$ F m$^{-1}$). The calculated capacitance and dielectric thickness are listed in table 2.1, which reveal that the dielectric thicknesses of the lipid layers with or without lutein are very consistent.

| | Capacitance of the hybrid bilayer (μF/cm$^2$) | Capacitance of the lipid layer (μF/cm$^2$) | Dielectric thickness of the lipid layer (Å) |
|---|---|---|---|
| C12SH/POPC/2% $C_{63}$ | 0.93 | 2.45 | 9.7 |
| C12SH/POPC/2% $C_{63}$ + 2% Lutein | 0.93 | 2.43 | 9.8 |

**Table 2.1.** The capacitance and dielectric thickness of the bilayers and lipid layers.

In terms of their position and orientation in the lipid matrix, the amphiphilic malonic fullerenes ($C_{63}$) are expected to occupy positions at the lipid/water interface.[21,22]

As for lutein, two orientations[23,24] are deemed plausible, with the lutein chain either running parallel or threading perpendicularly to the lipid monolayer which is illustrated in Figure 2.2.

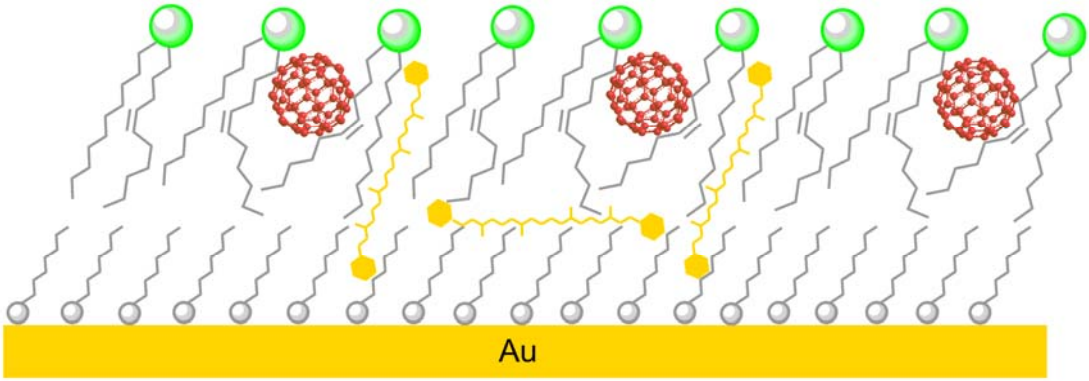


**Figure 2.2.** Schematic presentation of the experimental setup. In this structure, photoactive fullerene and lutein are organized on the gold electrode by an alkanethiol/lipid hybrid bilayer.

Cyclic voltammetry was used to determine the first redox potentials of lutein. As shown in Figure 2.3, the first positive sweep produced a single oxidation wave at 0.56 V vs Ag/AgCl; and this was accompanied by two small irreversible reduction waves in the returning scan, which may be caused by grafting of lutein on the electrode surface upon oxidation. The magnitude of the oxidation wave decreased and broadened into two peaks in the subsequent scans, while the corresponding reduction waves grew only slightly. In a separate measurement, a direct negative potential scan produced no reduction features before the reduction of solvent (not shown), i.e., at about -1.2 V vs. Ag/AgCl, indicating that the reduction of lutein must occur at still more negative potential regions.

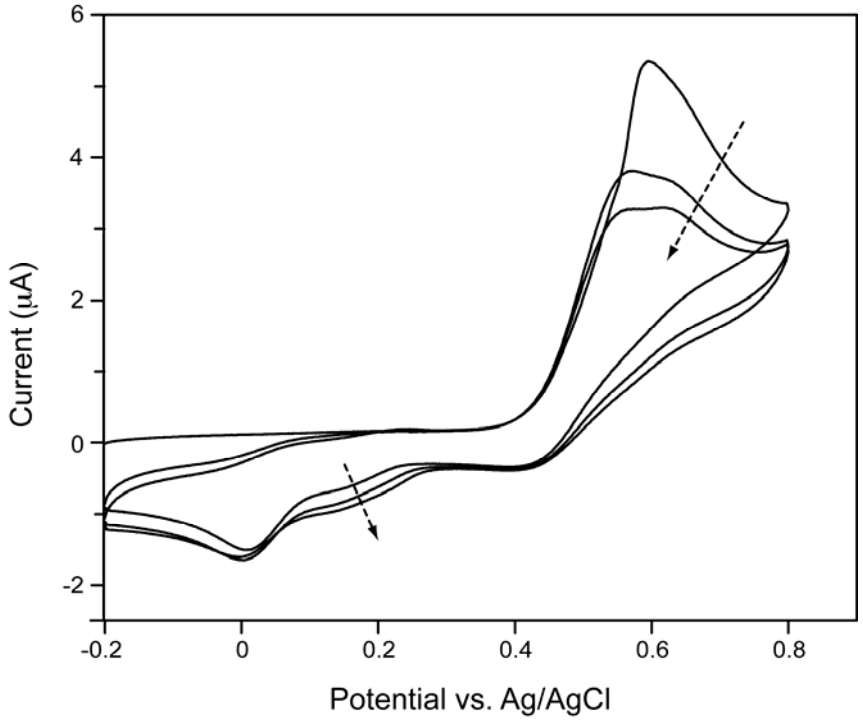


**Figure 2.3.** Cyclic voltammograms of lutein. The solution contains 0.5 mM lutein in dichloromethane with 0.1 M Bu4NBF4. The three-electrode setup contains a Au working electrode, a Pt counter electrode and a Ag/AgCl reference electrode. Scan rate: 100 mV/s. The arrows indicate the direction of growth/decay of the voltammogram in scans 1-3.

The quantitative incorporation of lutein in POPC liposomes was monitored by UV-vis absorption spectroscopy (Figure 2.4). For the UV-vis spectra of $C_{63}$/POPC liposomes, two main peaks at 260 and 328 nm correspond to the strongly allowed electronic transitions of $C_{60}$ fullerenes, with relatively weak absorption observable up to ~430 nm,[4] whereas for liposomes containing 1-3% lutein, the three peaks arising in between 400 and 500 nm (i.e., 429, 452 and 482 nm) are typical for the strongly allowed $S_0$-$S_2$ transition of carotenoids.[9] The inset of Figure 2.4 records the absorption spectrum of a C12-SAM/POPC hybrid bilayer assembled with 2% fullerene $C_{63}$ and 5% lutein, and the three-peak structure closely matches that seen in liposome samples.

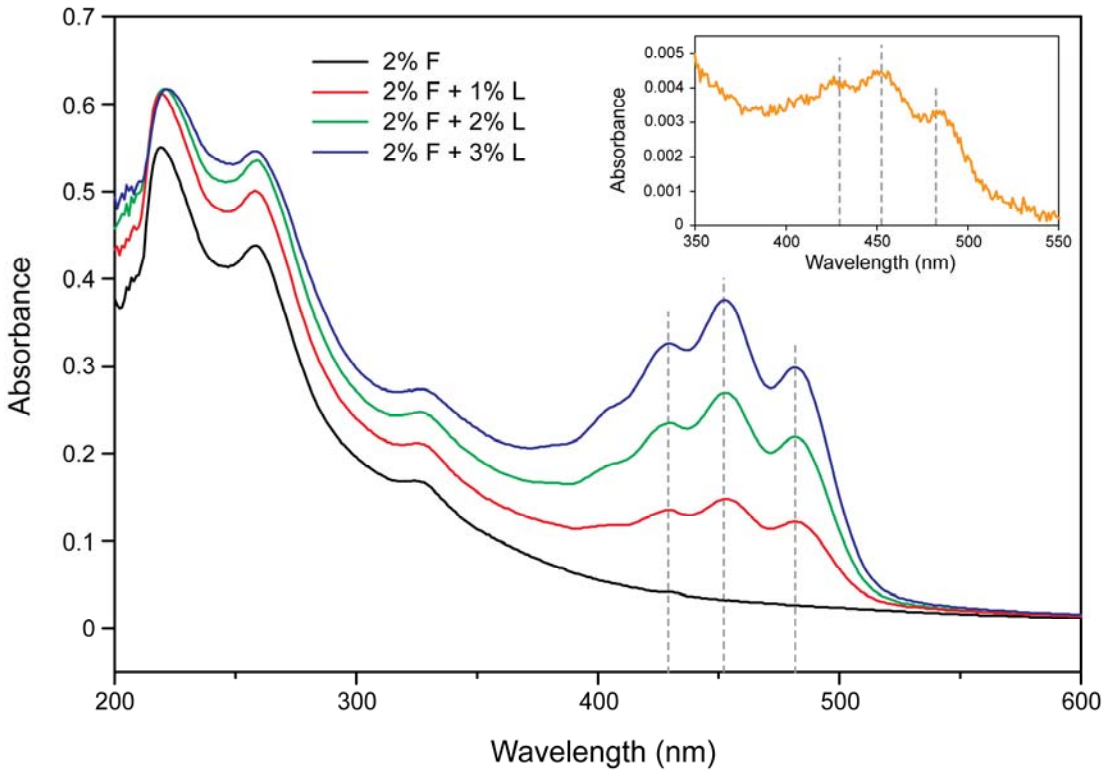


**Figure 2.4.** UV-vis spectra of POPC liposome samples containing 2% (mol) fullerene and 0-3% lutein (from bottom to top). The liposome solutions contain 0.25 mM POPC and are dispersed in 10 mM HEPES buffer saline (0.1 M NaCl, pH 7.7). Inset: absorption spectrum of 2% fullerene $C_{63}$ and 5% lutein assembled in a dodecanethiol/POPC bilayer on a semi-transparent gold substrate. The grey dashed lines correspond to the absorption peaks of the liposome samples. See Section 2.2.2 for details.

To investigate the variation of photocurrents as a function of the photon energy, photocurrent action spectra were obtained from bilayers containing either fullerenes alone or fullerenes together with luteins under both anodic and cathodic conditions (Figure 2.5). In the case of anodic photocurrent generation, the inclusion of more luteins in the bilayers generally caused the current to drop across the probed wavelength range. Between bilayers containing 1 and 2% lutein, such a drop is small but still distinctive. By contrast,

a higher cathodic photocurrent was obtained instead when both fullerenes and luteins were included in the bilayer. For the latter case, photoaction spectra from POPC alone and 2% lutein in POPC were also obtained for comparison.

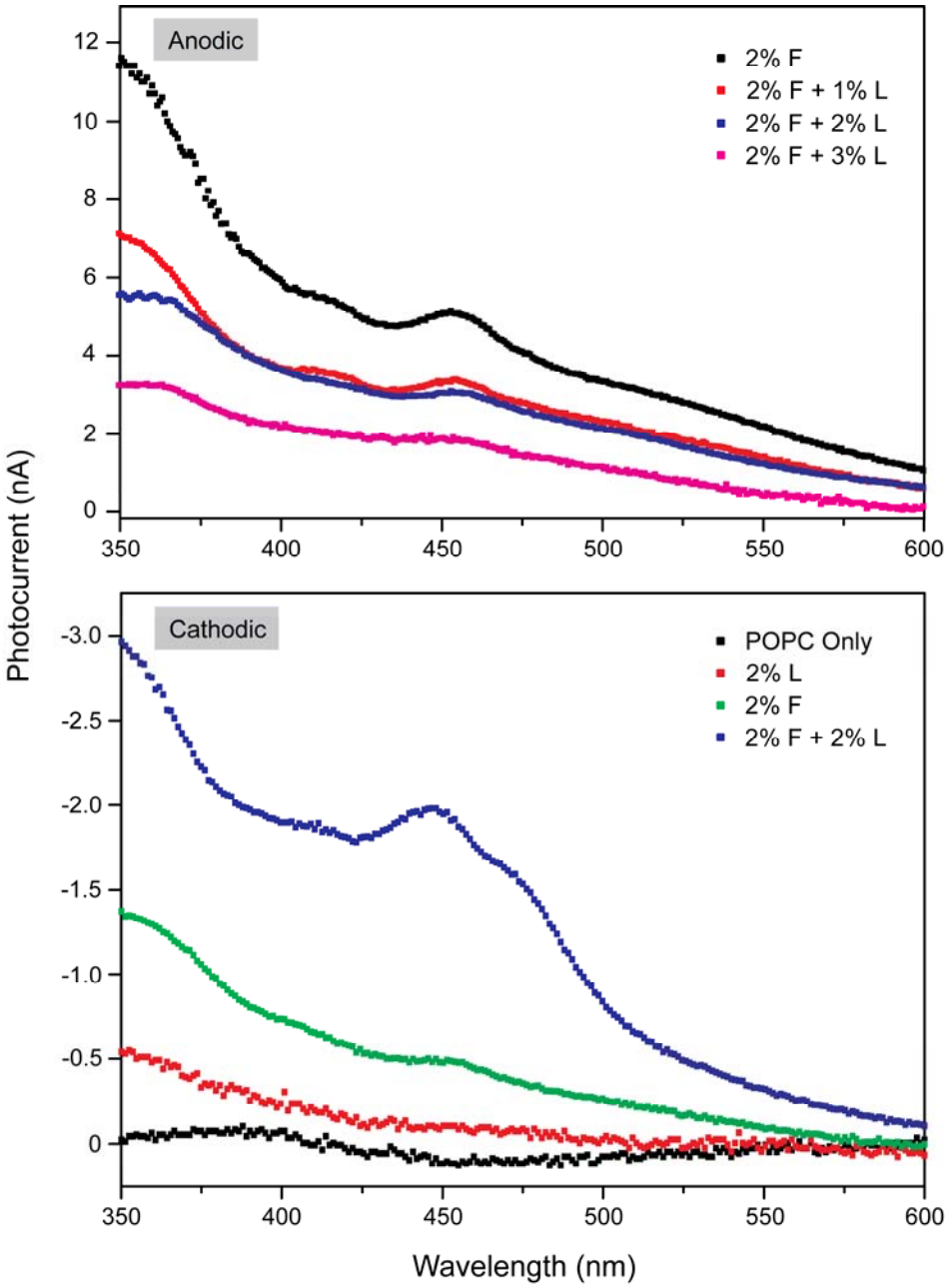


**Figure 2.5.** Photoelectrochemical action spectra of 2 mol% fullerene C63 assembled in C12-SAM/POPC hybrid bilayers with/without various amounts of lutein. The anodic action spectra (top) were generated in 50 mM ascorbate dissolved in HEPES buffer (10

mM HEPES, 100 mM NaCl, pH 7.7). Removal of oxygen in solutions was achieved by adding 50 mM glucose, 50 units/mL glucose oxidase, and 200 units/mL catalase. The cathodic spectra (bottom) were generated in an oxygen-saturated 0.1 M $Na_2SO_4$ aqueous solution containing 50 mM methyl viologen. The typical light intensity was in the range of 0.1-0.4 mW/cm$^2$, which was corrected with a photometer.

The observed photoactivity of lutein in the bilayer-based photoelectrochemical system prompted us to look further into its exact function(s) therein. Initially, we found that bilayers containing luteins alone were comparatively inefficient in generating photocurrents, i.e., approximately 2 and <−1 nA/cm$^2$ in the anodic and cathodic process, respectively (Figure 2.6). This low performance can be understood by considering the fast decay dynamics[10] of lutein's excited states as well as its relatively slow electron transfer rate, which lead to a rather insignificant photovoltaic process. In addition, the gold substrates can also depopulate the excited-state luteins via energy transfer. To actively modify the distribution of energy among all competing energy-dissipation channels and hence remedy the energy loss, one can introduce electron-accepting species into the system. Under favorable conditions (e.g., energetics, distance and orientation, etc.), a more efficient electron transfer between the electron donor and acceptor can be established, which then would direct a larger portion of the absorbed light energy to the pathway of charge separation. Considering the known electron-accepting capability of fullerenes, we further studied the photoconversion behavior of fullerenes in the presence of luteins. As shown in Figure 2.7, adding 1, 2, 3% lutein in the bilayers caused the anodic photocurrents obtained from 2% fullerene $C_{63}$ to decrease by 14, 22 and 43%, respectively; whereas under cathodic conditions, these devices produced a series of

enhanced photocurrents, i.e., 1.9, 2.7 and 4.2 times higher current for 1, 2 and 3% luteins. Thus, under our experimental conditions, i.e., 1-3% photoactive species in hybrid lipid bilayers, a sufficiently efficient electronic communication between excited lutein and fullerene can be obtained.

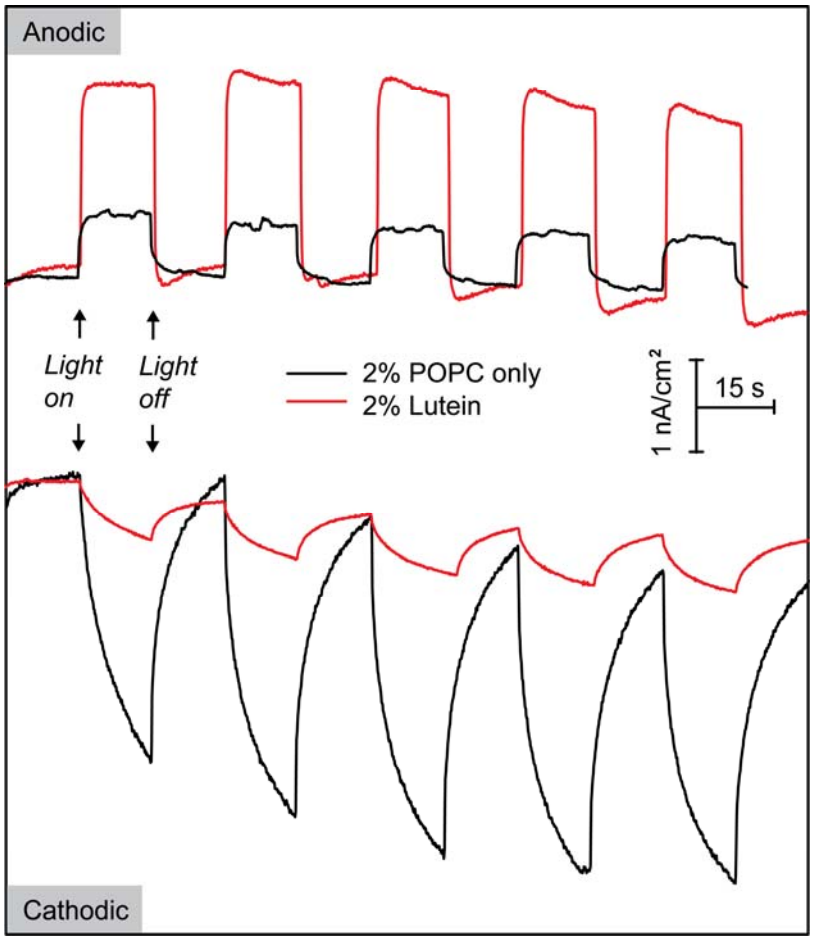


**Figure 2.6.** Background photocurrents. Currents were generated from POPC alone (traces in black) or 2% lutein in POPC (in red) monolayer formed on C12SH SAMs. The anodic photocurrents were generated in 50 mM ascorbate dissolved in HEPES buffer (10 mM HEPES, 100 mM NaCl, pH 7.7). Removal of oxygen in solutions was achieved by adding 50 mM glucose, 50 units/mL glucose oxidase, and 200 units/mL catalase. The

cathodic photocurrents were obtained from 50 mM methyl viologen dissolved in the same buffer. All photocurrents were collected with the three-electrode electrochemical cell as described above. The excitation light was provided by a Hg lamp filtered at 417±30 nm; average intensity: 40 mW/cm$^2$.

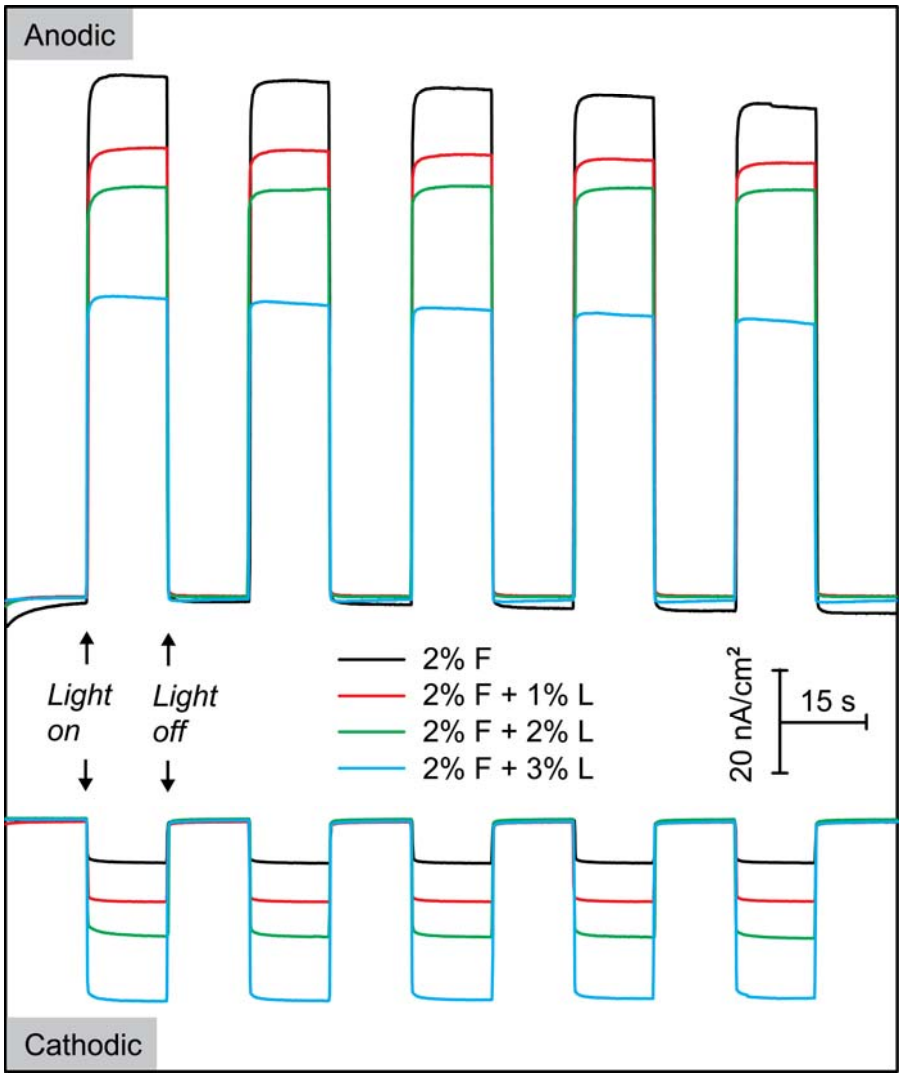


**Figure 2.7.** Photocurrent generation from 2% fullerene $C_{63}$ and 1-3% lutein assembled in C12-SAM/POPC bilayers. Other conditions are idential to those described in Figure 2.6. All the photocurrent results were repeated at least five times, same with all the results in other chapters.

To account for the observed photocurrent modulation effect, we further consider the mechanisms of energy/electron transfer between lutein and fullerene under light irradiation. Previous time-resolved spectroscopic studies of covalently linked carotene-fullerene complexes[18,19] revealed that electron transfer generally occurs in such systems and both carotenoid and fullerene are capable of producing charge separation upon photoexcitation. In the cases where both electron/energy transfer mechanisms are found to be involved, their relative significance depends critically on the solvents in which these conjugates are dispersed. Using transient absorption spectroscopy, for example, Berera and coworkers[18] studied the electron/energy transfer of a conjugated carotene-$C_{60}$ dyad in hexane and toluene. While the lifetime of carotene $S_2$ excited state was not directly determined due to its extremely short timescale, their results established that electron transfer between covalently linked carotene and fullerene could occur even from carotene's $S_2$ state. By assuming the energy transfer characteristic of the conjugate is solvent independent, they were able to further estimate that ~16% of $S_2$ carotene population directly undergoes charge transfer with ground-state fullerenes. Considering that both fullerene and lutein are situated in a relatively heterogeneous matrix, i.e., a single hybrid lipid bilayer interfacing water, and the observed direction-dependent modulation of photocurrents by lutein, we can postulate that electron transfer between lutein and fullerene should be at play in the present system. However, without further evidence from time-resolved spectroscopy, we cannot rule out the possibility of energy transfer between lutein and fullerene in our system or if so, its relative contribution as compared to electron transfer. For these considerations, we focus the following

discussion on the plausible electron transfer pathways that might be involved in the present photocurrent generation system.

The reduction potentials of excited lutein (L*) can be estimated as follows,

$$E^0(*L/L^+) = E^0(L/L^+) - E_{0,0}(L^*)$$

where $E^0(L/L^+)$ is the ground-state oxidation potential (0.56 V vs. Ag/AgCl) and $E_{0,0}(L^*)$ is the zero-zero transition energy of lutein (i.e., 1.74 eV for the $S_0 \rightarrow S_1$ transition, Ref. 10). This gives $E^0(*L/L^+)$ of -1.18 V vs. Ag/AgCl as the photoreduction driving force. Combining these values with redox potentials of fullerene and electron donor/acceptor in the solution, energy diagrams describing anodic and cathodic photocurrent generation processes can be sketched (Figure 2.8). Importantly, as the fullerene and lutein species are directionally organized in the bilayers, the resulting charge separation between the two is likewise vectorially oriented. In the cathodic process, specifically, the separated charges are aligned in parallel with the electron flow direction, giving rise to higher currents compared to devices containing fullerenes only. At both ground and excited states, luteins assist to relay the electrons outwards via a downhill electrochemical cascades, i.e., the electrode→lutein→fullerene→methyl viologen/oxygen, which thermodynamically favor cathodic photocurrent generation and suppress the backward charge recombination.[25,26] By contrast, in the anodic process and in the presence of lutein, the collective orientation of separated charges between fullerenes and luteins runs against the direction of the electron flow, which sets to decrease the overall photocurrents as lutein cation radicals ($L^{\bullet+}$) situated deep in the bilayer can intercept the incoming electrons injected by fullerene anions ($F^{\bullet-}$).

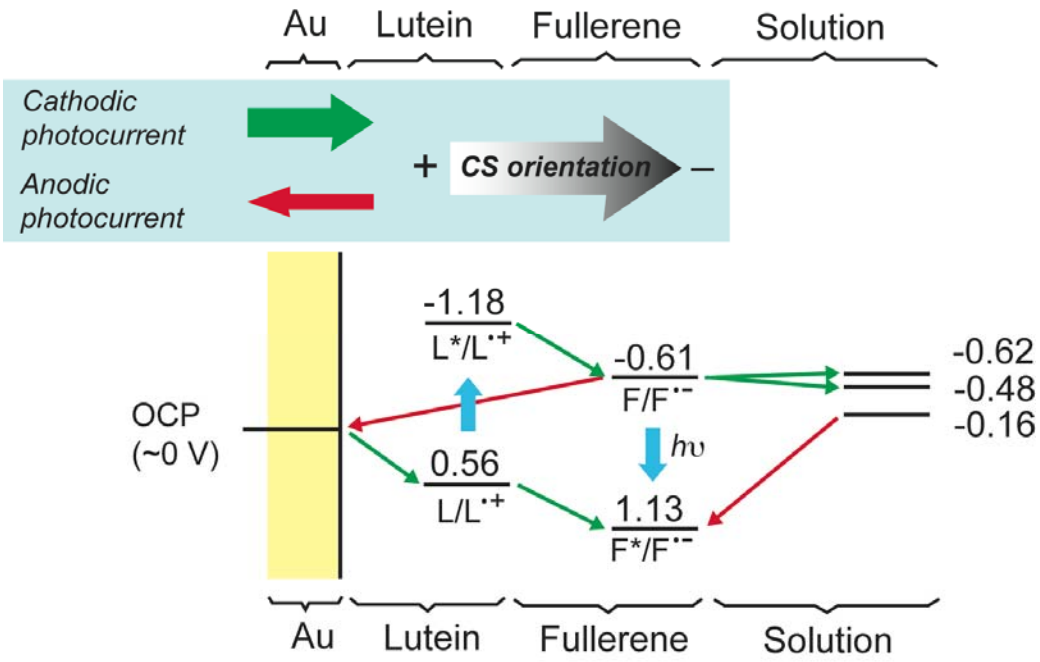


**Figure 2.8.** Energy diagrams for the anodic/cathodic photocurrent generation. Thick blue arrows indicate light absorption, whereas directions of electron flow are indicted by red (anodic) and green (cathodic) arrows. Sacrificial species used in the anodic process is ascorbate ($AscH^-$ - $e^-$ - $H^+$ → $Asc^{\bullet-}$, -0.16 V vs. Ag/AgCl), whereas methyl viologen ($MV^{2+}$ + $e^-$ → $MV^{\bullet+}$, -0.62 V) and oxygen ($O_2$ + $e^-$ → $O_2^{\bullet-}$, -0.48 V) are used in the cathodic process.

While the above discussion only invokes singlet-state fullerenes, it does not in any way exclude the possible involvement of triplet fullerenes in the electron transfer steps or in energy transfer. Since lutein and fullerene species are assembled in the lipid bilayer (as compared to covalently linked conjugates), the intersystem crossing of photoexcited fullerenes may occur in the regions where the distance/orientation of electron transfer between the two are not ideal. While the present study is focused on the photoactivity and photocurrent modulation effect of lutein in hybrid bilayer based photovoltaic models, further studies, particularly with time-resolved spectroscopy tools,

are clearly needed for a better understanding of the electron/energy transfer dynamics and mechanisms of such systems.

## 2.4 Conclusions

We report here a hybrid lipid-based molecular photovoltaic system consisting photoactive fullerene and lutein. While lutein itself is inefficient in producing photocurrent in the lipid bilayer matrix, it can effectively modulate photocurrents produced by the co-assembled fullerene, presumably via electron transfer mechanism. Our results point to the possibility of utilizing natural light-harvesting pigments such as carotenoids in artificial photoconversion system and in addition, the versatility of lipid-based membranes in assembling and organizing hydrophobic as well as amphiphilic species on electrodes.

## References:

1. Hagfeldt, A.; Grätzel, M. Molecular Photovoltaics. *Acc. Chem. Res.* **2000**, *33*, 269-277.

2. Grätzel, M. Molecular Photovoltaics That Mimic Photosynthesis. *Pure Appl. Chem.* **2001**, *73*, 459-467.

3. Imahori, H.; Fukuzumi, S. Porphyrin- and Fullerene-Based Molecular Photovoltaic Devices. *Adv. Funct. Mater.* **2004**, *14*, 525-536.

4. Zhan, W.; Jiang, K. A Modular Photocurrent Generation System Based on Phospholipid-Assembled Fullerenes. *Langmuir* **2008**, *24*, 13258-13261.

5. Jiang, K.; Xie, H.; Zhan, W. Photocurrent Generation from $Ru(bpy)_3^{2+}$ Immobilized on Phospholipid/Alkanethiol Hybrid Bilayers. *Langmuir* **2009**, *25*, 11129-11136.

6. Zhan, W.; Jiang, K.; Smith, M. D.; Bostic, H. E.; Best, M. D.; Auad, M. L.; Ruppel, J. V.; Kim, C.; Zhang, X. P. Photocurrent Generation from Porphyrin/Fullerene Complexes Assembled in a Tethered Lipid Bilayer. *Langmuir* **2010**, *26*, 15671-15679.

7. Blankenship, R. E. Molecular Mechanisms of Photosynthesis. Blackwell Science Ltd, Oxford, UK. 2002.

8. Ritz, T.; Damjanović, A.; Schulten, K.; Zhang, J.-P.; Koyama, Y. Efficient Light Harvesting Through Carotenoids. *Photosynth. Res.* **2000**, *66*, 125-144.

9. Fraser, N.; Hashimoto, H.; Cogdell, R. Carotenoids and Bacterial Photosynthesis: The Story So Far. *Photosynth. Res.* **2001**, *70*, 249-256.

10. Polívka, T.; Sundström, V. Ultrafast Dynamics of Carotenoid Excited States−From Solution to Natural and Artificial Systems. *Chem. Rev.* **2004**, *104*, 2021-2072.

11. Formaggio, E.; Cinque, G.; Bassi, R. Functional Architecture of the Major Light-Harvesting Complex from Higher Plants. *J. Mol. Biol.* **2001**, *314*, 1157-1166.

12. Dall'Osto, L.; Lico, C.; Alric, J.; Giuliano, G.; Havaux, M.; Bassi, R. Lutein is Needed for Efficient Chlorophyll Triplet Quenching in the Major LHCII Antenna Complex of Higher Plants and Effective Photoprotection in Vivo Under Strong Light. *BMC Plant Biology* **2006**, *6*, 32.

13. Wasielewski, M. R.; Kispert, L. D. Direct Measurement of the Lowest Excited Singlet State Lifetime of all-trans-β-Carotene and Related Carotenoids. *Chem. Phys. Lett.* **1986**, *128*, 238-243.

14. Kandori, H.; Sasabe, H.; Mimuro, M. Direct Determination of a Lifetime of the S2 State of β-Carotene by Femtosecond Time-Resolved Fluorescence Spectroscopy. *J. Am. Chem. Soc.* **1994**, *116*, 2671-2672.

15. Miyasaka, T.; Honda, K. Photoelectrochemical Observations on Chlorophyll-Carotene Interactions in a Lipid Bilayer Film. *Thin Solid Films,* **1983,** *102,* 173-185.

16. Sereno, L.; Silber, J. J.; Otero, L.; del Valle Bohorquez, M.; Moore, A. L.; Moore, T. A.; Gust, D. Photoelectrochemistry of Langmuir−Blodgett Films of Carotenoid Pigments on ITO Electrodes. *J. Phys. Chem.* **1996**, *100*, 814-821.

17. Fungo, F.; Otero, L.; Durantini, E. N.; Silber, J. J.; Sereno, L.; Mariño-Ochoa, E.; Moore, T. A.; Moore, A. L.; Gust, D. Photoelectrochemistry of a Pigment Used in Artificial Photosynthesis: An Anilinocarotenoid. *J. Phys. Chem. B* **2001**, *105*, 4783-4790.

18. Imahori, H.; Cardoso, S.; Tatman, D.; Lin, S.; Noss, L.; Seely, G. R.; Sereno, L.; de Silber, J. C.; Moore, T. A.; Moore, L. A.; Gust, D. Photoinduced Electron Transfer in a Carotenobuckminsterfullerene Dyad. *Photochem. Photobiol.* **1995**, *62*, 1009-1014.

19. Berera, R.; Moore, G. F.; van Stokkum, I. H. M.; Kodis, G.; Liddell, P. A.; Gervaldo, M.; van Grondelle, R.; Kennis, J. T. M.; Gust, D.; Moore, T. A.; Moore, A. L. Charge Separation and Energy Transfer in a Caroteno-$C_{60}$ Dyad: Photoinduced Electron Transfer from the Carotenoid Excited States. *Photochem. Photobiol. Sci.* **2006**, *5*, 1142-1149.

20. Xie, H.; Jiang, K.; Zhan, W. Modular Molecular Photovoltaic System Based on Phospholipid/Alkanethiol Hybrid Bilayers: Photocurrent Generation and Modulation. *Phys. Chem. Chem. Phys.* **2011**, *13*, 17712-17721.

21. Bortolus, M.; Parisio, G.; Maniero, A. L.; Ferrarini, A. Monomeric Fullerenes in Lipid Membranes: Effects of Molecular Shape and Polarity. *Langmuir* **2011**, *27*, 12560-12568.

22. Li, L.; Davande, H.; Bedrov, D.; Smith, G. D. A Molecular Dynamics Simulation Study of C60 Fullerenes Inside a Dimyristoylphosphatidylcholine Lipid Bilayer. *J. Phys. Chem. B* **2007**, *111*, 4067-4072.

23. Gruszecki, W. I.; Strzałka, K. Carotenoids as Modulators of Lipid Membrane Physical Properties. *Biochim. Biophys. Acta* **2005**, *1740*, 108-115.

24. Landrum, J. T. (Ed.) Carotenoids: Physical, Chemical, and Biological Functions and Properties. CRC Press, Boca Raton, FL, 2010.

25. Warshel, A.; Schlosser, D. W. Electrostatic Control of the Efficiency of Light-Induced Electron Transfer across Membranes. *Proc. Natl. Acad. Sci. USA* **1981,** *78*, 5564-5568.

26. Mauzerall, D. C. Photoinduced Electron Transfer. Fox, M. A. and Chanon, M. (Eds.) Part A, Elsevier Science Publishers B. V., Amsterdam, The Netherlands, 1988, pp 207-244.

# Chapter Three

## Molecular Photovoltaic Systems Based on Phospholipid/Alkanethiol Hybrid Bilayers: The Role of Oriented Surface Dipole

### 3.1 Introduction

Unlike single-crystal semiconductor solar cells, light excitation in the low-dielectric organic solar devices initially generates excitons and polarons, whose separation into free charge carriers critically depends on the interfacial and morphological characteristics of the organic matrices.[1,2] Understanding each of these properties can be difficult to achieve at the device level as they often appear convoluted and interdependent. To this end, recent research based on theoretical modeling[3,4] has proved to be very fruitful. Experimentally, molecular model architectures, based on single donor/acceptor layers,[5-7] are ideally suited to study various interfacial processes in organic photovoltaics (OPV). Along this line, we have successfully introduced several solid-supported lipid bilayer structures into the study of photoinduced electron transfer processes at water/lipid/electrode interfaces.[8-11] These systems allow a rich series of parameters critical to fundamental photovoltaic processes to be accessed, often in well defined single-component settings. Control of dosing, position and directionality of multiple electron donor/acceptor (synthetic or natural) in a single bilayer can be thus

achieved. Using porphyrin and fullerene as model photoagents, we report here that polar alkanethiols included in these bilayers can significantly modulate the resulting photovoltaic responses. These results not only allow us to make connections with the practice in organic electronic devices of using polar organic adsorbates to tune the work function of metals and hence the charge injection efficiency, but also highlight the subtle interplay of orientated surface dipole with other factors related to the photoagents, such as their location and orientation, in an alkane/lipid bilayer matrix.

Of particular relevance is the research in organic light-emitting diodes and other related fields that employ polar organic adsorbates to tune the work function of electrode materials and hence the charge injection barriers. The fundamental concept[12] here is the use of an organic layer to modify the potential difference of electrons inside and outside a metal, $\zeta$, which is related to the metal work function ($\phi_{\mathrm{m}}$) by equation $\phi_{\mathrm{m}} = \zeta - E_F$, where $E_F$ is the Fermi level of the metal. The importance of $\zeta$ in affecting the work function of metals was recognized as early as in the 1930s, when a monolayer of alkali atoms was found to reduce $\phi_{\mathrm{m}}$ of metals by more than half in study of photoelectric effects.[13,14] These experimental observations made Bardeen realize that work function is essentially a surface property of a metal that is determined largely by its uppermost atomic layers.[15] More recently, Campbell and coworkers[16] demonstrated that thiols self-assembled on noble metals could be fruitfully used to tune the work function of these metals. Generally, when a monolayer of polar alkanethiols is absorbed on a metal, it sets up a dipole layer (sometimes called an electrostatic double layer) at the metal/organic interface, which imposes a localized potential that can electrostatically impede or ease the extraction of electrons from the metal. Systematic tuning of the metal work function can be realized by

controlling the structure, size and substituent groups of organic absorbates.[17] The reason that such an interfacial dipole layer can affect the charge injection from/to organic materials layered further atop, which sometimes are macroscopic, is simply because it is positioned within the charge injection path. Owing to the ease of preparation and well-defined structures of self-assembled thiols on noble metals, this method has since then evolved into a versatile and powerful strategy that is widely employed in several fields such as organic light-emitting diodes and organic field-effect transistors.[18,19]

More recent work has also shown such a strategy can be successfully employed to control and improve OPV systems. Using a C16 SAM, for example, Mihailetchi et al.[20] were able to lower Ag work function by 0.6 eV, which allowed the researchers to build electron-dominant devices in studying poly(phenylene vinylene)/fullerene based bulk-heterojunction solar cells. In another study, Kim and coworkers[21] showed that enhancement of power conversion efficiency could be achieved in OPV cells fabricated with SAM-covered gold substrates. The effectiveness of using polar SAMs to modify injection barriers for electrogenerated as well as photogenerated charges underscores the general importance of energy alignment in achieving efficient interfacial charge injection.

In this study, we set to determine quantitatively how SAMs with well-defined dipoles influence the photovoltaic responses of lipid/alkanethiol hybrid bilayer-based model cells. These arguably are one of the simplest models to look at this interesting interfacial phenomenon, with a single dipole layer sandwiched in between an electrode and a photoagent-assembled lipid monolayer. Our results confirm the general trend established by previous studies and in addition, demonstrate the usefulness and controllability of alkane/lipid hybrid structures in probing photovoltaic processes.

## 3.2 Experimental Section

### 3.2.1 Reagents

Phospholipids such as 1-palmitoyl-2-oleoyl-*sn*-glycero-3-phosphocholine (POPC) and 1,2-dioleoyl-*sn*-glycero-3-phosphoethanolamine (DOPE) were received from Avanti Polar Lipids with purity better than 99%. Monomalonic fullerene ($C_{63}$) were prepared according to previously reported procedures.[8] The synthesis of Zinc Complex 5-(4-Carboxyphenyl)-10,15,20-tris-(3,5,di-methoxyphenyl) porphyrin phosphatidylethanolamine was previously reported.[22] Dodecanethiol, 1H,1H,2H,2H-perfluorodecanethiol ($CF_3(CF_2)_7(CH_2)_2SH$), 4-(2-hydroxyethyl) piperazine-1-ethanesulfonic acid (HEPES), methyl viologen dichloride hydrate ($MV^{2+}$), L(+)-ascorbic acid sodium salt, D-(+)-glucose, glucose oxidase (type X-S from *Aspergillus niger*) and catalase from bovine liver were obtained from Sigma-Aldrich. All chemicals received are of the highest grade available. All solutions were prepared using 18.2 MΩ•cm deionized water (Millipore).

### 3.2.2 Preparation of SAMs and HBMs

The formation of SAMs on gold substrates was accomplished by immersing gold-coated substrates in 1 mM ethanol solution of alkanethiols at room temperature for at least 15 h. Prior to this step, the gold-coated substrates were thoroughly cleaned in piranha solution (3:1, concentrated $H_2SO_4$ to 30% $H_2O_2$ solution, v/v) for 15 min, and rinsed by water and ethanol and dried by an argon stream. The SAM-modified gold substrates were carefully rinsed with ethanol and DI water, dried in argon, and immediately assembled in homemade Teflon cells to be used either for impedance analysis or photoelectrochemical measurements. Preparation of liposome samples

containing fullerenes[8] or porphyrin-conjugated lipids[10] was reported previously. Briefly, POPC and 2 mol% of either photoagent were mixed in chloroform and thoroughly dried. The resulting lipid films were re-suspended in 10 mM HEPES buffer saline (0.1 M NaCl, pH 7.7) to give final solutions of 2.5 mM POPC. Liposome solutions of these precursors were prepared by extruding the corresponding suspensions consecutively through porous polycarbonate membranes with average pore diameters of 400 and 80 nm. To form lipid/alkanethiol hybrid bilayers, typically 0.3 mL aliquots of such liposome solutions were added to the cell and incubated for 2 h. The unbound vesicle solutions in the cells were replaced by the same HEPES buffer solution before moving on to further measurements.

### 3.2.3 UV-vis Spectroscopy

UV-vis spectra were acquired with a UV-visible spectrophotometer (Cary 50 Bio, Varian). To obtain absorption spectra of chlorophyll *a* assembled in hybrid bilayers, a home-made Teflon cell was fitted to the sample holder of the spectrometer and so optically aligned. The cell is configured to have an all-through liquid reservoir that can be sandwiched between two planar substrates, one of which is a semi-transparent gold substrates (10 nm Au coated on glass slides, Sigma-Aldrich) and the other microscope cover slides (VWR).

### 3.2.4 Impedance Spectroscopy

Impedance spectroscopy measurements of the alkanethiol SAMs and corresponding alkanethiol/lipid hybrid bilayers were conducted on a Gamry

electrochemical impedance analyzer system (Reference 600). Homemade Teflon cells used herein contain a film-modified Au working electrode (effective area: ~1.13 $cm^2$), a Ag/AgCl reference electrode and a Pt counter electrode immersed in 10 mM KCl aqueous solution. During the impedance measurements, the electrochemical cells were biased with a 10 mV a.c. voltage operated in the frequency range from 10 to 10 kHz. The obtained impedance data were fitted to a series-*RC* circuit model using a modeling package included in Gamry Echem Analyst.

### 3.2.5 Electrochemical and Photoelectrochemical Measurements

Electrochemical and photoelectrochemical measurements were carried out with a potentiostat (CHI 910B, CH Instruments) in the above Teflon cells housing three electrodes. Photocurrents were measured amperometrically with potentials set equal to the open circuit potential of each cells determined separately under dark conditions; whereas photovoltages were acquired in the open-circuit potential mode. In both measurements, the cells were irradiated with light from a Hg lamp (X-Cite, series 120 PC, EXFO) filtered at 417±30 nm (average intensity: 40.0 $mW/cm^2$). A 50 mM ascorbate in HEPES buffer (10 mM HEPES, 100 mM NaCl or $Na_2SO_4$, pH 7.7) was used as sacrificial electron donor in the anodic generation; oxygen was removed from the cells by adding 50 mM glucose, 50 units/mL glucose oxidase, and 200 units/mL catalase in the solutions. Under cathodic conditions, the un-deaerated electrolyte solutions contained 50 mM methyl viologen and 100 mM $Na_2SO_4$ in HEPES buffer.

## 3.3 Results and Discussion

### 3.3.1 Construction/Characterization of Hybrid-Bilayer Based Photocells

Figure 3.1 shows schematically the structure of lipid/thiol hybrid bilayers and photoactive agents used in this study. To form such bilayers, a SAM of either dodecanethiol (C12SH) or heptadecafluoro-1-decanethiol (C10F17SH) is first formed on clean gold substrates, which is then covered with a monolayer of phospholipids upon exposure to a liposome solution containing either malonic fullerene or DOPE-conjugated zinc porphyrin (ZnP-DOPE). Electrochemical impedance analysis of these films reveals hybrid structures that conform with a bilayer model[9,,23] (Table 3.1 and Figure 3.2), confirming that monolayer quantities of lipids can be deposited on a fluorinated alkanethiol SAM similar to those based on *n*-alkanethiols as previously reported.[24] Additional measurements based on UV-vis of such hybrid bilayers further indicate that the top POPC monolayers formed on the two SAMs exhibit comparable lipid loading and packing density ( Figure 3.3).

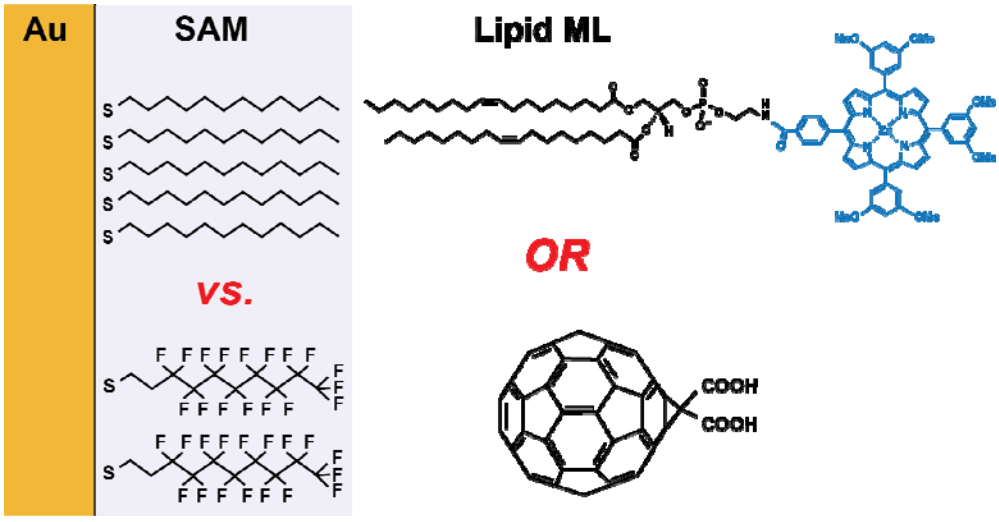


**Figure 3.1.** Schematic presentation of photovoltaic models based on lipid/alkanethiol hybrid bilayers. The bilayers comprise a SAM of either dodecanethiol (shorthanded as

C12SH) or heptadecafluoro-1-decanethiol (C10F17SH) and an upper POPC lipid monolayer assembled with either zinc porphyrin (ZnP) or malonic fullerene ($C_{63}$). Chemic al structures are not drawn to scale with each other.

| | Capacitance of SAM layer ($C_{SAM}$: μF/cm$^2$) | Dielectric thickness of SAM layer (Å) | Capacitance of the bilayer ($C_{BL}$: μF/cm$^2$) | Capacitance of the lipid layer ($C_{lipid}$: μF/cm$^2$) | Dielectric thickness of lipid layer (Å) |
|---|---|---|---|---|---|
| C12SH | 1.51± 0.004 | 13.5 | 0.90 ± 0.01 | 2.25 | 10.6 |
| C10F17SH | 1.53 ± 0.01 | 12.2 | 0.92 ± 0.05 | 2.30 | 10.4 |

**Table 3.1.** Capacitance and calculated dielectric thickness values of SAMs and lipid layers. These thicknesses are obtained by fitting the impedance data shown in Figure 3.2 into a series-*RC* equivalent circuit. These fits directly give capacitance values of SAMs and hybrid bilayers, whereas that of the lipid monolayer is calculated using equation: $C_{lipid}^{-1} = C_{BL}^{-1} - C_{SAM}^{-1}$. The thicknesses of the each layers were then calculated with the following relationship: $1/C = d/\varepsilon\varepsilon_0$, where $d$ is the thickness of the dielectric medium that separates the two conducting plates (i.e., the gold electrode and the electrolyte solution), $\varepsilon$ is the dielectric constant of the separating medium (i.e., 2.3 for C12SH, 2.1 for C10F17SH and 2.7 for POPC), and $\varepsilon_0$ is the permittivity of free space ($\varepsilon_0 \approx 8.854\times10^{-12}$ F m$^{-1}$). Standard deviations are obtained from three measurements.

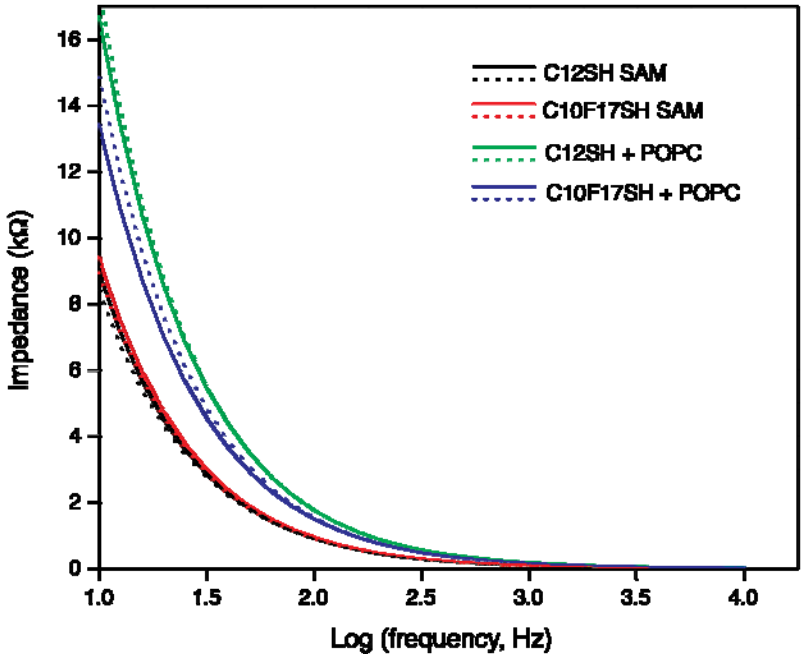


**Figure 3.2.** Impedance profile of SAMs and hybrid bilayers as a function of the applied *ac* frequency. The supporting electrolytes contain 10 mM KCl in DI water. Curves in dotted line are fitting results based on a series *RC* circuit model. See the Experimental Section for more details.

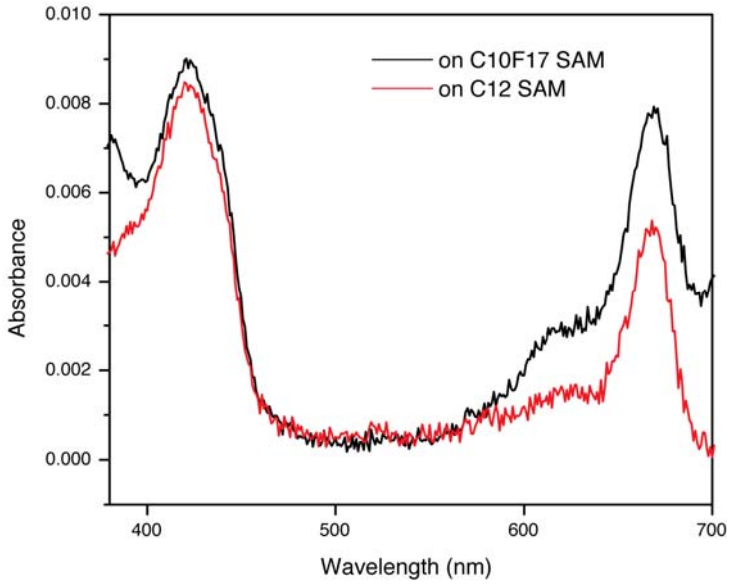

**Figure 3.3.** UV-vis spectra of 5 mol% chlorophyll *a* in the POPC layer formed on either C12SH SAM (in red) or C10F17SH SAM (in black). To form such bilayers, POPC liposomes (~1.25mM in HEPES buffer saline) incorporated with 5% chlorophyll *a* were incubated with the SAMs for 2h. Assuming the transfer of POPC and chlorophyll *a* onto the SAMs is quantitative, these data indicate the quantity of lipid deposition on the two SAMs is comparable.

### 3.3.2 Photovoltaic Behaviors of Hybrid-Bilayer Based Photocells

Figure 3.4a compares the anodic/cathodic photocurrents obtained from hybrid bilayers containing 2 mol% ZnP-DOPE in the top POPC layer. As discussed in our previous work,[10] these photocurrents result from photoinduced electron transfer processes between excited porphyrin and sacrificial redox agents in solution. Here in the anodic process, a photocurrent of ~130 nA/cm$^2$ was generated from bilayers having C12 SAM as the underlayer, whereas a lower current of ~50 nA/cm$^2$ was obtained when the underlying SAM is of C10F17SH instead. The difference in the anodic currents is not due to different loadings of ZnP-DOPE on the two SAMs during the hybrid bilayer formation, as an opposite trend was seen from the cathodic photocurrents obtained from the same devices (dashed traces, Figure 3.4a). These responses indicate the photocurrent generation process is instantaneous and relatively stable in these devices.

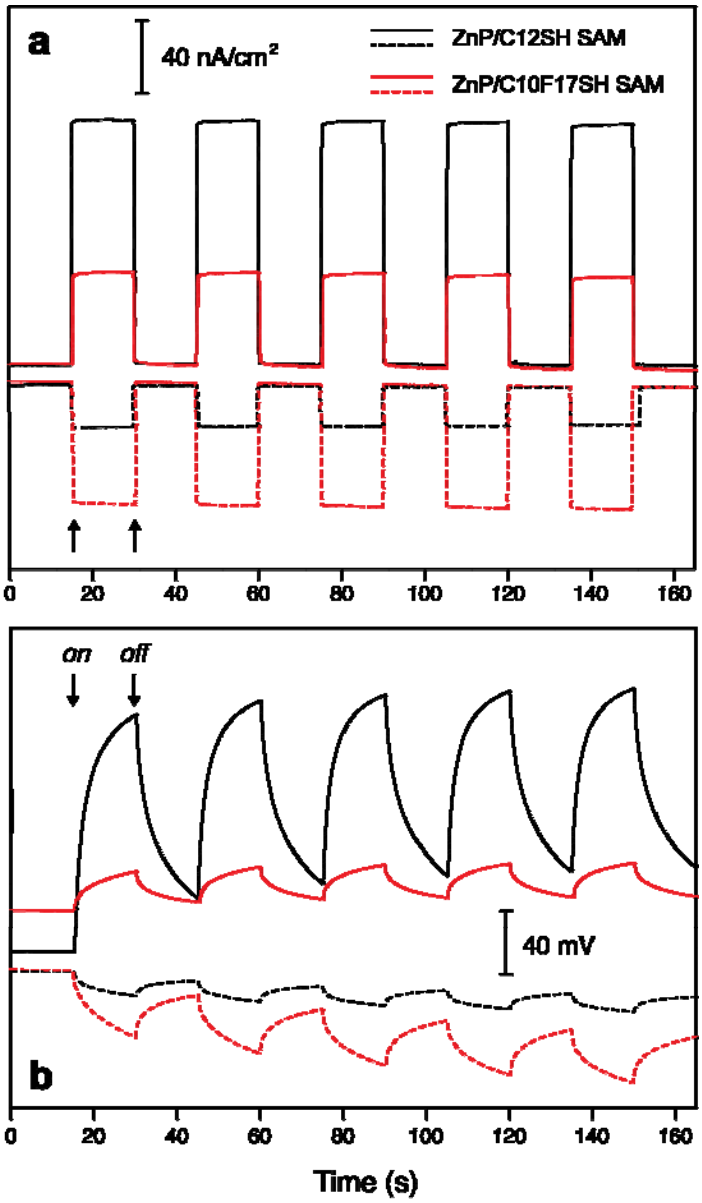


**Figure 3.4.** Photocurrent (a) and photovoltage (b) signals generated from 2% ZnP-DOPE in POPC lipid monolayers on either C12SH SAM (traces in black) or C10F17SH SAM (in red). The anodic photocurrents (solid-lined traces) were generated in 50 mM ascorbate (sacrificial electron donor) dissolved in HEPES buffer (10 mM HEPES, 100 mM $Na_2SO_4$, pH 7.7), in which oxygen was depleted by adding 50 mM glucose, 50 units/mL glucose oxidase, and 200 units/mL catalase, whereas the cathodic photocurrents (dashed traces) were obtained from 50 mM methyl viologen (primary electron acceptor)

dissolved in the same buffer. All photocurrents were collected with the three-electrode electrochemical cell as described in the Experimental Section; the excitation light was provided by a Hg lamp filtered at 417±30 nm with an average intensity of 40 mW/cm$^2$. Arrows indicate the times the light is turned on/off.

The photovoltages recorded from devices subject to similar dark/light cycles display a similar trend, i.e., higher voltage amplitudes accompanying higher currents and vice versa (Figure 3.4b). Unlike the photocurrents, the photovoltages increase only gradually upon photoexcitation and cannot reach steady states in a given light on/off cycle (15 s). This sluggish behavior reflects the dynamic response of the charging/discharging processes of this bilayer-based photoelectrochemical system under photoexcitation. In particular, the relatively steep rise of photovoltage as the light is just turned on reflects the fast initial accumulation of charges around the bilayer as a result of photoinduced electron transfer; as such a process continuously charges up the bilayer, the latter approaches its capacity, causing further charging to slow down.

When bilayers containing 2 mol% $C_{63}$ in the top POPC layer are subjected to similar photocurrent/photovoltage generation, a similar, although less marked, trend is observed (Figure 3.5). Here, a lower anodic current (i.e., 60 vs. 85 nA/cm$^2$) and a higher cathodic current (i.e., 18 vs. 10 nA/cm$^2$) is obtained when C10F17SH SAMs replace C12 SAMs as the underlying layer in the bilayers. Photovoltages again follow photocurrents. In all cases, bilayers cells with no photoagents included only produced negligible currents (not shown).

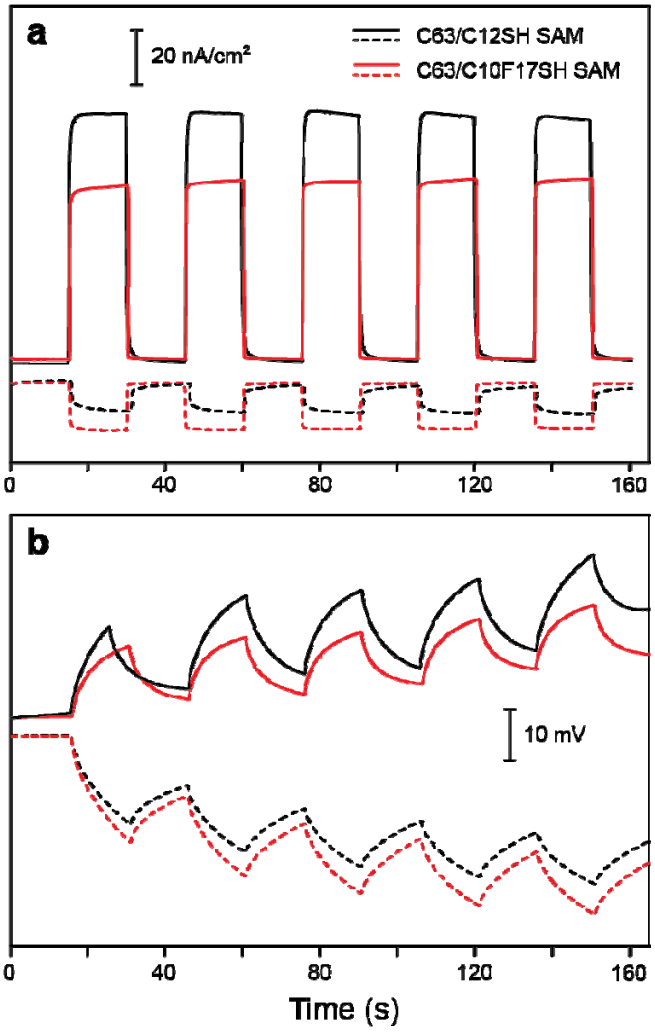


**Figure 3.5.** Photocurrent (a) and photovoltage (b) responses obtained from 2% fullerene $C_{63}$ assembled in POPC lipid monolayers on either C12SH SAM (traces in black) or C10F17SH SAM (in red). Here, the anodic photocurrents are marked by solid traces and the cathodic photocurrents by the dashed traces. All other conditions are identical to those in Figure 3.4.

### 3.3.3 Mechanisms of Photocurrent/Photovoltage Modulation: Considerations Regarding the Organization of Photoagents in the Lipid Monolayer

To account for the modulated photovoltaic behaviors of lipid-assembled photoagents by the underlying SAMs, we next consider the organization, position and orientation of these two agents in the bilayers. In terms of organization, the ZnP complex is directly linked to DOPE via the amine headgroup, whereas fullerenes are incorporated into lipids noncovalently. As such, the porphyrin moieties are expected to take position at the top of the lipid monolayer surface upon lipid fusion on the SAMs. On the other hand, the malonic group on fullerene $C_{63}$ renders amphiphicity to the sphere-shaped molecule, which should position itself relatively snugly within the surrounding amphiphilic lipids, so that the exposure of its hydrophobic bulk (/polar malonic group) to water (/lipid acyl chains) can be simultaneously minimized. Thus, fullerene $C_{63}$ is located closer to the SAM and the gold surface compared to ZnP in a hybrid bilayer.

So just how deeply is the malonic fullerene embedded in the POPC monolayer and how close is it to the underlying SAM? To answer these questions, we next evaluate its size and position in relation to the thickness of the POPC monolayer. First of all, the spherical fullerene tends to avoid space immediately below the carbonyls of the lipids, that is, the space occupied by the uppermost methylene groups in the acyl chains, because its bulky size would otherwise increase the interspace between lipids and thus break the balance of various forces[25] that stabilize the lipid/water interface. To minimize such an energy penalty, the fullerene preferentially takes positions about midway of the lipid hydrocarbon region.[26] This picture also holds true for singly modified fullerenes. For example, Bortolus et al.[27] have found that several singly regio-derivatized fullerenes tend to occupy spaces below the lipid/water interface in the lipid matrix similar to pristine $C_{60}$. On the other hand, the hydrophobic thickness of POPC bilayers has been determined to

be 25.8 Å by NMR[28] and 27.1 Å by X-ray scattering.[29] Assuming the thickness of POPC monolayer remains the same in a hybrid bilayer configuration, it follows that the bottom edge of the POPC-assembled fullerene (diameter of ~10 Å) should be fairly close to the hydrocarbon end of the lipid monolayer (i.e., within 3-4 Å). The highly disordered nature of liquid-crystalline POPC matrix as well as the likely site distribution of thus assembled occupants may further shorten this gap.

### 3.3.4 Mechanisms of Photocurrent/Photovoltage Modulation: Dipole Potentials Contributed by the Lipid Monolayer and SAMs

The observed modulation effects clearly arise from the different physiochemical characteristics built into the two hybrid-bilayer based matrices. In this section, we evaluate how and to what extent each layer can modify the effective energy levels of the two photoagents. For the upper layer, it is understood that several membrane-associated electrostatic potentials will develop as lipids assemble to form monolayers and bilayers at water/organic or water/water interfaces. Of particular importance here is the so-called membrane dipole potential.[30-32] which is formed between the lipid polar headgroups and the low-dielectric hydrocarbon chains by aligned dipoles of the lipid headgroup moieties, including choline, phosphate and carbonyl, as well as the hydration water molecules surrounding these groups. Because the choline(+)-phosphate(-) dipoles are found to be oriented almost parallel to the monolayer/bilayer surface[33] and the headgroup charges are overcompensated by the water molecules,[34] this dipole potential is largely attributed to the oriented water molecules that organized at/near the lipid/water interface. As determined by voltage-sensitive dye fluorescence measurements,[31,35] this typically results

in a potential of ~200 mVs across a zwitterionic POPC monolayer, with the water side negative. Considering the assembled position of the two photoagents in the lipid monolayer, one finds that the DOPE-conjugated ZnP moieties occupy little space in the hydrocarbon region of the lipid matrix, in which the most significant dipole potential drop develops. By contrast, the lipid-assembled fullerenes reside right in this dipole-active zone owing to their penetration into the hydrocarbon region of the lipid matrix. Since the electric field associated with a dipole layer is extremely localized (normally dropping to zero a few Å away from the initiating layer[36]), the different positions occupied by the two photoagents critically determine whether and to what extent the membrane dipole can shift their respective energy levels. Moreover, since the modulated photoelectrochemical responses result from charge transfer processes occurring between the layer of photoagents and the gold electrode, only dipoles situated in between these two layers are expected to directly impact these processes. This leads us to conclude that the lipid associated dipole only plays a minor role in modifying the energetics in fullerene-based devices – as it lies at the outside of the assembled fullerenes; whereas for the ZnP-containing cells, the same membrane dipole sits right within the confinement of the electrode and lipid headgroups and therefore, a dipole potential of 0.2 eV is specifically included in this case (vide infra).

Similarly, dipole potential contributions can be expected of the underlying SAMs to modify the interfacial energetics. Specifically, the more electronegative sulfur atom in the C12 thiol pulls electron density away from the adjacent methylene groups, forming a dipole with the sulfur as the negative pole; the opposite is true for C10F17SH, with electron clouds being pulled towards the distal fluorinated side of the molecule. This is

further shown by the calculated dipole moments[37] of the two adsorbates: 1.79 D for C12 thiol and −1.28 D for C10F17SH. Upon formation of self-assembled monolayers on gold, these polar molecules will yield a collective dipole that contains a non-zero component normal to the gold surfaces.

### 3.3.5 Mechanisms of Photocurrent/Photovoltage Modulation: A Combined Analysis

We next combine the two sources of dipole potentials in a more quantitative analysis of the overall cell energetics. For devices governed by tunneling-based charge injection processes, the efficiency of hole (/electron) injection can be significantly influenced by the energy differences between the Fermi potential level of the electrode and the HOMO(/LUMO) level, respectively, of the organic semiconductor immobilized on top of the electrode, i.e., the hole/electron injection barriers.[3,39] As discussed in the Introduction, one exploitable strategy of minimizing the charge injection barriers and thus enhancing the injection efficiency is using a dipole layer to interface the organic material and the electrode. Depending on its dipole orientation relative to the electrode, the dipole layer acts to shift up (or down) the effective vacuum energy level, which makes the removal of electrons from the metal more (or less) energetically costly, resulting in an increase (or a decrease) in the work function of the metal. When the same process additionally involves an organic (photoagent) layer at the outside, the HOMO/LUMO levels of the latter can be shifted by the inserted dipole layer as well, since it shares a common effective vacuum level with the gold substrate during the charge injection process.[39]

Following solid-state physics convention, the HOMO energy of ZnP is estimated from its first oxidation potential[40] and converted to absolute scale (5.6 eV) vs. the vacuum (i.e., potential of the latter is taken as 4.5 eV[41] vs. NHE). Its LUMO level, 3.5 eV, is estimated from the Weller relationship: $E_{LUMO} = E_{HOMO} - \Delta E_{0,0}$, where $\Delta E_{0,0}$ is the 0→0 transition energy of ZnP (i.e., ~2.1 eV as determined from ZnP fluorescence emission spectrum, Figure 3.6). A value of 4.9 eV is used as the work function of gold under ambient condition.[42] In the case of dipole potentials rendered by alkanethiol SAMs, Kelvin probe measurements[42] by de Boer et al. determined that C10F17SH SAM could increase the work function of gold by 0.6 eV relative to the unmodified gold, whereas the oppositely polarized C16 alkanethiol effectively lowered the gold work function by 0.8 eV.

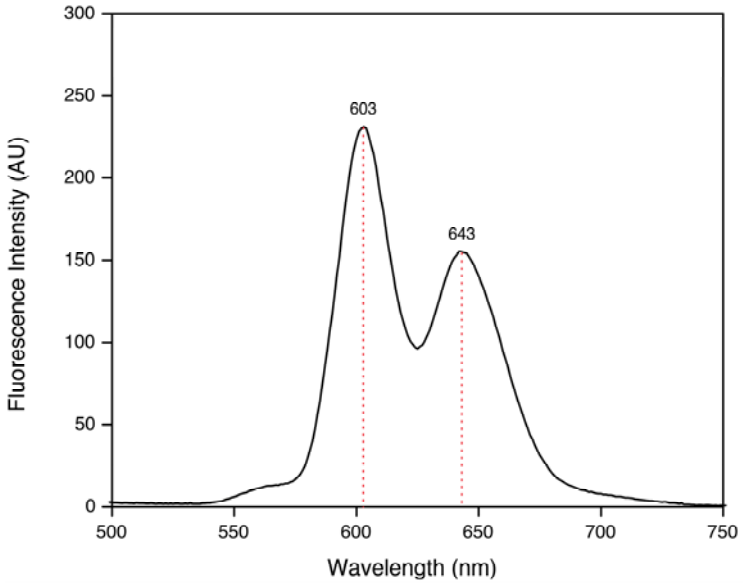


**Figure 3.6.** Fluorescence emission spectra of ZnP in POPC liposome. The liposome sample contains 0.25 mM POPC and ~5 μM ZnP-DOPE in 10 mM HEPES buffer saline (0.1 M NaCl, pH 7.7) solution. Excitation is made at 425 nm.

These values,[43] together with the contribution from the lipid membrane dipole, are taken into the analysis of energetics responsible for ZnP based bilayer cells (Figure 3.7). As shown in Figure 3.7b, the dipole associated with the C12 SAM brings down the HOMO/LUMO levels of ZnP vs. vacuum, which is partially counteracted by the lipid dipole that points to the opposite direction. In consequence, its effective LUMO level (4.1 eV) is now more closely aligned with the Fermi level of gold ($E_F$ = 4.9 eV), whereas the gap between its HOMO and the gold Fermi level is enlarged. These changes accordingly produce an electron-injection barrier (EIB) of 0.8 eV and a hole-injection barrier (HIB) of 1.3 eV in thus-prepared bilayer devices. By contrast, the effective energy levels associated with ZnP will be shifted further up when C10F17SH is used to form the bilayers, which result in a very small HIB (0.1 eV) and a very large EIB (2.2 eV) (Figure 3.7c). Together, the dipole potentials from SAMs and lipids in these hybrid bilayers modify the thermodynamic barrier for charge injection to occur, leading to a more efficient anodic photovoltaic process (due to a small EIB) in the case of C12 thiol and a facile cathodic process (due to a small HIB) for the fluorinated thiol as shown in Figure 3.4.

Similar energy diagrams for $C_{63}$ based devices can be sketched by putting together the respective potential energy levels of each participating component (Figure 3.8). As discussed above, the contribution from the lipid membrane dipole in the overall energetics is expected to be small because of its small overlap with the charge-injection path. Hence, a maximal anodic photocurrent can be predicted for the C12 SAM based cells as the estimated EIB is zero, i.e., LUMO of assembled $C_{63}$ = 4.1 − (−0.8, C12 SAM) = 4.9 eV, whereas a higher cathodic generation is expected for the C11F17SH base cells

due to a lower HIB. These estimates again agree with experimental data shown in Figure 3.5.

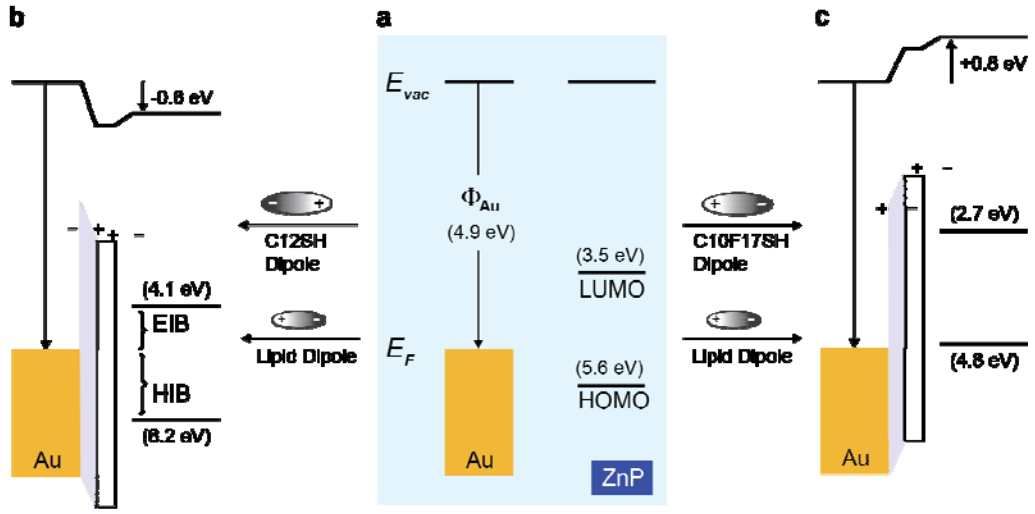


**Figure 3.7**. Energy diagrams of ZnP based photovoltaic systems. In panel a), the gold Fermi energy level ($E_F$) and the HOMO/LUMO levels of ZnP are separated in vacuum. b) Lowering of HOMO/LUMO levels of ZnP vs. $E_F$(Au) induced by the dipole of C12SH SAM situated in between the electrode and the photoagent. c) Upshifting of HOMO/LUMO levels of ZnP vs. $E_F$(Au) induced by the dipole of C10F17SH SAM situated in between the electrode and the photoagent. In both configurations, a 0.2 eV contributed by the lipid membrane dipoles is included.

While a similar trend is shared by the two photoagents investigated here, the level of modulation is noticeably smaller in the fullerene-based devices. For example, the anodic photocurrents obtained from fullerenes assembled on the two SAMs differ only by ~30%, despite the estimate that their EIBs are 2.4 eV apart. The relatively weak modulation of fullerene-based cells is likely due to its location in the bilayer as well as its high molecular polarizability (e.g., the ground-state polarizability[44] of $C_{60}$ is 84 $Å^3$).

Assembled as such, the polarizable molecule framework of fullerene may directly experience the surrounding dipoles and electronically dampen the polarization imposed by the latter, giving rise to a weakened modulation. In a sense, this counteracting effect bears similarity with the depolarization effect seen in the SAM formation on a substrate,[36] where individual adsorbates only display a dipole less than their gas-phase value due to a compensating electric field originated between the substrate and the SAM pointing in the opposite direction. This depolarization effect may pose a limit on employing polar SAMs to substantially modify charge-injection barriers in fullerene-based OPV systems. Follow-up computational studies of the present system may lead to more insights into the mechanism and control of such an effect in the near future.

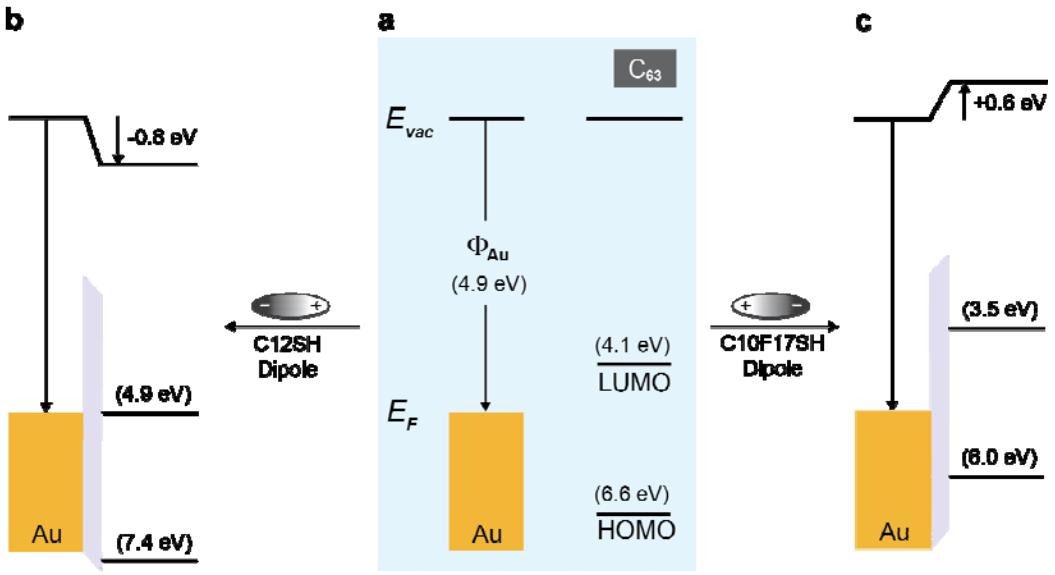


**Figure 3.8.** Energy diagrams of $C_{63}$ based photovoltaic systems. In panel a), the gold Fermi energy level ($E_F$) and the HOMO/LUMO levels of fullerene $C_{63}$ are separated in vacuum. b) Shifting of HOMO/LUMO levels of $C_{63}$ vs. $E_F$(Au) by the dipole of C12SH

SAM. c) Shifting of HOMO/LUMO levels of $C_{63}$ vs. $E_F$(Au) by the dipole of C10F17SH SAM.

### 3.4 Conclusions

We have found in this work that the intrinsic dipoles of lipids and alkanethiols can be used to modulate photoinduced charge injection processes in alkanethiol/lipid based bilayer photovoltaic systems. These modulation effects are satisfactorily explained by dipole-induced modification of work function of the metal substrates and hence the Shockley energy barriers[12,18,36,39] – a concept well established and broadly exploited in organic light-emitting diodes and field-effect transistors. Together, our results reveal the intricacy of orientated surface dipole in influencing the photovoltaic processes, and its subtle interplay with other related factors, such as the polarizability, location and orientation of the photoagents. These findings clearly point to the potential of controlling electronic and dielectric properties of organic devices using self-assembled structures, which we hope can be of use in designing new thin-film based photovoltaic and organoelectronic systems.

**References:**

1. Kippelen, B.; Bredas, J.-L. Organic Photovoltaics. *Energy Environ. Sci.* **2009**, *2*, 251-261.

2. Graetzel, M.; Janssen, R. A. J.; Mitzi, D. B.; Sargent, E. H. Materials Interface Engineering for Solution-Processed Photovoltaics. *Nature* **2012**, *488*, 304-312.

3. Heimel, G.; Romaner, L.; Zojer, E.; Bredas, J.-L. The Interface Energetics of Self-Assembled Monolayers on Metals. *Acc. Chem. Res.* **2008**, *41*, 721-729.

4. Beljonne, D.; Cornil, J.; Muccioli, L.; Zannoni, C.; Bredas, J.-L.; Castet, F. Electronic Processes at Organic-Organic Interfaces: Insight from Modeling and Implications for Opto-electronic Devices. *Chem. Mater.* **2011**, *23*, 591-609.

5. Imahori, H.; Mori, Y.; Matano, Y. Nanostructured Artificial Photosynthesis. *J. Photochem. Photobiol. C* **2003,** *4*, 51-83.

6. Konishi, T.; Ikeda, A.; Shinkai, S. Supramolecular Design of Photocurrent-Generating Devices Using Fullerenes Aimed at Modeling Artificial Photosynthesis. *Tetrahedron* **2005**, *61,* 4881-4899.

7. Kondo, T.; Uosaki, K. Self-Assembled Monolayers with Photo-Functionalities. *J. Photochem. Photobiol. C* **2007**, *8,* 1-17.

8. Zhan, W.; Jiang, K. A Modular Photocurrent Generation System Based on Phospholipid-Assembled Fullerenes. *Langmuir* **2008**, *24*, 13258-13261.

9. Jiang, K.; Xie, H.; Zhan, W. Photocurrent Generation from $Ru(bpy)_3^{2+}$ Immobilized on Phospholipid/Alkanethiol Hybrid Bilayers. *Langmuir* **2009**, *25*, 11129-11136.

10. Zhan, W.; Jiang, K.; Smith, M. D.; Bostic, H. E.; Best, M. D.; Auad, M. L.; Ruppel, J. V.; Kim, C.; Zhang, X. P. Photocurrent Generation from Porphyrin/Fullerene Complexes Assembled in a Tethered Lipid Bilayer. *Langmuir* **2010**, *26*, 15671-15679.

11. Xie, H.; Jiang, K.; Zhan, W. Modular Molecular Photovoltaic System Based on Phospholipid/Alkanethiol Hybrid Bilayers: Photocurrent Generation and Modulation. *Phys. Chem. Chem. Phys.* **2011**, *13*, 17712-17721.

12. Kao, K. C. *Dielectric Phenomena in Solids.* Elsevier Academic Press. San Diego, CA, 2004, Chapter 6.

13. Ives, H. E.; Olpin, A. R. Maximum Excursion of the Photoelectric Long Wave Limit

of the Alkali Metals. *Phys. Rev.* **1929,** *33,* 117-128.

14. Brady, J. J. The Photoelectric Properties of Alkali Metal Films as a Function of their Thickness. *Phys. Rev.* **1932,** *41,* 613-626.

15. Bardeen, J. Theory of the Work Function. II. The Surface Double Layer. *Phys. Rev.* **1936,** *49,* 653-663.

16. Campbell, I. H.; Rubin, S.; Zawodzinski, T. A.; Kress, J. D.; Martin, R. L.; Smith, D. L.; Barashkov, N. N.; Ferraris, J. P. Controlling Schottky Energy Barriers in Organic Electronic Devices Using Self-Assembled Monolayers. *Phys. Rev. B* **1996,** *54,* 14321-14324.

17. Alloway, D. M.; Hofmann, M.; Smith, D. L.; Gruhn, N. E.; Graham, A. L.; Colorado, R. Jr.; Wysocki, V. H.; Lee, T. R.; Lee, P. A.; Armstrong, N. R. Interface Dipoles Arising from Self-Assembled Monolayers on Gold: UV-Photoemission Studies of Alkanethiols and Partially Fluorinated Alkanethiols. *J. Phys. Chem. B* **2003**, *107*, 11690-11699.

18. Tung, R. T. Recent Advances in Schottky Barrier Concepts. *Mater. Sci. Eng. R* **2001,** *35,* 1-138.

19. Braun, S.; Salaneck, W. R.; Fahlman, M. Energy-Level Alignment at Organic/Metal and Organic/ Organic Interfaces. *Adv. Mater.* **2009**, *21*, 1450-1472.

20. Mihailetchi, V. D.; Koster, L. J. A.; Blom, P. W. M.; Melzer, C.; de Boer, B.; van Duren, J. K. J.; Janssen, R. A. J. Compositional Dependence of the Performance of Poly(p-phenylene vinylene):Methanofullerene Bulk-Heterojunction Solar Cells. *Adv. Funct. Mater.* **2005**, *15*, 795-801.

21. Kim, J.; Khang, D.-Y.; Kim, J.-H.; Lee, H. H. The Surface Engineering of Top Electrode in Inverted Polymer Bulk-Heterojunction Solar Cells. *Appl. Phys. Lett.* **2008**,

*92*, 133307.

22. Tanasova, M.; Vasileiou, C.; Olumolade, O. O.; Borhan, B. Enhancement of Exciton Coupled Circular Dichroism with Serically Encumbered Bis-Porphyrin Tweezers. *Chirality*, **2009**, *21*, 374-382.

23. Plant, A. L. Self-Assembled Phospholipid/Alkanethiol Biomimetic Bilayers on Gold. *Langmuir* **1993**, *9*, 2764-2767.

24. Silin, V. I.; Wieder, H.; Woodward, J. T.; Valincius, G.; Offenhausser, A.; Plant, A. L. The Role of Surface Free Energy on the Formation of Hybrid Bilayer Membranes. *J. Am. Chem. Soc.* **2002**, *124*, 14676-14683.

25. Israelachvili, J. N. *Intermolecular and Surface Forces,* 3rd Ed. Elsevier Inc. The Netherlands, 2011.

26. Li, L.; Davande, H.; Bedrov, D.; Smith, G. D. A Molecular Dynamics Simulation Study of $C_{60}$ Fullerenes Inside a Dimyristoylphosphatidylcholine Lipid Bilayer. *J. Phys. Chem. B* **2007**, *111*, 4067-4072.

27. Bortolus, M.; Parisio, G.; Maniero, A. L.; Ferrarini, A. Monomeric Fullerenes in Lipid Membranes: Effects of Molecular Shape and Polarity. *Langmuir* **2011**, *27*, 12560-12568.

28. Nezil, F. A.; Bloom, M. Combined Influence of Cholesterol and Synthetic Amphiphilic Peptides Upon Bilayer Thickness in Model Membranes. *Biophys. J.* **1992**, *61*, 1176-1183.

29. Kucerka, N.; Tristram-Nagle, S.; Nagle, J. F. Structure of Fully Hydrated Fluid Phase Lipid Bilayers with Monounsaturated Chains. *J. Membr. Biol.* **2005**, *208*, 193-202.

30. Brockman, H. Dipole Potential of Lipid Membranes. *Chem. Phys. Lipids* **1994**, *73*, 57-79.

31. Clarke, R. J. The Dipole Potential of Phospholipid Membranes and Methods for Its Detection. *Adv. Colloid Interface Sci.* **2001,** *89-90,* 263-281.

32. Demchenko, A. P.; Yesylevskyy, S. O. Nanoscopic Description of Biomembrane Electrostatics: Results of Molecular Dynamics Simulations and Fluorescence Probing. *Chem. Phys. Lipids* **2009**, *160*, 63-84.

33. Hauser, H.; Pascher, I.; Pearson, R. H.; Sundell, S. Preferred Conformation and Molecular Packing of Phosphatidylethanolamine and Phosphatidylcholine. *Biochim. Biophys. Acta* **1981,** *650,* 21-51.

34. Gawrisch, K.; Ruston, D.; Zimmerberg, J.; Parsegian, V. A.; Rand, R. P.; Fuller, N. Membrane Dipole Potentials, Hydration Forces, and the Ordering of Water at Membrane Surfaces. *Biophys. J.* **1992,** *61,* 1213-1223.

35. Clarke, R. J. Effect of Lipid Structure on the Dipole Potential of Phosphatidylcholine Bilayers. *Biochim. Biophys. Acta* **1997,** *1327,* 269-278.

36. Natan, A.; Kronik, L.; Haick, H.; Tung, R. T. Electrostatic Properties of Ideal and Non-ideal Polar Organic Monolayers: Implications for Electronic Devices. *Adv. Mater.* **2007**, *19*, 4103-4117.

37. Calculation was also performed on the neutral radicals of the two thiols using procedures similar to references 13 and 14, which gives 2.00 D for C12SH and −0.91 D for C10F17SH, respectively. Dipole calculation based on these neutral radicals is known to underestimate the contribution of Au-S bond to the overall dipole of the gold-attached thiol molecules (ref. 38) but is expected to produce the correct trend in our case.

38. Wang, L.J.; Rangger, G. M.; Ma, Z.Y.; Li, Q.K.; Shuai, Z.; Zojer, E.; Heimel, G. Is There a Au-S Bond Dipole in Self-Assembled Monolayers on Gold? *Phys. Chem. Chem. Phys.* **2010**, *12*, 4287-4290.

39. Ishii, H.; Sugiyama, K.; Ito, E.; Seki, K. Energy Level Alignment and Interfacial Electronic Structures at Organic/Metal and Organic/Organic Interfaces. *Adv. Mater.* **1999**, *8*, 605-625.

40. Imahori, H.; Yamada, H.; Nishimura, Y.; Yamazaki, I.; Sakata, Y. Vectorial Multistep Electron Transfer at the Gold Electrodes Modified with Self-Assembled Monolayers of Ferrocene-Porphyrin-Fullerene Triads. *J. Phys. Chem. B* **2000**, *104*, 2099-2108.

41. Bard, A. J.; Faulkner, L. R. *Electrochemical Methods: Fundamentals and Applications.* John Wiley & Sons. New York, 2001.

42. de Boer, B.; Hadipour, A.; Mandoc, M. M.; van Woudenbergh, T. Blom, P. W. M. Tuning of Metal Work Functions with Self-Assembled Monolayers. *Adv. Mater.* **2005**, *17*, 621-625.

43. Here, the shifted potentials of C12 SAMs were approximated by using data of C16 thiol reported in ref. 42.

43. Renge, I. Solvent Effects on the Absorption Maxima of Fullerenes $C_{60}$ and $C_{70}$. *J. Phys. Chem.* **1995**, *99*, 15955-15962.

## Chapter Four

# Lipid/Alkanethiol Hybrid-Bilayer Based Molecular Photovoltaic Systems: The Role of Cholesterol

## 4.1 Introduction

The research with molecular photovoltaics has gained a lot attention ever since the discovery of photoelectric effect.[1-3] The idea of turning sunlight into electric power became more promising with the development of new materials and techniques, especially with the invention of dye-sensitized solar cell in 1988 which is also known as Grätzel cell.[1,4] Based on solid-supported chromophores incorporated lipid/alkanethiol hybrid-bilayer, we have reported several molecular photovoltaic systems[5-8] and also demonstrated the antenna effect of natural compound lutein in this system.[8] A new two-component system will be described here, which shows the addition of cholesterol into the lipid layer can significantly modulate the photocurrent generation of fullerene in different ways depend on the lipid matrix.

Cholesterol is a major component of all cell membranes in nature.[9] It comprises approximately 20-50 mol% of most animal cell membranes, and up to 70 mol% of ocular lens membranes.[10] The molecular structure of cholesterol is shown in Figure 4.1, which includes a tetracyclic fused ring skeleton with a hydroxyl group on one end and an iso-octyl hydrocarbon side chain on another end.[11] The hydroxyl group makes cholesterol

amphiphilic which enables it to orient in lipid membranes. In a lipid bilayer matrix, the cholesterol orients itself with the hydroxyl group pointing toward to the aqueous phase, while the rigid and hydrophobic steroid ring being parallel to the hydrocarbon chains of the lipids.[12]

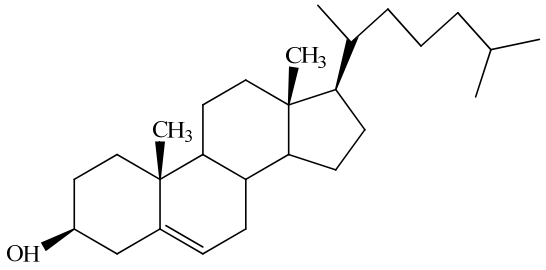


**Figure 4.1.** The molecular structure of cholesterol

Cholesterol has many functions in membranes and can modulate the structure and physicochemical properties of the membranes in several different ways. From physical perspective, cholesterol can increase the mechanical strength and the internal electrical dipole potential of the membranes which can modulate the transport of small molecules across the membranes correspondingly.[9,13] And also, cholesterol has the ability to regulate the fluidity and phase properties of the membranes.[14,15] At the molecular level, cholesterol can affect the ordering and packing density of the surrounding lipids, which will change the area occupied by a lipid.[10,16] The effects of cholesterol on the lipid molecules can be in opposite direction. When the temperature is above $T_m$ (gel-to-liquid crystal phase transition temperature), which means the lipids are in their fluid state, cholesterol can increase the ordering of the lipid membranes. It affects the ordering in the opposite way when the temperature is below $T_m$.[10]

Using a lipid/alkanethiol hybrid-bilayer based molecular photovoltaic model, we have investigated in this study the influence of morphology and ordering of organic matrices on the efficiency of photoinduced electron transfer processes. For the system containing fullerene $C_{63}$ assembled in a hybrid-bilayer of 1-palmitoyl-2-oleoyl-*sn*-glycero-3-phosphocholine (POPC, $T_m = -2$ °C) and 1-dodecanethiol, addition of 10-50% cholesterol into the lipids was found to increase the photocurrent output by 30-120% compared to the cholesterol-free devices. This enhancement of performance might due to the formation of a more ordered, gel-like POPC lipid matrix upon cholesterol addition, which lowers the energy loss caused by matrix relaxation during electron transfer. This analysis is supported by responses obtained from the system using 1,2-dipalmitoyl-*sn*-glycero-3-phosphocholine (DPPC, $T_m = 41$ °C) to form the lipid layer, in which case addition of cholesterol to the lipids causes the photocurrents to decrease. In both systems, evidence collected from UV-Vis and fluorescence spectroscopy has ruled out the possibility that the variation in photovoltaic responses is caused by cholesterol-induced condensing/ordering of the lipid matrices and thus different loadings of photoagents among devices. Implications of our findings in the improvement of organic photovoltaic devices are discussed.

## 4.2 Experimental Section

### 4.2.1 Reagents

Phospholipid 1-palmitoyl-2-oleoyl-*sn*-glycero-3-phosphocholine (POPC) and 1,2-dipalmitoyl-*sn*-glycero-3-phosphocholine (DPPC) were obtained from Avanti Polar Lipids with purity better than 99%. Synthesis of monomalonic fullerene ($C_{63}$) were

reported previously.[17] Cholesterol was purchased from Sigma-Aldrich with purity better than 99%. Sodium sulfate and sodium chloride were obtained from Fisher Scientific. Other reagents, including dodecanethiol ($C_{12}SH$), 4-(2-hydroxyethyl)piperazine-1-ethanesulfonic acid (HEPES), methyl viologen dichloride hydrate ($MV^{2+}$), L(+)-ascorbic acid sodium salt (sodium ascorbate), D-(+)-glucose, glucose oxidase (type X-S, *from Aspergillus niger*), and catalase from bovine liver were purchased from Sigma-Aldrich. All solutions employed in these experiments were prepared using 18.2 MΩ·cm deionized water (Millipore).

### 4.2.2 Synthesis of $Ru(bpy)_3^{2+}$-DOPE

$Ru(bpy)_3^{2+}$-DOPE was synthesized in one step by reacting $Ru(bpy)_3^{2+}$-NHS with DOPE. First, 2.5 μmol of DOPE (186 μL) in chloroform was added to a round bottom flask and dried under an argon stream prior to the addition of 0.8 mL of DMF and 25 μmol of triethylamine (3.48 μL) followed by stirring for 30 min. 5 μmol of $Ru(bpy)_3^{2+}$-NHS in DMF were then injected into the flask and thoroughly mixed. The reaction proceeded overnight at room temperature in dark. The resulting products were dried with 0.2g silicon and then separated on a silica gel column (200-400 mesh) using three subsequent mobile phases: ~500 mL of chloroform, a 90:10:0.5 mixture of chloroform/methanol/water, and the same in a 65:25:4 v/v ratio. The production of $Ru(bpy)_3^{2+}$-DOPE was confirmed by EIS-MS (calculated molecular weight: 1352.6; found: $[M+H]^+$: 1353.6; $[M+H]^{2+}$: 676.8).

### 4.2.3 Assembly of SAMs and Hybrid Bilayers

Gold-coated substrates were fabricated by sputtering gold onto chromium-coated silicon wafers. The thickness of the gold layer was about 200 nm. Prior to the self-assembly of alkanethiol monolayers, the gold-coated substrates were cleaned in piranha solution (3:1 v/v concentrated $H_2SO_4$/30% $H_2O_2$ solution) for 15 min and thoroughly rinsed with water and then ethanol and dried under an argon stream. The cleaned gold electrodes were incubated in 1 mM alkanethiol in ethanol solution at room temperature for at least 12 h. The SAM-modified gold substrates were then rinsed with copious amount of ethanol and DI water, dried in argon, then assembled in a homemade Teflon photoelectrochemical cell for further use.

To prepare octadecyltrichlorosilane (OTS) SAMs on glass substrates, glass slides (precleaned micro slides, VWR) were first cleaned by sonication in a series of media including dilute detergent, DI water, acetone, and DI water again, each of which persisted for 30 min. The treated slides were then boiled in a mixture of DI water/$H_2O_2$ (30%)/$NH_4OH$ (30%) (5:1:1, v/v) for 1 h. The slides were then rinsed with copious amount of DI water and thoroughly dried under an argon stream. The slides were immediately transferred into a glovebox in which the water vapor level is regulated at a level typically under 3 ppm. To form the OTS SAMs, the cleaned slides were immersed in a 2.5 mM OTS solution in anhydrous toluene for 45min. After silanization, the slides were further rinsed by toluene and methanol to remove the unbound silane and finally, annealed at 120ºC for 2 h. These slides are normally used to form lipid/SAM bilayers within 24 h.

Preparation of liposome samples containing fullerene $C_{63}$ [17] or $Ru(bpy)_3^{2+}$-DOPE [5] was reported previously. During the current investigation, cholesterol was added to the

liposome samples. Briefly, appropriate quantities of POPC (DPPC), cholesterol, $C_{63}$, or $Ru(bpy)_3^{2+}$-DOPE in chloroform were thoroughly mixed in a flask and then dried to a film by rotary evaporation. This mixture was then sonicated (Bransonic, model: 3510-DTH) in HEPES buffer solution (10 mM HEPES, 100 mM NaCl, pH 7.7) at room temperature (for POPC) or at 50 ºC (for DPPC) for 2h. The resulting solution was then extruded sequentially through polycarbonate membranes (Nuclepore, Whatman) of 400 and 80 nm-diameter pore at room temperature (for POPC) or at 50 ºC (for DPPC). The total lipid concentration of the final product was approximately 1.25 mM. The precise concentration of each composition used in the preparation will be specified later in this chapter.

The formation of phospholipid/alkanethiol hybrid bilayers was done by adding a 300-μL liposome solution (total lipid concentration: 1.25 mM) onto a SAM above prepared and incubated for 2 h at room temperature (for POPC), or 1 h at 50 ºC and another 1 h after the heat was turned off (for DPPC). The unbound liposome solution was then removed from the cell by thorough solution exchange with the fresh buffer solution repeated about 30 times(10 mM HEPES, 100 mM NaCl, pH 7.7).

### 4.2.4 Impedance Spectroscopy

The impedance measurements of the alkanethiol/lipid hybrid bilayers were carried out using a μAutolab Type III/FRA2 electrochemical impedance analyzer system (Metrohm Autolab B.V., Netherlands). Impedance measurements were analyzed by FRA 4.8 software. A conventional three-electrode setup was employed which contains bilayer-modified gold electrodes as the working electrodes, a Ag/AgCl (KCl saturated) reference

electrode and a Pt wire as the counter electrode. The electrochemical cells were biased with a 5 mV a.c. voltage operated in the frequency range from 10 to 10 kHz. The obtained impedance data were fitted to a series-*RC* circuit model using a modeling package included in FRA 4.8. The typical fitting errors were less than ±5%.

### 4.2.5 UV-vis Absorption and Fluorescence Spectroscopy

UV-vis spectroscopy was carried out using a UV-visible spectrophotometer (Cary 50 Bio, Varian).

The fluorescence emission spectra of the $Ru(bpy)_3^{2+}$-containing hybrid bilayer on glass slides were acquired using a PI Acton spectrometer (SpectraPro SP 2356, Acton, NJ) which is connected to the side port of an epifluorescence microscope (Nikon TE-2000U, Japan). The emission signal was recorded by a back illuminated digital CCD camera (PI Acton PIXIS:400B, Acton, NJ) operated by a PC. The excitation was generated by a mercury lamp (X-Cite 120, EXFO, Ontario, Canada) filtered by a band-pass filter at 470±20 nm. The exposure time was 50 ms. The emission signal was filtered by a long-pass filter with a cutoff wavelength of 515 nm.

### 4.2.6 Photoelectrochemical Measurements

The photoelectrochemical measurements were carried out in a Teflon, three-electrode photoelectrochemical cell. The three-electrode setup contains the gold substrate with a lipid/SAM bilayer as the working electrode, a Pt counter electrode and an Ag/AgCl (KCl-saturated) reference electrode. The effective area of the gold electrode is ~1.13 $cm^2$. Photocurrents were measured amperometrically with potentials set equal to

the open circuit potential of each cell determined separately under dark conditions; whereas photovoltages were acquired in the open-circuit potential mode. For both measurements the cells were irradiated with light from a Hg lamp (X-Cite, series 120 PC, EXFO) filtered at 417±30 nm with an average intensity of 40.0 mW/cm$^2$. The light was switched on and off every 15 s for 165 s total for photocurrent measurement whereas it was switched on and off every 30 s for 210 s total for photovoltage measurements. A 50 mM ascorbate in HEPES buffer (10 mM HEPES, 100 mM NaCl, pH 7.7) was used as sacrificial electron donor in the anodic current generation; the electrolyte containing 50mM methyl viologen in 0.1 M $Na_2SO_4$ was used for cathodic current generation. In the case of anodic current generation, oxygen in the cell was removed by adding 50 mM glucose, 50 units/mL glucose oxidase, and 200 units/mL catalase in the solution. The resulting photocurrents and photovoltages were recorded by a potentiostat (CHI 910B, CH Instruments).

## 4.3 Results and Discussion

### 4.3.1 Characterization of Liposome Samples and Hybrid Bilayer Matrix

A series of 1.25 mM POPC with cholesterol (10%, 25%, 50%) liposome samples containing either 2% $C_{63}$ or $Ru(bpy)_3^{2+}$ were prepared by an extrusion-based method as described in experimental section. UV-vis absorption spectra were obtained to monitor the quantitative incorporation of $C_{63}$ or $Ru(bpy)_3^{2+}$ in POPC/cholesterol liposome samples which are shown in Figure 4.2 (for $C_{63}$) and Figure 4.3 (for $Ru(bpy)_3^{2+}$). For the UV-vis spectra of $C_{63}$/POPC with/without cholesterol liposomes, two main peaks at 260 and 328 nm correspond to the strongly allowed electronic transitions of $C_{60}$ fullerenes

while the relatively weak absorption at 429 nm is characteristic of [6,6]-closed-ring bridged fullerenes, such as $C_{63}$.[17] The small variations between the UV-vis absorption of POPC/$C_{63}$/cholesterol (0-50%) samples may due to the liposome preparation or solution property change induced by cholesterol, we can still assume that the addition of cholesterol didn't significantly affect the amount of $C_{63}$ incorporated into liposomes. The UV-vis spectrum of $Ru(bpy)_3^{2+}$ has a broad peak with maximum absorption at 450 nm which is assigned to metal-to-ligand charge transfer ($t_{2g}$ (Ru)→π*(bpy) transition).[18,19] Same small variations were observed with the spectra of POPC/$Ru(bpy)_3^{2+}$/ cholesterol (0-50%) liposome samples and same assumption can be made.

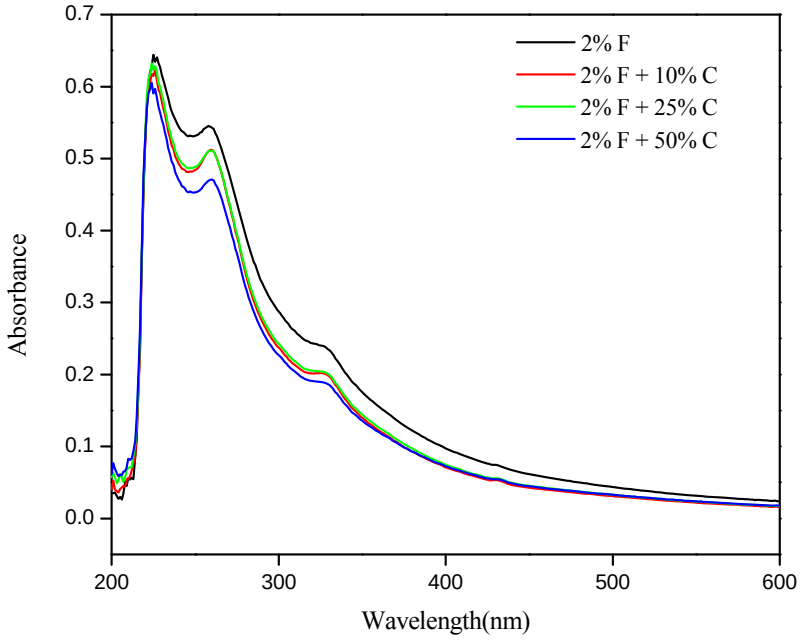


**Figure 4.2.** UV-vis spectra of POPC liposome samples containing 2% (mol) fullerene and 10, 25, 50% cholesterol. The liposome solutions contain 0.25 mM POPC and are dispersed in 10 mM HEPES buffer saline (0.1 M NaCl, pH 7.7).

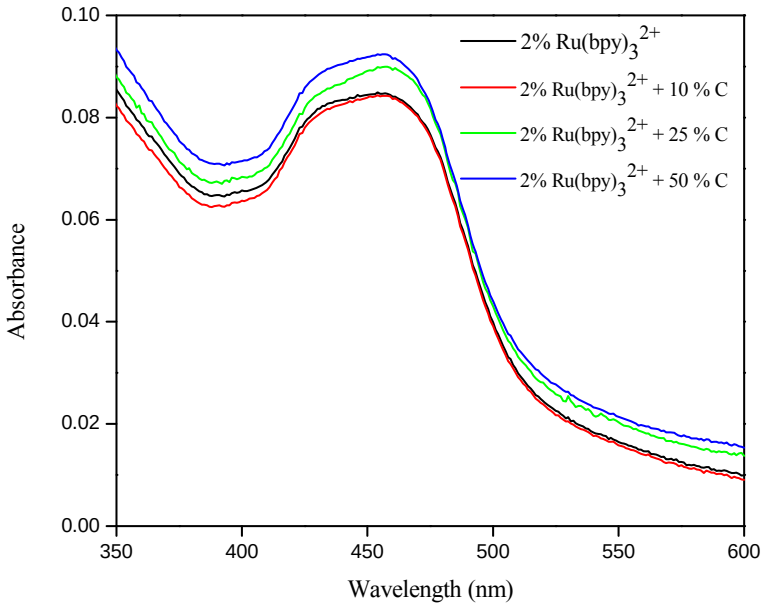


**Figure 4.3.** UV-vis spectra of POPC liposome samples containing 2% (mol) $Ru(bpy)_3^{2+}$ and 10, 25, 50% cholesterol. The liposome solutions contain 0.25 mM POPC and are dispersed in 10 mM HEPES buffer saline (0.1 M NaCl, pH 7.7).

To further confirm the assumption that the addition of cholesterol didn't interfere the appropriate amount of fullerene or $Ru(bpy)_3^{2+}$ incorporated into liposomes or the following composites loading for hybrid bilayer formation, fluorescence emission measurements were carried out with diluted liposome samples (Figure 4.4) and POPC/$Ru(bpy)_3^{2+}$/cholesterol-containing hybrid bilayers on semitransparent gold-coated glass slides (Figure 4.5). The fluorescence spectra with four liposome samples are quite comparable and also the hybrid bilayers prepared from 2% $Ru(bpy)_3^{2+}$ POPC liposomes containing 0-25% cholesterol share almost exact the same fluorescence emission spectra which indicate the similar loading of $Ru(bpy)_3^{2+}$ in the liposomes and also with these

bilayers. The fluorescence spectrum of hybrid bilayer assembled with 2% $Ru(bpy)_3^{2+}$/ POPC/50% cholesterol had a minor red shift along with two peaks broadening into one while sharing similar fluorescence intensity to other spectra. This may due to the decreased rigidity of the lipid membrane matrix induced by the addition of 50% cholesterol,[20] and $Ru(bpy)_3^{2+}$ emits light with longer wavelength in a more fluid matrix than in a more rigid membrane.[21] In a more fluid matrix, once $Ru(bpy)_3^{2+}$ gets excited, the solvent molecules surrounding it can quickly reorient to solvent the highly polar $Ru(bpy)_3^{2+}$ excited state. These surrounding solvent dipoles can further stabilize the excited state of $Ru(bpy)_3^{2+}$ and make the fluorescence emission of $Ru(bpy)_3^{2+}$ occur at a longer wavelength (lower energy level).[21]

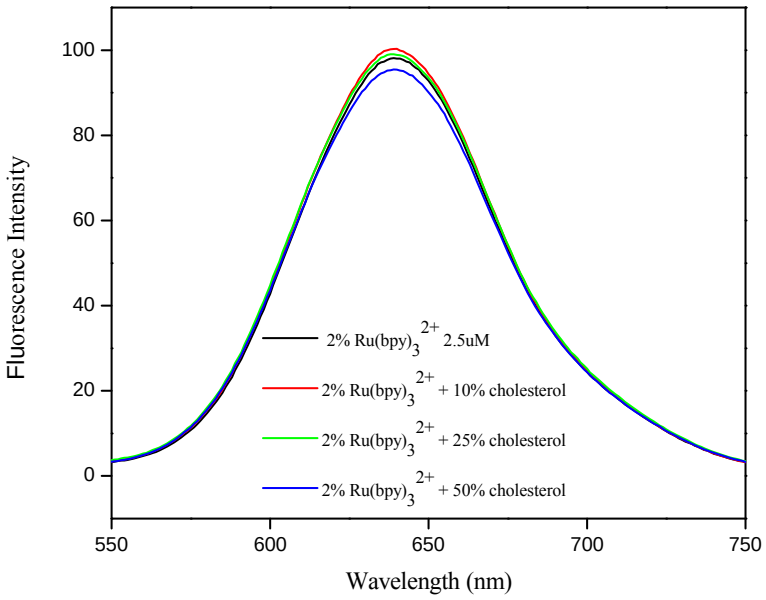


**Figure 4.4.** Fluorescence emission spectra of 2% (mol) $Ru(bpy)_3^{2+}$/POPC liposome samples with 0-50% cholesterol. The total lipid concentration is 2.5 μM.

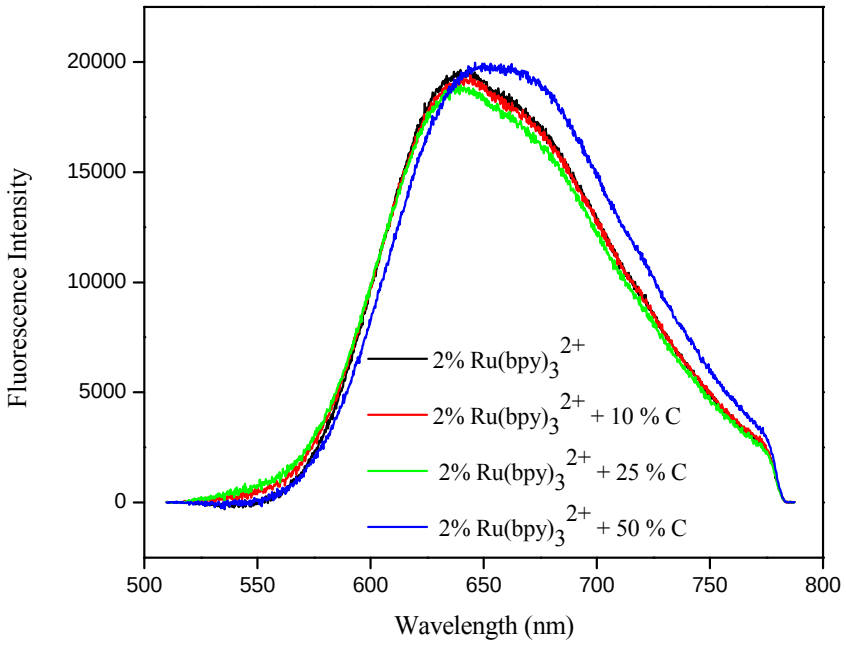


**Figure 4.5.** Fluorescence emission spectra of 2% (mol) $Ru(bpy)_3^{2+}$ in lipid monolayers on OTS modified glass slides. The lipid monolayers were formed form POPC liposomes containing 2% $Ru(bpy)_3^{2+}$ with (0-50%) cholesterol.

### 4.3.2 Photocurrent/Photovoltage Generation and Modulation

The obtained anodic and cathodic photocurrent from hybrid bilayers based photovoltaics containing 2% fullerene $C_{63}$ with (0-50%) cholesterol in top POPC lipid layer are shown in Figure 4.6 and Figure 4.7. As it is demonstrated in Figure 4.6, the addition of 10, 25, 50% cholesterol enhanced the anodic photocurrent of $C_{63}$ by 36, 57, 100%. Similarly, the cathodic photocurrent generated by $C_{63}$ alone was increased by 47, 87, and 220% via adding 10, 25, 50% of cholesterol. Since cholesterol itself cannot contribute to the photocurrent generation, the modulation of photocurrent may come from the effect of cholesterol on the lipid membrane matrix.

At room temperature, which is higher than the $T_m$ of POPC, the POPC lipid membrane is in a fluid phase. Adding cholesterol to the lipid layer increases the orientational order of POPC alkyl tails and the effect is dependent on cholesterol concentration up to 50%.[10] This more ordered lipid matrix lowers the energy loss during photoinduced electron transfer process. Also, the added cholesterol can decrease the lateral diffusion coefficient of the POPC lipids, which slows down the lateral dynamics in the lipid layer.[22,23] The suppressed lateral dynamics can indirectly enhance the vectorial electron transfer efficiency which is crucial to photocurrent generation.[5]

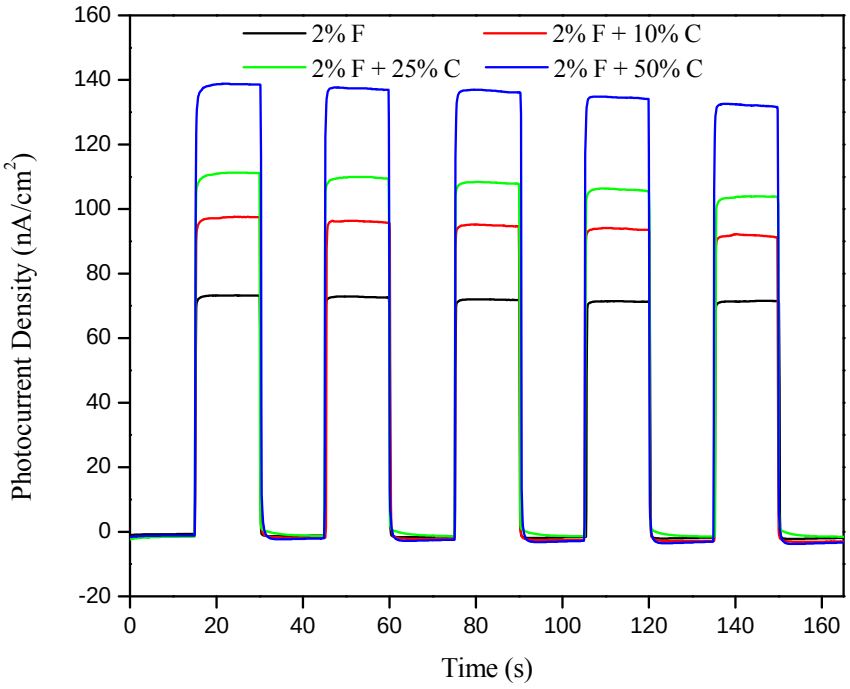


**Figure 4.6.** Anodic photocurrent generation from 2% fullerene $C_{63}$ and 10-50% cholesterol assembled in C12-SAM/POPC bilayers. They were generated in 50 mM ascorbate dissolved in HEPES buffer (10 mM HEPES, 100 mM NaCl, pH 7.7). Removal of oxygen in solutions was achieved by adding 50 mM glucose, 50 units/mL glucose

oxidase, and 200 units/mL catalase. The excitation light was provided by a Hg lamp filtered at 417±30 nm; average intensity: 40 mW/cm$^2$.

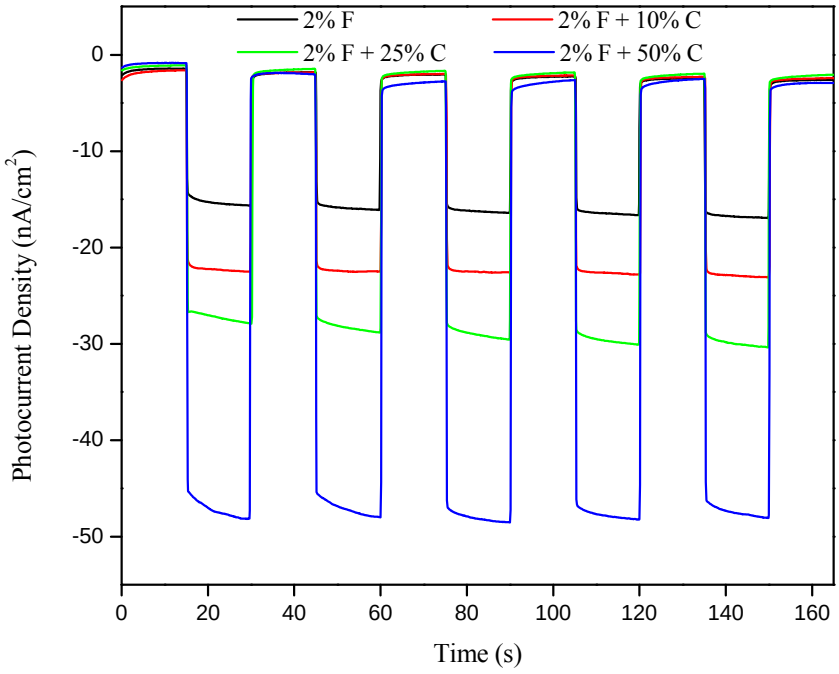


**Figure 4.7.** Cathodic photocurrent generation from 2% fullerene $C_{63}$ and 10-50% cholesterol assembled in C12-SAM/POPC bilayers. They were obtained from 50 mM methyl viologen in 0.1 M $Na_2SO_4$. Same light source as it for anodic photocurrent generation.

The effect of added cholesterol on POPC lipid layer was further confirmed by impedance spectroscopy. The measured capacitance of C12SH SAM ($C_{SAM}$) is 1.642 μF/cm$^2$. The measured capacitance of the hybrid bilayer ($C_{BL}$) and the calculated capacitance of lipid layer ($C_{lipid}$) based on $C_{lipid}^{-1} = C_{BL}^{-1} - C_{SAM}^{-1}$ are listed in Table 4.1. The capacitance of the layer can be defined as $C = \varepsilon\varepsilon_0$ A/d, where $\varepsilon$ is the dielectric

permittivity of the separating medium, $\varepsilon_0$ is the permittivity of free space ($\varepsilon_0 \approx 8.854\times10^{-12}$ F m$^{-1}$), A denotes the electrode area and d represents the layer thickness.[24] The addition of cholesterol into $C_{63}$/POPC layer increases the thickness of the lipid layer,[25,26] and imposes ordering and condensing effect on the matrix, as result of which, there will be less solvents in the lipid layer.[10] Less solvents produce smaller dielectric permittivity, along with bigger thickness lead to smaller capacitance.[24,27] So a higher concentration of cholesterol in the POPC layer corresponds to a smaller $C_{\text{lipid}}$, which agrees with the data in Table 4.1.

| | 2% F | 2% F + 10% C | 2% F + 25% C | 2% F + 50% C |
|---|---|---|---|---|
| $C_{\text{BL}}$ (μF/cm$^2$) | 1.042 | 1.065 | 0.997 | 0.972 |
| $C_{\text{lipid}}$ (μF/cm$^2$) | 2.85 | 3.031 | 2.538 | 2.382 |

**Table 4.1.** The measured capacitance of the 2% $C_{63}$/POPC/SAM bilayers containing 0-50% cholesterol and the calculated capacitance of the lipid layers.

The photovoltages obtained from the same device with 30 s dark/light cycles display a similar trend, i.e., higher photovoltage generation accompanying higher currents with higher cholesterol concentration and also the other way around (Figure 4.8 for anodic photovoltages, Figure 4.9 for cathodic photovoltages). Unlike the photocurrents, the photovoltages increase only gradually upon photoexcitation and cannot reach steady states in a 30 s. This sluggish behavior reflects the dynamic response of the charging/discharging processes of this bilayer-based photovoltaics under photoexcitation.

In particular, the relatively steep rise of photovoltage as the light is initially turned on reflects the fast accumulation of charges around the bilayer as a result of photoinduced electron transfer. As the bilayer is continuously being charged, the further charging process will slow down while reaching its capacity.

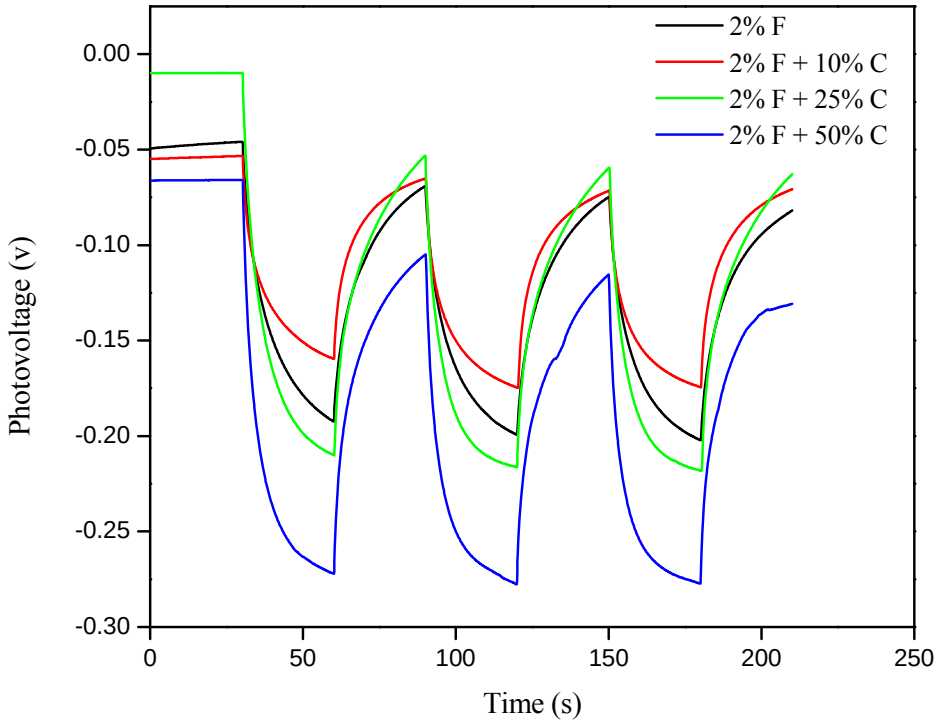


**Figure 4.8.** Anodic photovoltage generation from 2% fullerene $C_{63}$ and 10-50% cholesterol assembled in C12-SAM/POPC bilayers. Other conditions are idential to those described in Figure 4.6.

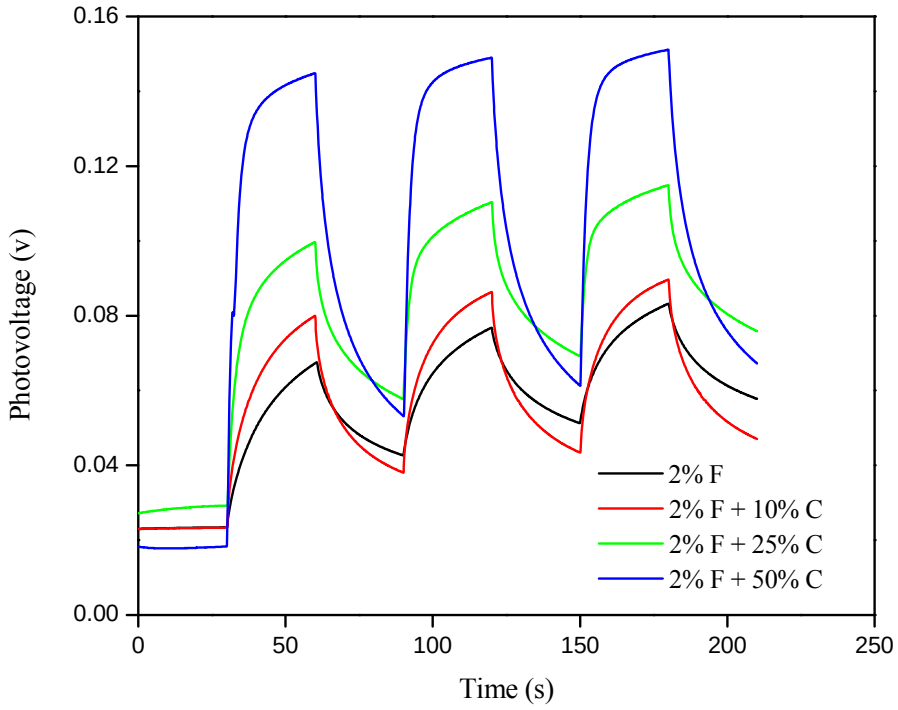


**Figure 4.9.** Cathodic photovoltage generation from 2% fullerene $C_{63}$ and 10-50% cholesterol assembled in C12-SAM/POPC bilayers. Other conditions are idential to those described in Figure 4.7.

The same photocurrent measurements were carried out with 2% fullerene $C_{63}$ /(10-50) cholesterol incorporated in DPPC lipid layer. The obtained anodic/cathodic currents are shown in Figures 4.10 and 4.11. Compared to $C_{63}$/POPC/C12SH system, the $C_{63}$/DPPC/C12SH based photovoltaics generated much higher currents compared to $C_{63}$/POPC/C12SH system, i.e., 170 nA/cm$^2$ to 70 nA/cm$^2$ for anodic current, 50 nA/cm$^2$ to 15 nA/cm$^2$ for cathodic current. Also, the anodic (cathodic) current generated by $C_{63}$ alone was decreased by 47, 18, 79% (38, 26, 72%) with 10, 25, 50% addition of cholesterol, which is quite contrary to the photocurrent generation trend in POPC matrix.

These variations correspond to the different lipid matrices and different effects asserted by the cholesterol. Unlike POPC, DPPC is a saturated lipid and in a gel phase at room temperature (25 ºC). Quite opposite to what it does to the lipids in fluid state, cholesterol promotes the fluidity of lipid matrix while in the gel state,[10] which increases the energy loss during electron transfer process and therefore smaller photocurrents after cholesterol incorporation. Since cholesterol has a stronger interation with fully saturated lipids, such as DPPC, than that with unsaturated lipids, like POPC,[10,16] it had a larger impact on the $C_{63}$ photocurrent generation in DPPC matrix (170 to 35 nA/cm$^2$ with 50% cholsterol) than that in POPC matrix (70 to 140 nA/cm$^2$ with 50% cholsterol).

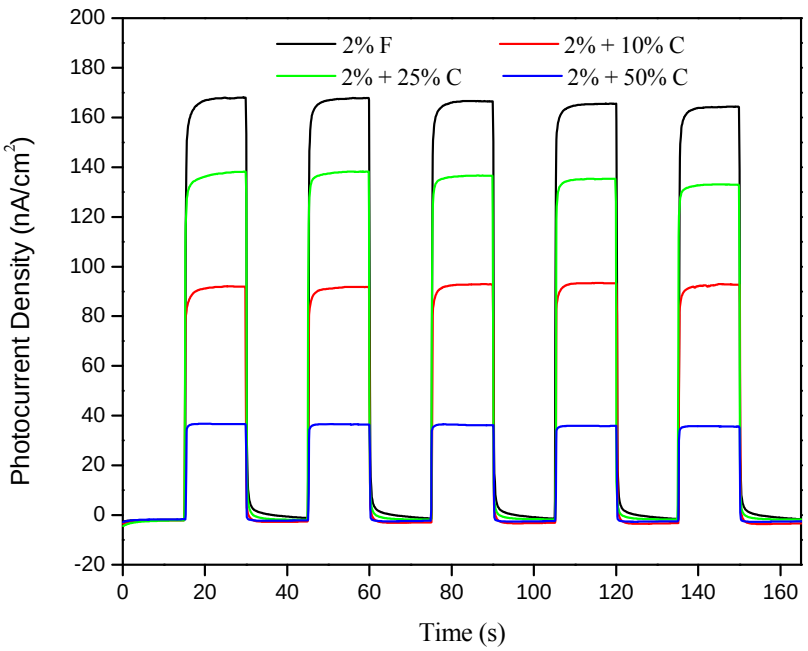


**Figure 4.10.** Anodic photocurrent generation from 2% fullerene $C_{63}$ and 10-50% cholesterol assembled in C12-SAM/DPPC bilayers. Other conditions are idential to those described in Figure 4.6.

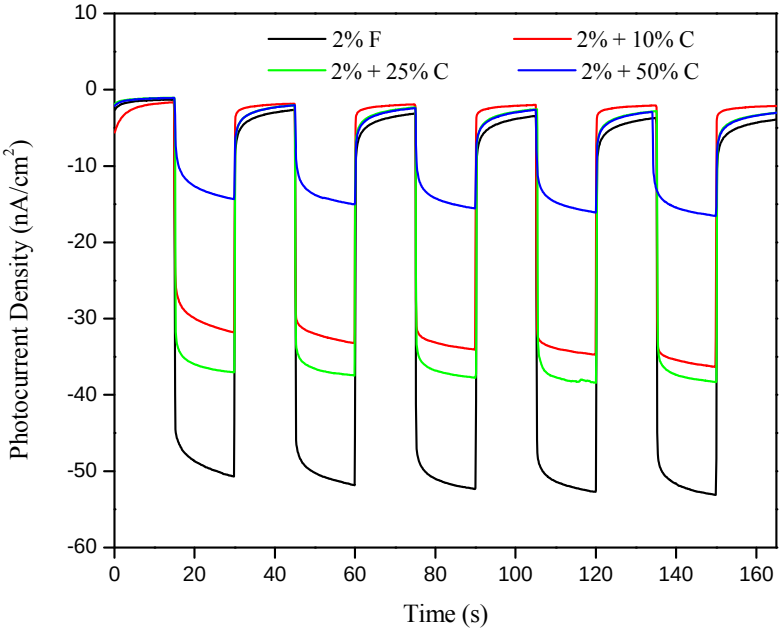


**Figure 4.11.** Cathodic photocurrent generation from 2% fullerene $C_{63}$ and 10-50% cholesterol assembled in C12-SAM/DPPC bilayers. Other conditions are idential to those described in Figure 4.7.

### 4.4 Conclusion

Two new hybrid lipid-based molecular photovoltaic systems were studied here, which were built with photoactive fullerene $C_{63}$ and cholesterol (0-50%) either in POPC or DPPC lipid matrix. Due to the dual effects of cholesterol on lipid membrane - it increases the ordering and rigidity in fluid phase while decreasing them in gel state, the incorporated cholesterol can modulate the photocurrent generation of this two systems in an opposite direction. This results provide more opportunity to modify molecular

photovoltaics using natural compound cholesterol, or through altering the lipid matrix phase either by choosing different lipids or by changing the temperatures.

**References:**


1. Hagfeldt, A.; Grätzel, M. Molecular Photovoltaics. *Accounts of Chemical Research*. **2000**, *33*, 269-277.

2. Kippelen, B.; Bredas, J.-L. Organic photovoltaics. *Energy & Environmental Science*. **2009**, *2*, 251-261.

3. Imahori, H.; Fukuzumi, S. Porphyrin- and Fullerene-Based Molecular Photovoltaic Devices. *Advanced Functional Materials*. **2004**, *14*, 525-536.

4. Gratzel, M. Photoelectrochemical cells. *Nature*. **2001**, *414*, 338-344.

5. Jiang, K.; Xie, H.; Zhan, W. Photocurrent Generation from Ru(bpy)32+ Immobilized on Phospholipid/Alkanethiol Hybrid Bilayers. *Langmuir*. **2009**, *25*, 11129-11136.

6. Xie, H.; Jiang, K.; Zhan, W. A modular molecular photovoltaic system based on phospholipid/alkanethiol hybrid bilayers: photocurrent generation and modulation. *Physical Chemistry Chemical Physics*. **2011**, *13*, 17712-17721.

7. Zhan, W.; Jiang, K.; Smith, M. D.; Bostic, H. E.; Best, M. D.; Auad, M. L.; Ruppel, J. V.; Kim, C.; Zhang, X. P. Photocurrent Generation from Porphyrin/Fullerene Complexes Assembled in a Tethered Lipid Bilayer. *Langmuir*. **2010**, *26*, 15671-15679.

8. Liu, L.; Zhan, W. Molecular Photovoltaic System Based on Fullerenes and Carotenoids Co-assembled in Lipid/Alkanethiol Hybrid Bilayers. *Langmuir*. **2012**, *28*, 4877-4882.

9. Starke-Peterkovic, T.; Turner, N.; Vitha, M. F.; Waller, M. P.; Hibbs, D. E.; Clarke, R. J. Cholesterol effect on the dipole potential of lipid membranes. *Biophysical journal*. **2006**, *90*, 4060.

10. Róg, T.; Pasenkiewicz-Gierula, M.; Vattulainen, I.; Karttunen, M. Ordering effects of cholesterol and its analogues. *Biochimica et Biophysica Acta (BBA) - Biomembranes*. **2009**, *1788*, 97-121.

11. Ohvo-Rekilä, H.; Ramstedt, B.; Leppimäki, P.; Peter Slotte, J. Cholesterol interactions with phospholipids in membranes. *Progress in Lipid Research*. **2002**, *41*, 66-97.

12. Brown, R. E. Sphingolipid organization in biomembranes: what physical studies of model membranes reveal. *Journal of Cell Science*. **1998**, *111*, 1-9.

13. Finkelstein, A.; Cass, A. Effect of Cholesterol on the Water Permeability of Thin Lipid Membranes. *Nature*. **1967**, *216*, 717-718.

14. El-Sayed, M. Y.; Guion, T. A.; Fayer, M. D. Effect of cholesterol on viscoelastic properties of dipalmitoylphosphatidylcholine multibilayers as measured by a laser-induced ultrasonic probe. *Biochemistry*. **1986**, *25*, 4825-4832.

15. Jedlovszky, P.; Mezei, M. Effect of Cholesterol on the Properties of Phospholipid Membranes. 2. Free Energy Profile of Small Molecules. *The Journal of Physical Chemistry B*. **2003**, *107*, 5322-5332.

16. Pandit, S. A.; Chiu, S.-W.; Jakobsson, E.; Grama, A.; Scott, H. L. Cholesterol Packing around Lipids with Saturated and Unsaturated Chains: A Simulation Study. *Langmuir*. **2008**, *24*, 6858-6865.

17. Zhan, W.; Jiang, K. A Modular Photocurrent Generation System Based on Phospholipid-Assembled Fullerenes. *Langmuir*. **2008**, *24*, 13258-13261.

18. Cook, M. J.; Lewis, A. P.; McAuliffe, G. S. G.; Skarda, V.; Thomson, A. J.; Glasper, J. L.; Robbins, D. J. Luminescent metal complexes. Part 1. Tris-chelates of substituted 2,2[prime or minute]-bipyridyls with ruthenium (II) as dyes for luminescent solar collectors. *Journal of the Chemical Society, Perkin Transactions 2*. **1984**, *0*, 1293-1301.

19. Ward, M. D. Metal-metal interactions in binuclear complexes exhibiting mixed valency; molecular wires and switches. *Chemical Society Reviews*. **1995**, *24*, 121-134.

20. Gracia, R. S.; Bezlyepkina, N.; Knorr, R. L.; Lipowsky, R.; Dimova, R. Effect of cholesterol on the rigidity of saturated and unsaturated membranes: fluctuation and electrodeformation analysis of giant vesicles. *Soft Matter*. **2010**, *6*, 1472-1482.

21. Innocenzi, P.; Kozuka, H.; Yoko, T. Fluorescence Properties of the Ru(bpy)32+ Complex Incorporated in Sol−Gel-Derived Silica Coating Films. *The Journal of Physical Chemistry B*. **1997**, *101*, 2285-2291.

22. Falck, E.; Patra, M.; Karttunen, M.; Hyvönen, M. T.; Vattulainen, I. Lessons of Slicing Membranes: Interplay of Packing, Free Area, and Lateral Diffusion in Phospholipid/Cholesterol Bilayers. *Biophysical journal*. **2004**, *87*, 1076-1091.

23. Rubenstein, J.; Smith, B. A.; McConnell, H. M. Lateral diffusion in binary mixtures of cholesterol and phosphatidylcholines. *Proceedings of the National Academy of Sciences*. **1979**, *76*, 15-18.

24. Steinem, C.; Janshoff, A.; Ulrich, W.-P.; Sieber, M.; Galla, H.-J. Impedance analysis of supported lipid bilayer membranes: a scrutiny of different preparation techniques. *Biochimica et Biophysica Acta (BBA) - Biomembranes*. **1996**, *1279*, 169-180.

25. Bretscher, M.; Munro, S. Cholesterol and the Golgi apparatus. *Science*. **1993**, *261*, 1280-1281.

26. Kučerka, N.; Marquardt, D.; Harroun, T. A.; Nieh, M.-P.; Wassall, S. R.; de Jong, D. H.; Schäfer, L. V.; Marrink, S. J.; Katsaras, J. Cholesterol in Bilayers with PUFA Chains: Doping with DMPC or POPC Results in Sterol Reorientation and Membrane-Domain Formation. *Biochemistry*. **2010**, *49*, 7485-7493.

27. Salamon, Z.; Lindblom, G.; Tollin, G. Plasmon-waveguide resonance and impedance spectroscopy studies of the interaction between penetratin and supported lipid bilayer membranes. *Biophysical journal*. **2003**, *84*, 1796-1807.

# Chapter Five

## Self-Assembled Monolayers (SAM)/Lipid Multilayers on Indium Tin Oxide (ITO) Surfaces: Formation and Photoelectrochemical Applications

### 5.1 Introduction

Attempts were made in this study to 1) form hybrid alkane/lipid bilayers on indium tin oxide substrates and 2) use thus formed thin organic films to conduct photocurrent generation. A motivation of such efforts was to find alternative substrates to replace gold previously used in this lab to build molecular photovoltaic systems. Although gold's inertness and ease of formation of self-assembled monolayers were found useful in our previous studies, it also has several intrinsic shortcomings that prevent its general use in solar cells: its scarcity and thus high price, opaqueness and more importantly, its lack of band gap (thus high tendency of charge recombination) and quenching of photoexcitation due to its plasmon motion. Our general strategy here is to form monolayers of alkanesilanes on ITO substrates, which are then covered by monolayers of lipids via lipid fusion. Thus formed films were characterized by several techniques, including cyclic voltammetry and fluorescence microscopy.

Indium Tin Oxide (ITO) is a semiconductor material typically comprised of 90% $In_2O_3$, 10% $SnO_2$ by weight. ITO is most commonly employed as a thin film coated on solid substrates, such as silicon, or glass as is the case in the current investigation. The many properties of ITO include electrical conductivity, high optical transparency, thermal

stability and wide band gap[1] which enable its use in optoelectronic devices, such as liquid crystal displays, organic light emitting diodes (OLEDs) and solar cells.[2-4] Despite its widespread use, there are several drawbacks with the chemical and electronic properties of ITO, including relatively low work function, strong absorption in the blue light region and high polar hydrophilic surface, which limit its further applications.[5,6]

The formation of self-assembled monolayers (SAMs) on ITO has been an attractive field due to the widespread use of ITO and the sensitivity of its properties to the surface treatment. It has been shown that the work function and charge injection efficiency of ITO can be easily altered through the formation of SAMs.[7,8] Furthermore, different SAMs can be utilized to change the wettability of ITO surface to make it compatible with nonpolar organic materials such as those used in OLEDs or photovoltaic devices.[6] Thus far, phosphonic acids,[8,9] carboxylic acids,[10] thiols,[11] amines[12] and alkylsilane[13-15] have been used to form SAMs on ITO surface. Since the polar headgroups of carboxylic acids, thiols and amines do not bind strongly to ITO surface, the formation of stable, well-packed SAMs through them is very difficult.[15] Even with strong bonding, it is still quite challenging to form a densely-packed and defect-free SAM on ITO with phosphonic acids and alkylsilane because of the high surface roughness and low hydroxyl group coverage.[13]

The ability of alkanethiols to form densely-packed and well-ordered SAMs on gold surfaces has inspired the use of this combination in various molecular photovoltaic systems.[16-18] Due to the ability of the gold surface to quench the excited states of chromophores, it is hard to achieve a large quantum yield with this system but this can be overcome by switching to ITO substrates.[19] Over the past few years, several high

performance photovoltaics based on SAMs (especially donor-acceptor linked SAMs) on ITO have been reported.[20-23]

Within the current investigation, several molecular photovoltaic systems were constructed based on either lipid bilayer or hybrid bilayer matrices on ITO substrates and the photocurrent generation behaviors were investigated using $Ru(bpy)_3^{2+}$ or fullerene $C_{63}$ as the photoactive species. In either system, the hybrid bilayer-based photocell was able to generate higher anodic photocurrent as compared to the lipid bilayer-based system. The formation of octadecyltrichlorosilane (OTS) SAMs on bare glass or ITO as well as the surface roughness of these bare or modified substrates were also investigated and compared using electrochemical, fluorescence and atomic force microscopy (AFM) techniques.

## 5.2 Experimental Section

### 5.2.1 Reagents

Phospholipid 1-palmitoyl-2-oleoyl-*sn*-glycero-3-phosphocholine (POPC) was obtained from Avanti Polar Lipids. n-Octadecyltrichlorosilane (OTS, 95% purity) from Gelest and potassium hexacyanoferrate-(III) ($K_3Fe(CN)_6$) from Riedel-de Haën. Monomalonic fullerene ($C_{63}$)[24] and $Ru(bpy)_3^{2+}$-conjugated DOPE[25] were prepared according to previously published procedures. Sodium sulfate and sodium chloride were obtained from Fisher Scientific while 4-(2-hydroxyethyl)piperazine-1-ethanesulfonic acid (HEPES), L(+)-ascorbic acid sodium salt (sodium ascorbate), D-(+)-glucose, glucose oxidase (type X-S, *from Aspergillus niger*), and catalase from bovine liver were

purchased from Sigma-Aldrich. All solutions employed in these experiments were prepared using 18.2 MΩ·cm deionized water (Millipore).

### 5.2.2 The Patterning of Glass and ITO Substrates

Some of the glass and ITO slides were patterned for fluorescence imaging measurements. To do so, glass (precleaned micro slides, VWR) or ITO (Delta Technologies) substrates used in lipid monolayer/bilayer formation were first sonicated in Micro-90 washing solution (International Products Co.) for 1 h and then 0.5 h each in acetone, methanol and deionized water. A positive photoresist layer (15-20 $\mu$m thick, AZ P4620, Clariant Co., Somerville, NJ) was then spin coated onto these slides. The photoresist layer was patterned by illuminating the resist with an unfiltered Hg light source (EXFO X-Cite 120) through a photomask. The unpolymerized photoresist was removed by dipping the substrates into a suitable developer solution. After being carefully washed and thoroughly dried by argon, these substrates were then transferred into a glove box for the formation of trichloro(octadecyl)silane (OTS) monolayers on lithography-exposed surfaces. Immediately thereafter, the glass slides were washed with copious amounts of toluene and the remaining photoresist was removed with ethanol. Finally, these substrates with patterned OTS monolayers were thoroughly rinsed with DI water, dried and ready for lipid deposition.

### 5.2.3 Assembly of SAMs and Hybrid Bilayers

To prepare OTS SAMs on ITO and glass substrates, ITO or glass slides were first cleaned by sonication in a series of media including Micro-90 washing solution, DI

water, acetone, and DI water again, each of which persisted for 30 min. The treated slides were then boiled in a mixture of DI water/$H_2O_2$ (30%)/$NH_4OH$ (30%) (5:1:1, v/v) for 1 h. The slides were then rinsed with copious amount of DI water and thoroughly dried under an argon stream. The slides were immediately transferred into a glovebox in which the water vapor level is regulated at a level typically under 3 ppm. To form the OTS SAMs, the cleaned slides were immersed in a 2.5 mM OTS solution in anhydrous toluene for 45min. After silanization, the slides were further rinsed with toluene and methanol to remove the unbound silanes and finally, annealed at 120ºC for 2 h. These slides are then assembled in a homemade Teflon photoelectrochemical cell before further use usually within 24 h.

Preparation of liposome samples containing fullerene $C_{63}$ [24] or $Ru(bpy)_3^{2+}$-DOPE[25] was reported previously; the POPC/Rhodamine liposome was prepared according to the same procedure. Appropriate quantities of POPC and Rhodamine in chloroform were thoroughly mixed in a flask and then dried to a film by rotary evaporation. This mixture was then sonicated (Bransonic, model: 3510-DTH) in HEPES buffer solution (10 mM HEPES, 100 mM NaCl, pH 7.7) at room temperature for 2h. The resulting solution was then extruded consecutively through polycarbonate membranes (Nuclepore, Whatman) of 400 and 80 nm-diameter pore at room temperature. The total lipids concentration of the final product was approximately 1.25 mM.

The formation of POPC/OTS hybrid bilayers was done by adding a 300-μL liposome solution (total lipid concentration: 1.25 mM) onto an SAM above prepared and incubated for 2 h. Afterwards, the unbound liposome solution was completely removed

from the cell by thorough solution exchange with the buffer solution for about 30 times(10 mM HEPES, 100 mM NaCl, pH 7.7).

### 5.2.4 Electrochemical Measurements

The Cyclic voltammetry experiments were carried out with a potentiostat (CHI 910B, CH Instruments) in a three-electrode Teflon cell containing blank or OTS-covered (with/without lipid layer) ITO substrates as the working electrode, Pt wire as the counter electrode and Ag/AgCl (in saturated KCl) as the reference electrode. 10mM $K_3Fe(CN)_6$ solution was used as the electrolyte for the CV measurements. The scan rate was 100 mV/s.

### 5.2.5 Contact Angle Measurements

The ITO slides were first cleaned with the same procedure as described in 5.2.3 section. Water contact angle measurements were then carried out with the sessile drop method on a Ram´e-Hart20 model 200 automated goniometer (Ram´e-Hart, Inc. Mountain Lakes, NJ) using DRO Pimage Standard software.

### 5.2.6 Fluorescence Imaging and Intensity Measurements

The fluorescence images of the Rhodamine-containing hybrid bilayer on ITO or glass slides were acquired using a PI Acton spectrometer (SpectraPro SP 2356, Acton, NJ) which is connected to the side port of an epifluorescence microscope (Nikon TE-2000U, Japan). The image was recorded by a back illuminated digital CCD camera (PI Acton PIXIS:400B, Acton, NJ) operated by a PC. The excitation was generated by a

mercury lamp (X-Cite 120, EXFO, Ontario, Canada) filtered by a band-pass filter at 560±20 nm. The light intensity was about 40 mW. The exposure time was 50 ms.

Fluorescence intensity measurements of rhodamine solution were conducted using a Nanodrop 3300 fluorospectrometer (Thermo Scientific). The intensity of emission was measured at 575 nm. The rhodamine solution was obtained by first adding a 300 μL rhodamine/POPC liposome solution onto a bare or silanized glass/ITO substrate assembled in a photochemical cell and incubated for 2 h. Afterwards, the unbound liposome solution was completely removed from the cell by thorough buffer solution exchange. The remaining solution was then removed and the cell was allowed to dry naturally overnight, which was followed by dissolving the dry lipid film in ethanol and transferring the ethanol solution into a small glass vial. Finally, the ethanol was removed under argon while heating on a hot plate to 80 ºC followed by dissolving the rhodamine/POPC in 20 μL ethanol.

### 5.2.7 Photoelectrochemical Measurements

The photoelectrochemical measurements were carried out in a three-electrode Teflon photoelectrochemical cell. The three-electrode setup contains the ITO substrate with a lipid bilayer or a lipid/SAM hybrid bilayer as the working electrode, a Pt counter electrode, and a Ag/AgCl (KCl-saturated) reference electrode. The effective area of the gold electrode is ~1.13 $cm^2$. The anodic photocurrent was generated in 50 mM ascorbate in HEPES buffer solution. Oxygen in the cell was removed by mixing 50 mM glucose, 50 units/mL glucose oxidase, and 200 units/mL catalase. The cell was irradiated with light from a Hg lamp (X-Cite, series 120 PC, EXFO) filtered at 470±20 (average intensity: ~20

mW/cm$^2$) for $Ru(bpy)_3^{2+}$ systems and filtered at 417±30 nm (average intensity: ~40 mW/cm$^2$) for fullerene systems. The resulting photocurrents were recorded by a potentiostat (CHI 910B, CH Instruments). The spectral variation of excitation light intensity was corrected with a photometer (Thorlabs).

### 5.2.8 AFM Measurements

The AFM measurements of bare/SAM-coated ITO or glass slides were conducted with Veeco atomic force microscope (Dimension 3000) in a tapping mode. The etched Si tips (FM-20,Nanoworld) have a force constant of 2.8 N/m and resonance frequency of 75 kHz. The tip scanning was operated at 2 Hz. All images are presented without graphical enhancement.

## 5.3 Results and Discussion

### 5.3.1 Cyclic Voltammetry Blocking Behaviors

Cyclic voltammetry (CV) was used to monitor the formation of OTS and lipid/OTS on ITO. Four ITO slides were prepared according to the experimental section and used as the working electrodes to carry out the CV measurements with 10mM $K_3Fe(CN)_6$ as the electrolyte. The results are shown in Figure 5.1. The voltammetry of the bare ITO electrode exhibits the typical reversible shape for $Fe(CN)_6^{3-}$. The coating of an OTS layer without being annealed did not significantly decrease the peak current which indicates a poorly packed SAM. The peak current corresponding to the ITO electrode which was annealed at 120 ºC for 2 h right after the silanization was decreased significantly. This suggests that the baked OTS layer can partially block the access of

$Fe(CN)_6^{3-}$ molecules from the electrode surface. Furthermore, the formation of $Ru(bpy)_3^{2+}$ embedded POPC lipid layer on the baked OTS/ITO can also impose mass-transfer barrier for the redox species to reach the ITO surface thus resulting further reduced peaks. These results show that the annealing process is crucial for the formation of a well packed OTS SAM. On another hand, the existence of the reversible redox peaks even with an OTS/lipid hybrid layer indicates some pinholes are present and the ITO surface coverage is not close to unity.[15,26]

The formation of OTS SAM was further confirmed with contact angle measurement. The contact angle of clean, bare ITO was 22.6° while the contact angle of the OTS SAM-coated ITO after annealing was 108.1°. The latter value indicates a sharp increase in hydrophobicity due to the alkyl chains on the surface.

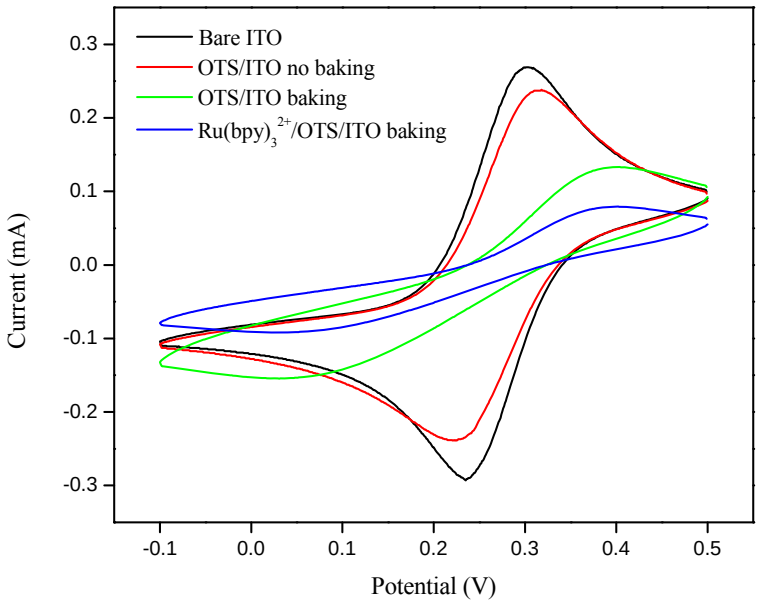


Figure 5.1. Cyclic voltammetry of bare ITO and SAM/ITO (with or without lipid layer) at a Scan rate of 100 mV/s.

### 5.3.2 Photocurrent Generation

The photocurrent obtained with the POPC lipid bilayer-based and POPC/OTS hybrid bilayer-based photovoltaics were compared in Figure 5.2 and 5.3. Regardless of the incorporated photosensitizer, the hybrid bilayer systems produced higher photocurrent than the lipid bilayer one. As shown in Figure 5.2, ~ 300 nA/cm$^2$ anodic current was generated by 2% $Ru(bpy)_3^{2+}$ in POPC lipid bilayer membrane (BLM) versus ~ 450 nA/cm$^2$ in POPC/OTS hybrid bilayer membrane (HBM) with the same photoagent. For fullerene systems, the photocurrent was 40 nA/cm$^2$ versus 115 nA/cm$^2$ (Figure 5.3). With the same hybrid bilayer on gold substrate, the obtained photocurrent was 29 nA/cm$^2$ for $Ru(bpy)_3^{2+}$ [25] and 75 nA/cm$^2$ for $C_{63}$ [24].

Compared to the suspended BLM, HBM has significantly more mechanical stability while preserving the dynamic nature of BLM. It has also been suggested that the HBM can organize the embedded molecules (proteins or photoagents) in a way which more closely resembles the eukaryote membrane which can enhance the vectorial electron transfer.[27] Furthermore, the SAM layer in HBM offers a better packed and lower fluidity environment, which can inhibit the energy loss during photoinduced electron transfer process and thus increase the photocurrent generation.

The more pronounced current enhancement with $C_{63}$ assembled in hybrid bilayer matrix can be explained by the different organization and location of fullerene in the membrane as compared to $Ru(bpy)_3^{2+}$. The $Ru(bpy)_3^{2+}$ groups are expected to locate at the top of the lipid monolayer facing the water/lipid interface since they are directly linked to DOPE lipids via the amine head group.[17] While it has been shown that the

fullerenes tend to reside in the hydrocarbon chain region in the lipid layer.[28] Thus the polar OTS SAMs in the hybrid bilayer matrix apply more impact on the fullerene $C_{63}$ system because of the shorter distance between the photoagents and the SAMs.

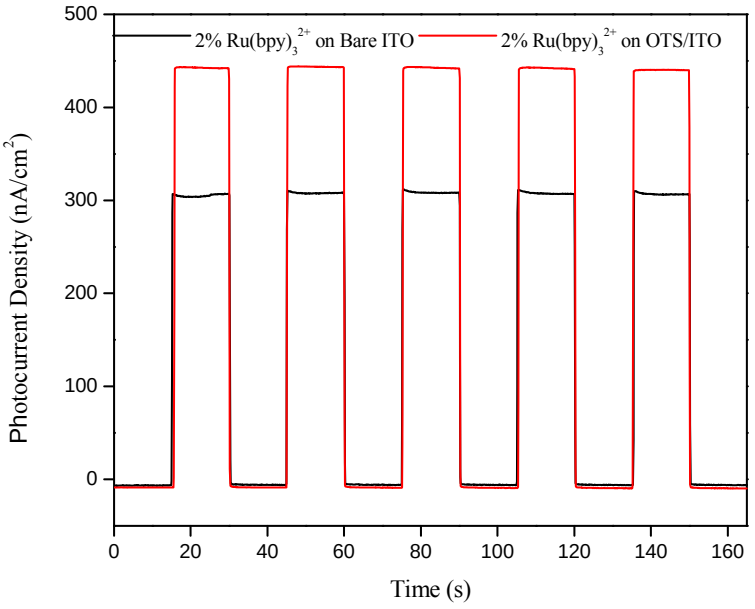


**Figure 5.2.** Photocurrent singles generated by 2% $Ru(bpy)_3^{2+}$ in POPC lipid bilayer ( in black) or in POPC/OTS hybrid bilayer (in red). The excitation light was provided by a Hg lamp filtered at 470±20 nm with an average intensity of 20 $mW/cm^2$.

### 5.3.3 Investigation of Bilayer Formation with Fluorescence Techniques

After observing the photocurrent enhancement with hybrid bilayer models, fluorescence techniques were employed to study the formation of the hybrid bilayers versus the lipid bilayers. Glass substrates were initially used to test the feasibility of the methods. A fluorescence image with a patterned glass slide is shown in the top of Figure 5.4. The dark regions represent the lithography-exposed surface during the patterning process, which corresponds to the rhodamine embedded, OTS/lipid-coated area. The

bright strips were covered with photomask during illumination and thus correspond to the regions with lipid layers. As shown in the bottom curve of Figure 5.4, the fluorescence intensity of the dark regions is one half of the intensity for the bright regions, which confirms the formation of the hybrid bilayer as well as the lipid bilayer.

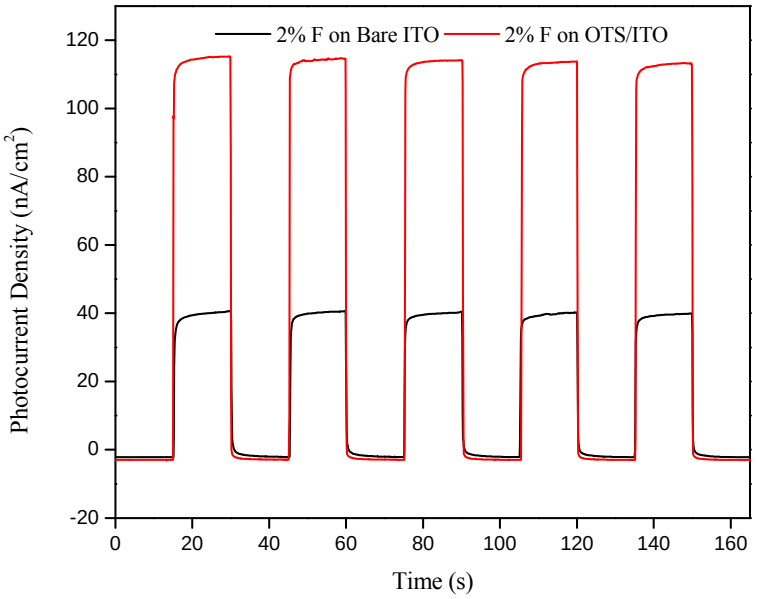


**Figure 5.3.** Photocurrent singles generated by 2% fullerene $C_{63}$ in POPC lipid bilayer ( in black) or POPC/OTS hybrid bilayer (in red). The excitation light was provided by a Hg lamp filtered at 417±30 nm; average intensity: 40 mW/cm$^2$.

The ratio of the amount of rhodamine corresponding to the hybrid or lipid bilayer on glass was further confirmed using a Nanodrop fluorospectrometer. The standard curve shown in Figure 5.5 reveals the linear relationship between [rhodamine]/M and fluorescence intensity. So the fluorescence intensity ratio of 502.82 : 1065.54 (0.47) in Table 5.1 indicates that the amount of rhodamine incorporated in the hybrid bilayer is

about one half of what was in the lipid bilayer, which demonstrates that a well packed OTS SAM and the subsequent lipid monolayer, as well as a lipid bilayer can be formed on glass. When the [rhodamine] in the lipid bilayer formed on glass was compared to that formed on the ITO surface, shown in Table 5.2, a ratio of 614.64 : 642.84 (0.96) was obtained which supports the formation of lipid bilayer on ITO. Unfortunately, similar fluorescence image/intensity results were not obtained involving OTS/lipid bilayer on ITO. This could be due to the large surface roughness of ITO compared to glass which was then studied by AFM.

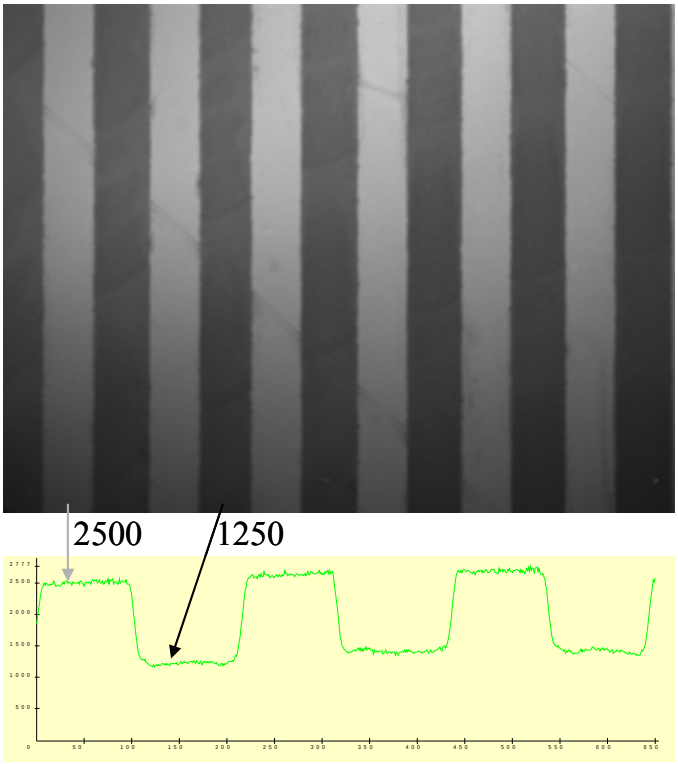


**Figure 5.4.** The fluorescence image (top) and its corresponding fluorescence intensity curve (bottom) of a patterned glass substrate with OTS/POPC hybrid bilayer or POPC lipid bilayer.

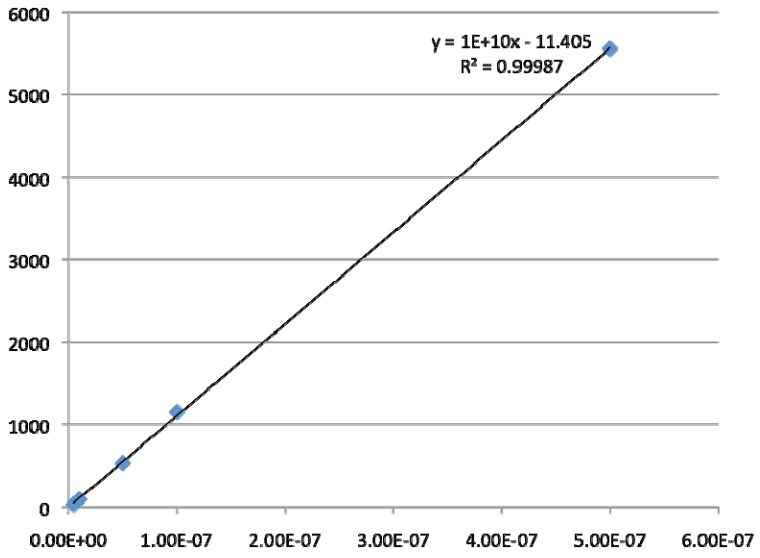


**Figure 5.5.** The standard curve of [Rhodamine]/M vs fluorescence intensity in ethanol.

| | Fluorescence intensity at 575 nm | | | | | Average |
|---|---|---|---|---|---|---|
| Hybrid bilayer on glass | 510.1 | 509.2 | 491.6 | 491.4 | 511.8 | 502.82 |
| Lipid bilayer on glass | 1039.4 | 1091.8 | 942.9 | 1132.8 | 1120.8 | 1065.54 |

**Table 5.1.** The fluorescence intensity of rhodamine solution obtained from the lipid bilayer on bare glass or the lipid monolayer on silanized glass.

| | Fluorescence intensity at 575 nm | | | | | Average |
|---|---|---|---|---|---|---|
| Lipid bilayer on glass | 602.5 | 631.6 | 640.7 | 570.5 | 627.9 | 614.64 |
| Lipid bilayer on ITO | 612.4 | 697.5 | 524.6 | 712.6 | 667.1 | 642.84 |

**Table 5.2.** The fluorescence intensity of rhodamine solution obtained from the lipid bilayer on bare glass or ITO.

### 5.3.4 Surface Roughness Study with AFM

As shown on the left of Figure 5.6, the surface of both bare and OTS-coated glass is very homogeneous and has a low roughness which is 0.918 and 0.852 (Table 5.3). Unlike glass substrate, the surface of bare ITO is non-uniform and has a much higher surface roughness (3.268) which makes it quite difficult to self-assemble a uniform and well packed OTS layer on it. That explains the rough surface of silanized ITO shown on the bottom right in Figure 5.6.

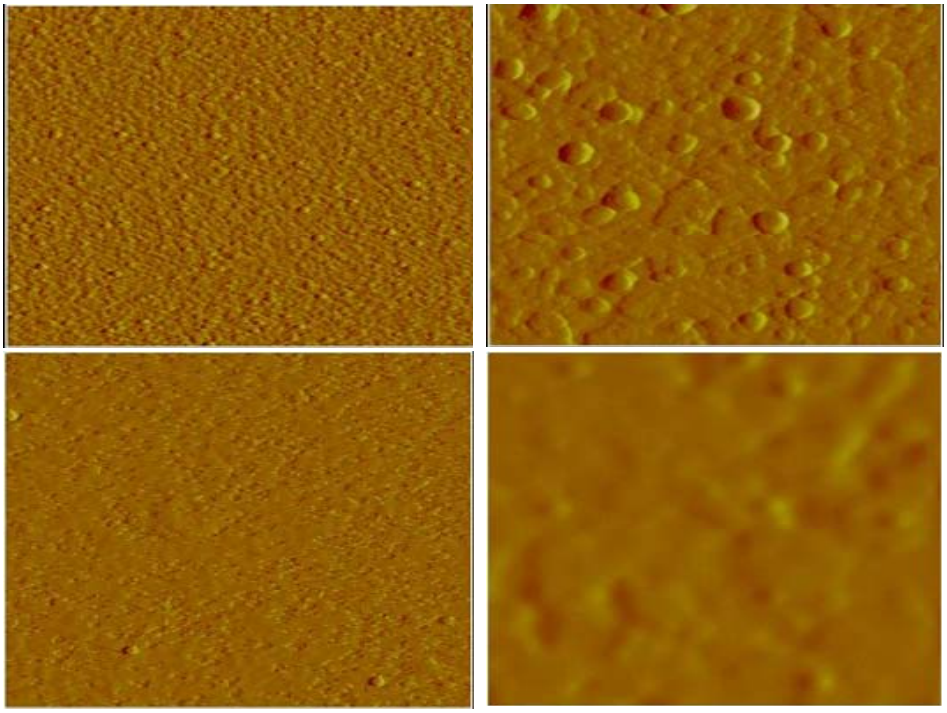

**Figure 5.6.** AFM images of bare glass (top left), bare ITO (top right), OTS-coated glass (bottom left) and OTS-coated ITO (bottom right). Size of the images is 2×2 μm, the scale of the z-axis: 10 nm for glass substrates, 50 nm for ITO substrates.

| Substrate | Bare glass | Bare ITO | OTS-coated glass | OTS-coated ITO |
|---|---|---|---|---|
| Roughness | 0.918 | 3.268 | 0.852 | 2.549 |

**Table 5.3.** The surface roughness of the substrates corresponding to Figure 5.6.

## 5.4 Conclusion

The ITO-based photovoltaic systems described here can generate higher photocurrent than the similar setup constructed on gold substrate. And the OTS/lipid matrix can significantly enhance the photocurrent generation as compared to the lipid bilayer system on bare ITO. Moreover, the annealing process is crucial for the formation of OTS SAMs on ITO/glass. This study also shows that lipid layers do not readily assemble on the rough surface such as ITO as compared to smooth surfaces. Because of its non-uniformity and high surface roughness, the formation of a homogeneous and densely packed OTS SAMs on ITO was unsuccessful in current investigation. This issue may be overcome or improved by using a different substrate cleaning procedures, such as UV-ozone, or by spin-coating another appropriate layer on top of ITO.

## References:


1. Samedov, K.; Aksu, Y.; Driess, M. Facile Molecular Approach to Transparent Thin-Film Field-Effect Transistors with High-Performance Using New Homo- and Heteroleptic Indium(III)–Tin(II) Single-Source Precursors. *Chemistry of Materials*. **2012**, *24*, 2078-2090.

2. Caruge, J. M.; Halpert, J. E.; Wood, V.; Bulovic, V.; Bawendi, M. G. Colloidal quantum-dot light-emitting diodes with metal-oxide charge transport layers. *Nat Photon*. **2008**, *2*, 247-250.

3. Yarema, M.; Pichler, S.; Kriegner, D.; Stangl, J.; Yarema, O.; Kirchschlager, R.; Tollabimazraehno, S.; Humer, M.; Häringer, D.; Kohl, M.; Chen, G.; Heiss, W. From Highly Monodisperse Indium and Indium Tin Colloidal Nanocrystals to Self-Assembled Indium Tin Oxide Nanoelectrodes. *ACS Nano*. **2012**, *6*, 4113-4121.

4. Harris, T. R. Review of Organic Light Emitting Diode Fabrication and Recent Progress. *Proceedings of Soft Electronics*. **2008**.

5. Marks, T. J.; Veinot, J. G. C.; Cui, J.; Yan, H.; Wang, A.; Edleman, N. L.; Ni, J.; Huang, Q.; Lee, P.; Armstrong, N. R. Progress in high work function TCO OLED anode alternatives and OLED nanopixelation. *Synthetic Metals*. **2002**, *127*, 29-35.

6. Li, J.; Wang, L.; Liu, J.; Evmenenko, G.; Dutta, P.; Marks, T. J. Characterization of transparent conducting oxide surfaces using self-assembled electroactive monolayers. *Langmuir*. **2008**, *24*, 5755-5765.

7. Donley, C.; Dunphy, D.; Paine, D.; Carter, C.; Nebesny, K.; Lee, P.; Alloway, D.; Armstrong, N. R. Characterization of indium-tin oxide interfaces using x-ray photoelectron spectroscopy and redox processes of a chemisorbed probe molecule: effect of surface pretreatment conditions. *Langmuir*. **2002**, *18*, 450-457.

8. Koh, S. E.; McDonald, K. D.; Holt, D. H.; Dulcey, C. S.; Chaney, J. A.; Pehrsson, P. E. Phenylphosphonic Acid Functionalization of Indium Tin Oxide: Surface Chemistry and Work Functions. *Langmuir*. **2006**, *22*, 6249-6255.

9. Ho, P. K. H.; Granström, M.; Friend, R. H.; Greenham, N. C. Ultrathin Self-Assembled Layers at the ITO Interface to Control Charge Injection and Electroluminescence Efficiency in Polymer Light-Emitting Diodes. *Advanced Materials*. **1998**, *10*, 769-774.

10. Asanov, A. N.; Wilson, W. W.; Oldham, P. B. Regenerable Biosensor Platform: A Total Internal Reflection Fluorescence Cell with Electrochemical Control. *Analytical Chemistry*. **1998**, *70*, 1156-1163.

11. Yan, C.; Zharnikov, M.; Gölzhäuser, A.; Grunze, M. Preparation and Characterization of Self-Assembled Monolayers on Indium Tin Oxide. *Langmuir*. **2000**, *16*, 6208-6215.

12. Oh, S.-Y.; Yun, Y.-J.; Kim, D.-Y.; Han, S.-H. Formation of a self-assembled monolayer of diaminododecane and a heteropolyacid monolayer on the ITO surface. *Langmuir*. **1999**, *15*, 4690-4692.

13. Choi, Y.; Noh, J. Structural Effect on Formation of Alkylsilane Self-Assembled Monolayers on Indium Tin Oxide Surface. *Molecular Crystals and Liquid Crystals*. **2008**, *492*, 165/[529]-171/[535].

14. Hillebrandt, H.; Tanaka, M. Electrochemical Characterization of Self-Assembled Alkylsiloxane Monolayers on Indium−Tin Oxide (ITO) Semiconductor Electrodes. *The Journal of Physical Chemistry B*. **2001**, *105*, 4270-4276.

15. Luscombe, C. K.; Li, H.-W.; Huck, W. T.; Holmes, A. B. Fluorinated silane self-assembled monolayers as resists for patterning indium tin oxide. *Langmuir*. **2003**, *19*, 5273-5278.

16. Huang, C.-H.; McClenaghan, N. D.; Kuhn, A.; Bravic, G.; Bassani, D. M. Hierarchical self-assembly of all-organic photovoltaic devices. *Tetrahedron*. **2006**, *62*, 2050-2059.

17. Zhan, W.; Jiang, K.; Smith, M. D.; Bostic, H. E.; Best, M. D.; Auad, M. L.; Ruppel, J. V.; Kim, C.; Zhang, X. P. Photocurrent generation from porphyrin/fullerene complexes assembled in a tethered lipid bilayer. *Langmuir*. **2010**, *26*, 15671.

18. Liu, L.; Zhan, W. Molecular Photovoltaic System Based on Fullerenes and Carotenoids Co-assembled in Lipid/Alkanethiol Hybrid Bilayers. *Langmuir*. **2012**, *28*, 4877-4882.

19. Yamada, H.; Imahori, H.; Nishimura, Y.; Yamazaki, I.; Ahn, T. K.; Kim, S. K.; Kim, D.; Fukuzumi, S. Photovoltaic Properties of Self-Assembled Monolayers of Porphyrins and Porphyrin−Fullerene Dyads on ITO and Gold Surfaces. *Journal of the American Chemical Society*. **2003**, *125*, 9129-9139.

20. Imahori, H.; Kimura, M.; Hosomizu, K.; Sato, T.; Ahn, T. K.; Kim, S. K.; Kim, D.; Nishimura, Y.; Yamazaki, I.; Araki, Y.; Ito, O.; Fukuzumi, S. Vectorial Electron Relay at ITO Electrodes Modified with Self-Assembled Monolayers of Ferrocene–Porphyrin–Fullerene Triads and Porphyrin–Fullerene Dyads for Molecular Photovoltaic Devices. *Chemistry – A European Journal*. **2004**, *10*, 5111-5122.

21. Cho, Y.-J.; Ahn, T. K.; Song, H.; Kim, K. S.; Lee, C. Y.; Seo, W. S.; Lee, K.; Kim, S. K.; Kim, D.; Park, J. T. Unusually High Performance Photovoltaic Cell Based on a [60]Fullerene Metal Cluster−Porphyrin Dyad SAM on an ITO Electrode. *Journal of the American Chemical Society*. **2005**, *127*, 2380-2381.

22. Yamada, H.; Imahori, H.; Nishimura, Y.; Yamazaki, I.; Fukuzumi, S. Enhancement of Photocurrent Generation by ITO Electrodes Modified Chemically with Self-Assembled Monolayers of Porphyrin–Fullerene Dyads. *Advanced Materials*. **2002**, *14*, 892-895.

23. Imahori, H.; Kashiwagi, Y.; Hasobe, T.; Kimura, M.; Hanada, T.; Nishimura, Y.; Yamazaki, I.; Araki, Y.; Ito, O.; Fukuzumi, S. Porphyrin and fullerene-based artificial photosynthetic materials for photovoltaics. *Thin Solid Films*. **2004**, *451–452*, 580-588.

24. Zhan, W.; Jiang, K. A Modular Photocurrent Generation System Based on Phospholipid-Assembled Fullerenes. *Langmuir*. **2008**, *24*, 13258-13261.

25. Jiang, K.; Xie, H.; Zhan, W. Photocurrent Generation from Ru(bpy)32+ Immobilized on Phospholipid/Alkanethiol Hybrid Bilayers. *Langmuir*. **2009**, *25*, 11129-11136.

26. Dayton, M. A.; Brown, J. C.; Stutts, K. J.; Wightman, R. M. Faradaic electrochemistry at microvoltammetric electrodes. *Analytical Chemistry*. **1980**, *52*, 946-950.

27. Plant, A. L. Supported Hybrid Bilayer Membranes as Rugged Cell Membrane Mimics. *Langmuir*. **1999**, *15*, 5128-5135.

28. Bortolus, M.; Parisio, G.; Maniero, A. L.; Ferrarini, A. Monomeric Fullerenes in Lipid Membranes: Effects of Molecular Shape and Polarity. *Langmuir*. **2011**, *27*, 12560-12568.

# Chapter Six

# Conclusion

Ever since the discovery of photovoltaic effect by Edmond Becquerel in 1839,[1] researchers have begun the journey of designing photovoltaics to convert sunlight into electric power. Two significant developments include the silicon-dominated semiconductor p-n junction solar cell which was first described in 1941[2] and the dye sensitized solar cell (DSSC) which was invented in 1988[3,4]. Distinct from the traditional solid state semiconductor-based photovoltaics, the DSSCs separate the light absorption and charger transfer processes which enables the use of low-cost materials and high efficiency.[5] Inspired by natural photosynthesis, several molecular photovoltaic (artificial photosynthetic) systems have been developed and reported which are based on chromophores embedded in solid-supported lipid bilayers[6] or alkanethiol/lipid hybrid bilayers [7,8].

One of the several advantages with the hybrid bilayer-based matrices over lipid bilayer systems is that they can be modified through both interfacial layers, a technique which was utilized in the current investigation to further study and develop these artificial photosynthetic systems. Due to their unique electrical and photochemical properties, fullerenes, porphyrin and $Ru(bpy)_3^{2+}$ are commonly used to serve as the photosensitizer in molecular photovoltaic devices and were also widely employed within our previous research. Instead of exploring new chromophore candidates, these three chromophores

were also included in building the molecular photovoltaics within the current investigation. But the photocurrent generated by these systems was modulated either through co-assembling some natural compounds, lutein or cholesterol, or by altering the bottom SAM layer. The hybrid bilayer-based photovoltaics were constructed on gold or ITO substrates via self-assembling an alkenthiol/OTS layer and a subsequent phospholipid monolayer from liposomes which were prepared with extrusion method. UV-vis and fluorescence spectroscopy were used to monitor the proportional incorporation of the photoactive agents in the liposome samples. Cyclic voltammetry, surface UV-vis, surface fluorescence and impedance spectroscopy were employed to study and characterize the SAM coated surface and hybrid bilayer structures. Photochemical action spectra, photocurrent and photovoltage generation were obtained to investigate the photovoltaic behaviors and the modulation effect of these systems. Energy diagrams were sketched to help understand the mechanisms and electron transfer processes.

Lutein itself is inefficient in generating photocurrent, but it can significantly modulate fullerene's photocurrent output via an electron transfer mechanism when co-assembled in the POPC lipid layer matrix. Addition of 1, 2, and 3% lutein in the bilayers decreased the anodic photocurrents generated from 2% fullerene $C_{63}$ by 14, 22 and 43% respectively while enhancing the cathodic photocurrents by factors of 1.9, 2.7 and 4.2.[9] By changing the fluidity, packing and phase properties of lipid membranes, up to 50% cholesterol can also be co-incorporated into lipid layers to regulate fullerene's photocurrent generation. Due to cholesterol's dual effect on different lipid membranes, adding 10, 25, and 50% cholesterol into POPC lipid matrices can enhance the anodic

photocurrent obtained from fullerene $C_{63}$ by 36, 57, and 100% and cathodic current by 47, 87, and 220%, respectively. While addition of the same amount of cholesterol into DPPC lipid membranes suppressed the photocurrent generation of fullerene $C_{63}$ by 47, 18, 79% in anodic condidions and 38, 26, 72% in cathodic conditions.

The intrinsic dipoles of alkanethiols can also be used to modulate photovoltaic responses in these alkanethiol/lipid hybrid bilayer based cells, which was demonstrated by comparing dodecanethiol (C12SH) and heptadecafluoro-1-decanethiol (C10F17SH) systems. By switching the underlying SAM from C12SH to C10F17SH, the anodic photocurrent of Zinc porphyrin (ZnP) was decreased from ~130 nA/cm$^2$ to ~50 nA/cm$^2$ while the cathodic photocurrent was increased from ~25 nA/cm$^2$ to ~65 nA/cm$^2$. And the same trend was observed with fullerene's photocurrents.

Contrary to the gold, the ITO substrate can be used to build these bilayer based photovoltaic cells without quenching chromophore excited states and is able to produce higher photocurrent as compared to the same structure and components on gold surface. But because of the high surface roughness and low hydroxyl group coverage, it is quite challenging to form a densely packed, well ordered SAM and subsequent lipid layer on ITO substrate which is a fundamental limitation endeavored by the current research efforts.

Several molecular photovoltaic devices were constructed and different strategies were successfully applied to modulate the photocurrent generation which is a significant step toward the development of artificial photosynthetic systems. Thus far the precise configuration of the hybrid bilayer structures as well as the orientation of the embedded chromophores remains unclear which will relay on new techniques to solve. And

hopefully, the light-to-power conversion efficiency with these photovoltaics can be improved in near future which will push them closer to practical application.

**References:**


1. Becquerel, E. *C.R. Acad. Sci.* **1839**, *9*, 145-149.

2. Ohl, R. S. Light-sensitive electric device. *US Patent No. 2,402,622*. **1941**, *27*.

3. Gratzel, M. Photoelectrochemical cells. *Nature*. **2001**, *414*, 338-344.

4. Hagfeldt, A.; Grätzel, M. Molecular Photovoltaics. *Accounts of Chemical Research*. **2000**, *33*, 269-277.

5. Green, M. A. Photovoltaic principles. *Physica E: Low-dimensional Systems and Nanostructures*. **2002**, *14*, 11-17.

6. Zhan, W.; Jiang, K. A Modular Photocurrent Generation System Based on Phospholipid-Assembled Fullerenes. *Langmuir*. **2008**, *24*, 13258-13261.

7. Jiang, K.; Xie, H.; Zhan, W. Photocurrent Generation from Ru(bpy)32+ Immobilized on Phospholipid/Alkanethiol Hybrid Bilayers. *Langmuir*. **2009**, *25*, 11129-11136.

8. Zhan, W.; Jiang, K.; Smith, M. D.; Bostic, H. E.; Best, M. D.; Auad, M. L.; Ruppel, J. V.; Kim, C.; Zhang, X. P. Photocurrent generation from porphyrin/fullerene complexes assembled in a tethered lipid bilayer. *Langmuir*. **2010**, *26*, 15671.

9. Liu, L.; Zhan, W. Molecular Photovoltaic System Based on Fullerenes and Carotenoids Co-assembled in Lipid/Alkanethiol Hybrid Bilayers. *Langmuir*. **2012**, *28*, 4877-4882